LA-14379
Approved for public release;
distribution is unlimited.

Enhanced Verification Test Suite for Physics Simulation Codes

Los Alamos
NATIONAL LABORATORY
EST. 1943

Los Alamos National Laboratory, an Affirmative Action/
Equal Opportunity Employer, is operated by Los Alamos
National Security, LLC, for the National Nuclear Security
Administration of the U.S. Department of Energy under
contract DE-AC52-06NA25396.

LA-14379
Issued: September 2008

Enhanced Verification Test Suite for Physics Simulation Codes

James R. Kamm
Jerry S. Brock
Scott T. Brandon*
David L. Cotrell*
Bryan Johnson*
Patrick Knupp**
William J. Rider**
Timothy G. Trucano**
V. Gregory Weirs**

* Lawrence Livermore National Laboratory, 7000 East Avenue, Livermore, CA 94551.
**Sandia National Laboratories, PO Box 5800, Albuquerque, NM 87185.

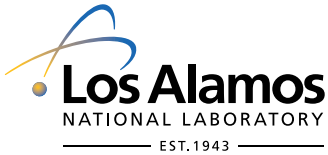

This page intentionally left blank.

LAWRENCE
LIVERMORE
NATIONAL
LABORATORY

LLNL-TR-411291

Enhanced Verification Test Suite for Physics Simulation Codes

J. R. Kamm, J. S. Brock, S. T. Brandon, D. L. Cotrell, B. Johnson, P. Knupp, W. Rider, T. Trucano, V. G. Weirs

March 16, 2009

This page intentionally left blank.

SANDIA REPORT

SAND2008-7813
Unlimited Release
Printed April 2009

Enhanced Verification Test Suite for Physics Simulation Codes

James R. Kamm[1], Jerry S. Brock[1], Scott T. Brandon[2], David L. Cotrell[2], Bryan M. Johnson[2], Patrick Knupp, William J. Rider, Timothy G. Trucano, and V. Gregory Weirs

[1] Los Alamos National Laboratory
[2] Lawrence Livermore National Laboratory

Prepared by
Sandia National Laboratories
Albuquerque, New Mexico 87185 and Livermore, California 94550

Sandia is a multiprogram laboratory operated by Sandia Corporation,
a Lockheed Martin Company, for the United States Department of Energy's
National Nuclear Security Administration under Contract DE-AC04-94-AL85000.

Issued by Sandia National Laboratories, operated for the United States Department of Energy by Sandia Corporation.

Available to DOE and DOE contractors from
U.S. Department of Energy
Office of Scientific and Technical Information
P.O. Box 62
Oak Ridge, TN 37831

Telephone: (865) 576-8401
Facsimile: (865) 576-5728
E-Mail: reports@adonis.osti.gov
Online ordering: http://www.doe.gov/bridge

Available to the public from
U.S. Department of Commerce
National Technical Information Service
5285 Port Royal Rd
Springfield, VA 22161

Telephone: (800) 553-6847
Facsimile: (703) 605-6900
E-Mail: orders@ntis.fedworld.gov
Online ordering: http://www.ntis.gov/help/ordermethods.asp?loc=7-4-0#online

SAND2008-7813
Unlimited Release
Printed April 2009

Enhanced Verification Test Suite for Physics Simulation Codes

James R. Kamm and Jerry S. Brock
Los Alamos National Laboratory
P.O. Box 1663
Los Alamos, NM 87545

Scott T. Brandon, David L. Cotrell, and Bryan M. Johnson
Lawrence Livermore National Laboratory
P.O. Box 808
Livermore, CA 94551-0808

Patrick Knupp
Applied Math and Applications

Timothy G. Trucano
Optimization and Uncertainty Quantification

William J. Rider and V. Gregory Weirs
Computational Shock and Multiphysics

Sandia National Laboratories
P.O. Box 5800
Albuquerque, NM 87185-0819

This page intentionally left blank.

Enhanced Verification Test Suite for Physics Simulation Codes

James R. Kamm, Jerry S. Brock
Los Alamos National Laboratory

Scott T. Brandon, David L. Cotrell, Bryan M. Johnson
Lawrence Livermore National Laboratory

Patrick Knupp, William J. Rider, Timothy G. Trucano, V. Gregory Weirs
Sandia National Laboratories

“In an age of spreading pseudoscience and anti-rationalism, it behooves those of us who believe in the good of science and engineering to be above reproach whenever possible. Public confidence is further eroded with every error we make… As Robert Laughlin noted in this magazine, ‘there is a serious danger of this power [of simulations] being misused, either by accident or through deliberate deception.’ Our intellectual and moral traditions will be served well by conscientious attention to verification of codes, verification of calculations, and validation, including the attention given to building new codes or modifying existing codes with specific features that enable these activities.”

Patrick Roache [Roa04]

Executive Summary

This document discusses problems with which to augment, in quantity and in quality, the existing tri-laboratory suite of verification problems used by Los Alamos National Laboratory (LANL), Lawrence Livermore National Laboratory (LLNL), and Sandia National Laboratories (SNL). The purpose of verification analysis is demonstrate whether the numerical results of the discretization algorithms in physics and engineering simulation codes provide correct solutions of the corresponding continuum equations. The key points of this document are:

- Verification deals with mathematical correctness of the numerical algorithms in a code, while validation deals with physical correctness of a simulation in a regime of interest. This document is about verification.
- The current seven-problem Tri-Laboratory Verification Test Suite, which has been used for approximately five years at the DOE WP laboratories, is limited.
- Both the methodology for and technology used in verification analysis have evolved and been improved since the original test suite was proposed.
- The proposed test problems are in three basic areas:
    1. Hydrodynamics
    2. Transport processes
    3. Dynamic strength-of-materials
- For several of the proposed problems we provide a "strong sense verification benchmark," consisting of (i) a clear mathematical statement of the problem with sufficient information to run a computer simulation, (ii) an explanation of how the code result and benchmark solution are to be evaluated, and (iii) a description of the acceptance criterion for simulation code results.
- It is proposed that the set of verification test problems with which any particular code be evaluated include some of the problems described in this document.

Analysis of the proposed verification test problems constitutes part of a necessary—but not sufficient—step that builds confidence in physics and engineering simulation codes. More complicated test cases, including physics models of greater sophistication or other physics regimes (e.g., energetic material response, magneto-hydrodynamics), would represent a scientifically desirable complement to the fundamental test cases discussed in this report.

The authors believe that this document can be used to enhance the verification analyses undertaken at the DOE WP Laboratories and, thus, to improve the quality, credibility, and usefulness of the simulation codes that are analyzed with these problems.

Contents

Introduction

The DOE/NNSA Advanced Simulation & Computing (ASC) Program directs the development, demonstration, and deployment of physics and engineering simulation codes. These codes, used at Los Alamos National Laboratory (LANL), Lawrence Livermore National Laboratory (LLNL), and Sandia National Laboratories (SNL), are arguably among the most complex simulation codes utilized in computational science. The defensible utilization of these codes for high-consequence decisions requires defensible verification and validation of the simulation software.

What is Verification?

Verification is the process of demonstrating that numerical solutions of the discretized algorithms in simulation software are the correct solutions of the corresponding continuum equations. Consequently, verification represents an important aspect of the development, assessment, and application of simulation software for physics and engineering. An essential element of the verification process is the quantitative analysis of simulation code performance on well-defined problems. The outcome of such analyses provides hard evidence of mathematical consistency between the mathematical statements of the physics models and their discrete analogues as implemented with numerical algorithms in the simulation codes.

One of the important lessons of the past ten years of the ASC program is the complexity and the importance of verification. The challenge of verification is compounded by the fact that, at any point in time, verification cannot be considered to be complete in a rigidly logical sense. Rather, just as in validation, the progress of verification is measured primarily by the accumulation of evidence that numerical solutions of the continuum equations are indeed rigorously correct and accurate for particular calculations. The degree to which verification has been achieved directly influences the conduct of validation, as well as our sense of the quality of specific applications calculations. The simplest meaning of this point is that verification provides quantification of the numerical component of the “error bar” around calculations. When this error bar component is incomplete or completely missing, it is difficult or impossible to specify the overall accuracy of calculations. For example, in the absence of verification evidence, “good agreement” of calculations with experimental data may be an irrelevant observation, as the numerical solution could be completely wrong and the experimental agreement completely accidental.

Verification and Code Development

Recognition of the importance of verification is the essential factor in devising rational and effective means of accomplishing it. We seek to determine necessary elements of verification, to sensibly use available resources to realize these elements, and to rigorously understand the products of these analyses. Verification is affected by the manner in which software is developed and the skill with which that software is used. Simply put, ASC software cannot be proven to be mathematically correct and,

consequently, the accumulation of quantitative evidence remains the exclusive basis for inferring the mathematical correctness. The practical view is that this evidence must be accumulated over the long run. This accumulation occurs throughout the on-going processes of code development as well as during the subsequent code usage. Both activities are sources of necessary evidence that ASC codes achieve mathematical conditions *necessary* for their stockpile stewardship applications.

Verification evidence emerging from code development is generated by software engineering processes applied (implicitly or explicitly) during that development, and by the specific testing practices employed by the development personnel. Code usage evidence is a more subtle, complex, and diverse body of information that emerges from a heterogeneous group of users. Testing executed under the umbrella of code development is not restricted to the verification test problems that we discuss in this report; nevertheless, we have as a goal that our problems become useful as critical testing elements for code developers. However, unlike other testing procedures applied by code developers (including, e.g., unit tests and the restricted cases applied in regression testing), verification test problems also are relevant to code users. In fact, many of these test problems originated in user communities associated with given subject matter expertise. In developing this report, we have strived to take best advantage of the overlapping domains of interest of code developers and of code users: this intersection distinguishes useful verification test problems. Correct execution of test problems as described here will increase the level of confidence of code developers *and* of code users.

Verification Test Problems

There exists an agreed-upon set of problems used by the Laboratories for verification purposes. This set of seven problems [Bro06] forms a nominal basis with which to assess code capabilities. In recent years, verification analysis capabilities have matured significantly, enabling augmentation of the test suite. An intensified desire has developed within the code community for an enhanced set of problems that extends the scope of the code physics assessed and further challenges code capabilities.

The purpose of this document is to list problems with which to augment, both in quantity and in quality, the existing Tri-Laboratory Test Suite (TLTS) of verification problems used by LANL, LLNL, and SNL. We propose more problems than would probably be included in a finalized verification suite: we do so to encourage discussion within the community regarding the advantages and disadvantages of each problem. The burden lies with the code community—model developers, code developers, analysts, and end-users—to agree upon an expanded set of problems that will improve verification analyses and, thereby, enhance the quality of the physics simulations.

We believe that one measure of success of this effort is providing a set of problems that adds to the code testing associated with the JOWOG-42 code comparison activity [JAI07]. Verification test problems provide evidence that a code is mathematically correct; this approach complements the JOWOG-42 problems, which typically serve to assess physics simulation capabilities for more complicated and ambiguous situations,

albeit with less definitive expectations as far as drawing conclusions from the analysis of the problems. These two aspects, viz., (i) the code comparison emphasis of JOWOG-42 and (ii) a rigorous process for applying a verification test suite, each serve distinct purposes, but we believe there is common ground that is worth recognizing. The future of both code verification and JOWOG-42 will be well served by evolving toward a unified and stable suite of mathematically rigorous test problems and analysis techniques. Among the necessary factors to achieve this goal are (i) enriching the physics associated with the verification test suite and (ii) applying more rigor to the analysis of the JOWOG-42 problems. This report makes some progress on both of these issues, but much remains to be accomplished.

Code Verification

Verification can be summarized as the analysis of whether the numerical solutions of the discrete algorithms provide accurate solutions of the corresponding continuum equations. Distinct numerical schemes based on the identical continuum equations can produce radically different quantitative (and qualitative) results; therefore, while one may obtain nominally *correct* solutions of the discretized schemes, those results might be *inaccurate* solutions of the underlying continuum equations. Consequently, verification analysis constitutes a critically important aspect of the development, assessment, and application of simulation software for physics and engineering. It is important to distinguish between verification for the purpose of proving code correctness, and for providing algorithmic assessment; both activities have high value, but differ in details and tenor. An essential element of any verification process is the quantitative analysis of the simulation code performance on well-defined problems. The outcome of such analyses provides defensible evidence of mathematical consistency between the mathematical statements of the physics models and their discrete analogues as implemented with numerical algorithms in the simulation codes.

Verification is needed for scientific simulation codes because these codes are designed to produce approximate solutions to mathematical problems for which (i) the exact solution is not known and (ii) knowledge of the error is potentially as valuable as (or more valuable than) knowledge of the solution, per se. Most software returns either exact solutions to problems with exact solutions (e.g., banking, spreadsheets) or results for non-mathematical problems having only a subjectively defined goal (image processing, photo management, word processors, etc.). Due to this critical aspect of scientific simulation, software quality practices from the broader industry (e.g., regression testing) are helpful but are not sufficient for high-consequence physics/engineering simulation codes. Additionally, it is important to recognize that sensitivity analysis (see, e.g., [Sal04, Tru06]) cannot replace verification. The determination of a relative lack of sensitivity to mesh density or time step size does not imply that the calculation is necessarily converged. Instead, a lack of sensitivity may result from a calculation being very far from the asymptotic range of convergence, a conclusion that can be drawn from the verification process.

At its core, verification of ASC calculations both quantifies numerical errors and defines a rigorous basis for believing that quantification. These two goals are inseparable. It is a useless activity to provide numerical error estimates without presenting evidence to support them. Providing an error estimate for complex problems falls under the purview of *solution* (or *calculation*) *verification*, while providing the rigorous basis for such estimates is achieved with *code verification*. The overall activity of verification is the combination of *both* code and solution verification. The verification test problems that are the subject of this report are intended to comprise necessary conditions for code verification, mainly because they provide an opportunity to link both code and calculation verification in a way that is both relevant to code developers and users.

Verification and Software Testing

Software testing is critical and has had an unquestionably positive presence in ASC software development. Testing that is closest to code development centers on software engineering techniques, such as unit testing; such testing primarily addresses the correct functioning of software. The major factor that drives interest in the creation and application of the verification test problems that we present is that ASC software can function perfectly and provide mathematically *in*correct solutions to the underlying continuum equations. A simple example of what can cause this is incorrect input: for example, a numerical mesh that is inadequate for required accuracy levels. Foremost, however, the problem is driven by the potential for incorrect mathematics to be instantiated in the implemented software. What distinguishes computational science from other kinds of software development are the inevitable challenges created by mathematical complexity: this stands as the single most important factor in driving the creation of verification test problems.

To amplify this point, we observe a persistent confusion of verification testing with regression testing. These are completely different testing procedures because they have completely different goals. Verification testing, as we define it here, aims to develop evidence of mathematical correctness in the implemented software. Regression testing is a software engineering technique that assesses the robustness of software to frequent changes. Regression tests properly need not have any element of mathematical correctness as their goal. Regression tests reduce to a (typically large) collection of relatively simple problems that are executed at a regular (typically frequent) time interval. Regression testing seeks principally to reduce the amount of software rework that is created by the introduction of mistakes in software additions. This reduction is accomplished by comparing today's code with yesterday's code via execution of the regression test suite. Thus, regression testing targets *software stability*, not *mathematical correctness*. Regression testing is very successful from this point of view, although there remain major issues related to the size and complexity of the regression test suite, the frequency of execution, the need to "re-baseline" as inevitable algorithm modifications are implemented, etc. (Indeed, the belief that code stability enabled by regression testing outweighs the relatively large effort for managing a regression test suite is disputed in some quarters.)

Another mistake made in the interpretation of verification tests versus regression tests is that if verification tests are truly different, then those test problems must not be able to be regularly executed by code developers. Verification test suites can be implemented, managed, and applied by code developers just like regression tests. The major differences are (i) it will take more resources (people, computers, time) to actually execute a verification test suite, especially if convergence analysis is included as part of the testing; (ii) the time interval of execution of a verification test suite must be different than for regression testing; and (iii) the brute force methods for comparing today's regression test suite results versus yesterday's baseline must be replaced by greater human involvement in judging the quality of execution of verification tests. Frankly, we view the increased human element required to assess the execution of verification tests to be desirable, and it certainly emphasizes the point made above, i.e., that an important value of verification tests is their use in engaging the user community around a code. It is certainly true that the resources required to properly execute and assess verification problems is far greater than for regression tests. Giving priority to verification at this degree of intensity has been one of the historical reasons that verification has not been embedded entirely successfully in the ASC program. Our document cannot and will not address the issue of programmatic priorities for verification, but this issue is clearly present.

Verification and Scientific Software

Thus, verification analysis of complicated physics/engineering simulation codes is an example of the assessment of a complex system for which the systematic gathering of appropriate evidence is required. While tests may demonstrate that software is manifestly incorrect, there is no clear-cut procedure with which to "prove" unambiguously that software behavior is completely correct. Thus, the process by which relevant verification evidence is generated and interpreted requires knowledge of the entire simulation and analysis chain. Such knowledge includes understanding of:

- the system being simulated (e.g., the relevant physics, physics models, and these models' representation in mathematical equations);
- the nature of the simulation (including the discrete algorithms used to obtain approximate solutions to the mathematical equations, these algorithms' limitations, the associated numerical analysis, and the software implementation of those algorithms); and
- the process by which the code results are analyzed in the verification process (including, e.g., theory, implementation, and interpretation of convergence analysis).

In its entirety, this body of knowledge is both large and complex; consequently, the determination of an appropriate set of verification problems requires guidance and consensus among experts in each of these fields.

Appropriate verification tests are the most valuable tests of mathematical accuracy available. Any test problem that reveals mathematical problems underlying implemented software should ideally be viewed as helpful by both code developers and code users. We seek to avoid any notion a test problem effort is perceived as undermining both code developers and code users. Instead, valuable test problems speak to the complexity of the

mathematics in ASC codes while simultaneously addressing the complexity of these codes' intended use. Such problems must be chosen to lie in the overlapping domain of code developers and code users. Consequently, one measure of success for such problems is the relevance that both communities attach to such problems (in distinction to regression tests, about which, frankly, users could not care less). Hence, for verification tests it is necessary to couple the science of constructing complex mathematical benchmarks that definitively test ASC software with the art of selecting benchmarks that users believe increase the likely success of the code for their own purposes.

Given the complexity of these issues, there arises the notion that favorable comparison of computed results with experimental data represents prima facie evidence of verification. For example, upon obtaining acceptable agreement between experimental data and numerical results from a simulation code having non-existent, unknown, or undocumented verification provenance, one might speculate, "If there were errors in the computed solution, then we would never have calculated results so close to the experimental data; therefore, this code must be adequately verified." Such reasoning not only blurs the divide between verification and validation (the latter of which addresses the correctness of the underlying models to the physical phenomena of interest), but also—and more gravely—stands as a textbook example of fallacious reasoning exhibiting a so-called "false-cause fallacy."[1] Code analysts must bear in mind that simulation software represents exquisitely intricate numerics algorithms coupled to a complicated hardware/system-software platform: simulation software is *not* a "physics engine" that generates instantiations of physical reality. Hence, documented, quantitative verification analysis is a necessary component for developing code confidence and credibility.

Verification and the Tri-Laborabory Test Suite

Familiarity with the many issues underlying verification guided the selection of test problems proposed in this document. The verification problems in the current Tri-Laboratory Test Suite represent a small subset of certain physics phenomena. An important characteristic of any enhanced Test Suite, therefore, is that it expand the scope of physics phenomena being assessed and increase the depth and value of that interrogation.

Given our task, the expectations for this document are straightforward: we view it as defining a verification test suite that addresses the issues discussed above. We acknowledge that the problems we propose will not meet all expectations. Therefore, with time we plan to increase the number of tests as well as the rigor and clarity of their definition, implementation, application, and assessment criteria. We hope that these verification problems will exhibit intuitive value and relevance for users, so that their use will become part of systematic periodic testing supporting code development.

We are mindful that the proposed verification test problems constitute part of a necessary—*but not sufficient*—activity that builds confidence in physics and engineering simulation codes. More complicated test cases, including, e.g., physics models of greater

[1] See http://hawaii.hawaii.edu/wwwreading/Fallacies/fallacydefinitions.htm for a list of errors in reasoning.

sophistication, would represent a scientifically desirable complement to the fundamental test cases discussed in this report. If we are successful, our effort will play a constructive role in building scientifically defensible confidence in simulation capabilities.

The Current Tri-Laboratory Verification Test Suite

There are currently seven problems in the Tri-Lab Verification Test Suite [Bro06]. These problems were defined by a specific, but very limited, ASC milestone. The physics modeled in these problems include gas dynamics (Noh and Sedov Problems), coupled gas dynamics and non-linear heat conduction (Reinicke/Meyer-ter-Vehn Problem), coupled gas dynamics and radiation-diffusion (Coggeshall-8 Problem), non-equilibrium radiation-diffusion (Su-Olson Problem), neutron transport (Sood Problem), and high explosives (either the Escape of HE Products or Mader Problem). A brief description of these problems is provided below, followed by a table that catalogues the test problems together with their relevant physics models.

1. *Noh Problem* [Noh87] Symmetric planar, cylindrical or spherical one-dimensional, inviscid, non-heat conducting, compressible gas dynamics of a polytropic gas, which tests a code's ability to convert kinetic energy into internal energy. This problem admits a closed-form self-similar solution.
2. *Sedov Problem* [Sed59] Symmetric planar, cylindrical or spherical one-dimensional, inviscid, non-heat conducting, compressible gas dynamics of a polytropic gas, which tests a code's ability to convert internal energy into kinetic energy. This problem admits a closed-form, self-similar solution that requires one numerical quadrature.
3. *Reinicke/Meyer-ter-Vehn (RMtV) Problem* [Rei91] Extension of the spherically symmetric Sedov problem to include non-linear heat conduction. This self-similar problem's solution requires the numerical solution of a non-linear eigenvalue problem in the form of coupled, non-linear ordinary differential equations.
4. *Coggeshall-8 (Cog-8) Problem* [Cog91] Spherically symmetric, one-dimensional problem that couples inviscid, compressible gas dynamics of a polytropic gas with radiation-diffusion. This problem admits a closed-form solution.
5. *Su/Olson Problem* [Su96] Non-equilibrium radiation-diffusion physics problem in one-dimensional, Cartesian (slab) geometry. This problem admits a solution that reduces to numerical quadrature.
6. *Sood Problem* [Soo03] Neutron transport problem in one-dimensional, Cartesian (slab) geometry. The solution to this problem is given in terms of an analytic eigenvalue and corresponding eigenfunction solution.

7a. *Escape of HE Products* [Fic74] A constant-velocity piston interacts with a one-dimensional, Cartesian (slab) high explosive with a polytropic gas equation of state initiating an unsupported detonation. Evaluation of the straight-line characteristics of this problem admits a closed-form solution.

7b. *Mader Problem* [Fic79] High explosives problem in one-dimensional, Cartesian (slab) geometry for a material with a polytropic gas equation of state. This

problem admits a closed-form solution for the material properties in the rarefaction wave behind a steady detonation.

Table 1. Identification of the *existing* ASC Tri-Lab Test Suite problems and their corresponding physics models

Test Problem	Gas Dynamics	Non-Linear Heat Conduction	Non-Equilib. Radiation Diffusion	Neutron Transport	High Explosives
1. Noh	•				
2. Sedov	•				
3. RMtV	•	•			
4. Cog-8	•		•		
5. Su-Olson			•		
6. Sood				•	
7. HE	•				•

Code Simulation Capabilities

Multi-physics computer codes contain simulation modules that span a range of physical phenomena. One principal difference between "engineering" and "physics" simulation codes occurs in the parameter regimes and representative timescales of interest for the respective applications. Such differences affect both the physics modules and numerical algorithms used in these codes. Nevertheless, both categories include modeling representations of the following five general categories.

1. Hydrodynamics encompasses the flow of compressible, strength-free materials and, thus, forms the backbone of many multiphysics simulation codes. In the present context, "hydrodynamics" refers to multimaterial shock-hydrodynamics, which, mathematically, means we are concerned with so-called weak solutions of the partial differential equations (PDEs). For the compressible Euler equations, admissible solutions are associated with *vanishing* disspation mechanisms rather than their complete absence. Consequently, the algorithmic considerations necessary to produce the correct solutions are subtle, including important aspects such as numerical dissipation and conservation (particularly of energy). Special care must be taken to assure that the solutions are converging to the analytical solutions. Obtaining the correct solution of the hydrodynamics equations is crucial as it provides the foundation for putting "the right material in the right place at the right time" in a simulation. The term "hydrodynamics" also includes the modeling of non-reactive multimaterial interactions, which are used to represent material interfaces that are either distinct (e.g., at material boundaries) or indistinct (e.g., as a result of mixing/interpenetration processes) relative to the resolution of the simulation.

2. Dynamic material response includes the effect of non-zero deviatoric stresses for materials that support shear stresses (such as solids). Such response encompasses the behavior of elastic (i.e., with recoverable deformation), plastic (which admits the dissipation of energy through irrecoverable plastic work), damaged (e.g., fractured or spalled), and more complex (e.g., porous) materials. Some researchers include dynamic material response under the rubric of "hydrodynamics," but we distinguish it here as a separate field. For dynamic material response, the constitutive models dominate material behavior. The material models used in practice are often phenomenological or defined by experimental data, which presents a different set of challenges to effective verification. Our approach is to emphasize well-defined analytic material models that, though less realistic, allow conclusive analysis of the simulation codes.

3. Transport processes is a catch-all phrase used somewhat imprecisely here to cover both true transport phenomena (e.g., as modeled with particle-based Monte Carlo methods) as well as the diffusion approximation (i.e., with a continuum approach) for neutral (e.g., neutron, photon) and charged-particle (e.g., ion) processes. Consequently, this category encompasses an extremely broad spectrum of physical phenomena and correspondingly wide range of modeling and numerical approximations (e.g., from Monte Carlo neutronics to heat transfer).

4. Energetic materials are those that inject kinetic energy to the overall material energy budget, e.g., through the transformation of chemical energy into kinetic energy in high explosives. While detailed models of the intricate physico-chemical processes associated with these important phenomena exist, here we refer only to highly simplified models that are often employed in multiphysics codes. Analysis of such simplified models does not provide unambiguous and complete verification evidence for complicated energetic material models; however, such analysis can provide compelling evidence of an algorithm's ability to solve the underlying mathematical equations in the presence of energy release. Analysis of such problems should be conducted with explicit acknowledgement that the models for energy release in practical simulations may not coincide with the energy release models amenable to analytical solution. In this document, we do not include any new test problems for energetic materials; we intend to do so in future revisions.

5. Magneto-hydrodynamics is required for a restricted class of problems, including e.g., above ground experiments (AGEX) associated with the Sandia Z-machine. Solutions of the ideal magneto-hydrodynamics (MHD) equations can contain interactions of many additional waves, which extend the hyperbolic wave families associated with conventional compressible hydrodynamics behavior related to shock processes, etc. Importantly, MHD evolves in the presence of a powerful physical constraint, viz., that the divergence of the magnetic field is identically zero. Maintaining this solenoidal magnetic field is a computationally challenging and necessary aspect of accurate MHD simulations and, therefore, is an important target for verification testing. Moreover, Z-machine related experiments require modeling of non-ideal resistive MHD processes. Algorithms and verification problems appropriate to a full range of resistive MHD applications are

required. As with energetic materials, we do not include any new test problems for MHD in this document but intend to do so in future revisions.

Proposed Enhanced Test Suite Problems

The test problems proposed here augment the original Tri-Lab Verification Test Suite in several different regimes. A brief description of these problems is provided below, followed by a table that catalogues the test problems together with their relevant physics models. Those problems marked with an asterisk (*) are for reference only and do *not* have complete specifications provided in the appendix.

1. Hydrodynamics

1a. *1-D Riemann Problems* The class of 1-D Riemann problems is well known in both the hydrodynamics algorithm development and code verification communities, since the exact solution can be computed for the one- and two-material cases for polytropic gases [Got98, Tor99] and the stiffened-gas equation of state (EOS) [Plo88]. The initial conditions for this problem consist of two different, initially uniform states separated by an ideal, massless barrier, the instantaneous removal of which leads to the dynamic evolution of the solution in time. For convex EOSs, several fundamentally different solution structures exist for this problem, based on the initial conditions. It is straightforward to devise initial conditions that lead to each of these states. Such problems are particularly convenient for code verification as (i) they are easy to set-up for Eulerian, Lagrangian, and ALE codes, (ii) the simulations run quickly, (iii) the exact solution allows unambiguous code verification analysis. A number of Riemann problems that have proven to be useful to the shock-capturing community are included in our proposed test suite.

A particular case of this problem, using a two-material water-air shock tube configuration [Sau99, Sau01], is widely used by the multiple-material hydrodynamics community to evaluate algorithm performance. This problem is a special case of the problem discussed above and allows one to verify multiple-material, planar shock phenomena for a case that is well-scrutinized in published literature.

Additionally, it is possible to examine phenomena that arise with non-convex EOSs* [Dah05, Men88, Mül06]. Using the appropriate tabular or analytic non-convex EOS, one can formulate shock tube initial conditions that lead to non-classical structures such as rarefaction shocks and compression fans, which are associated, e.g., with polymorphic phase transitions exhibited by certain metals [Joh99] and geologic materials [Swe90]. Numerical schemes that correctly resolve the wave patterns for convex EOSs may fail dramatically for non-convex EOSs. Consequently, this case provides a demanding test of hydrodynamics algorithm robustness for atypical (but not unheard-of) material behavior.

1b. *The Guderley Problem* Guderley [Gud42] considered the case of a spherically symmetric, polytropic, non-heat-conducting, inviscid gas with an infinitely strong shock

propagating toward the origin. The similarity solution to this problem is obtained by the evaluation of two nonlinear eigenvalue problems that together yield the entire self-similary flow-field, i.e., for both the pre-bounce, incoming phase and the post-bounce, outgoing flow (see also [Laz81, Mey82, Hir01, Pon06, Ram07]). This solution allows rigorous code-verification analysis of compressible flow in both convergent and divergent geometries. Moreover, this problem can be tested in 1D (spherical-*r*), 2-D (cylindrical *r*-*z*), and 3-D (Cartesian *x*-*y*-*z*) geometries (the latter two of which can be used to quantitatively evaluate solution sphericity). Although straightforward to set up and run in the Lagrangian frame of reference, this problem is difficult to specify in the Eulerian frame [Ram08].

1c. *The Cook-Cabot Riemann Invariant Problem* This 1-D, planar polytropic, non-heat-conducting, inviscid compressible flow problem, proposed in the literature by Cook & Cabot [Coo04], provides a precise measure of the accuracy of an algorithm as a smooth flow develops a discontinuity. This problem has an exact solution up to the time at which the shock wave forms, which is analogous to the wave-breaking phenomenon in Burgers' equation [Whi74]; indeed, a transformation of the Riemann invariant is used to define the analytical solution. The results for this problem are profitably examined both in physical and spectral spaces.

1d. *The Woodward-Colella Interacting Blast Wave Problem* Another 1-D, planar polytropic, non-heat-conducting, inviscid compressible flow configuration, this problem [Woo84] tests an algorithm's ability to handle strong and complex wave interactions. Although there is no exact solution, the Blast Wave problem has become a standard in the repertoire of tests for compressible flow algorithm development and, as such, the solution is well characterized. This problem keenly discriminates between methods for strong, interacting shock waves. Since there is no exact solution, however, the numerical solutions for this problem must be compared with a well-defined and demonstrably converged numerical solution.

1e. *The Shu-Osher Entropy Wave Problem* Another 1-D, planar polytropic, non-heat-conducting, inviscid compressible flow configuration, this problem [Shu89] tests an algorithm's ability to handle strong and complex wave interactions. Like the Blast Wave problem, the Shu-Osher problem does not have an exact solution but does have the rightfully earned status as a fixture in hydrodynamics algorithm development community. This problem is used to differentiate between methods with regard to the quality of solutions for shock waves interacting with turbulent or complex structure. As in the Blast Wave problem, the numerical solutions for this problem should be compared with a well-defined and demonstrably converged numerical solution.

1f. *The Taylor-Green Vortex (TGV) Problem* This 2-D* or 3-D problem harks back to Taylor [Tay38] and has been revisited since by many researchers (see, e.g., [Dri07]) as a model problem with which to examine the transition to turbulence from a well-characterized initial state. The TGV initial conditions consist of a regular pattern of sinusoidal variation in *x*- and *y*-velocities, with the pressure (which satisfies a Poisson equation) having sinusoidal variations about a fixed value P_0; the initial density assumes

a constant value, and the initial specific internal energy (SIE) is assigned to be consistent with the density and pressure fields through a polytropic EOS. Periodic boundary conditions are imposed on the initial domain, which has extent 2π in each direction. This initially regular configuration evolves through a phase where it is (nearly) singular to a disordered state. For the case of an incompressible fluid, Taylor & Green [Tay38] describe a process by which to obtain a series approximation to the exact solution, with the sinusoidal spatial dependence and an infinite polynomial expansion for the temporal dependence; this approximate solution, however, is only useful at early times. Although no exact solution for compressible fluids is known, for either early or late times, the TGV problem provides an important and widely-used test of multidimensional hydrodynamics of disordered flow. In particular, this problem can be applied to evaluate codes that are used to simulate large-scale turbulence without resorting to Reynolds averaging (or analogous closure approaches), i.e., to codes that employ (implicit) large eddy simulation.

1g. *Richtmyer-Meshkov (RM) and Rayleigh-Taylor* (RT) Problems* These fundamental hydrodynamic instabilities comprise important, challenging, and well-documented phenomena generated by density and pressure gradients. The RM problem considers the stability of an impulsively accelerated interface separating two compressible or incompressible fluids of different density [Mar57, Ric60, Mes69]. This instability is of fundamental importance in a variety of applications, spanning a wide range of length scales. At large scales RM instability generates mixing in supernovae [Arn89, Bur95]; at smaller scales it plays an important role in deflagration-to-detonation transition [Kho99] and enhances mixing in ramjet engines [Yan93, Cur96]; at even smaller scales it initiates shell break-up in inertial confinement fusion capsules [Lin95, Nie03]. The RM instability is often referred to as the impulsive or shock-induced Rayleigh-Taylor (RT) instability. Unlike RT, where the instability takes place only when the light fluid accelerates into the heavy fluid and the initial growth of perturbations is exponential in time, RM is unstable irrespective of the direction from which the shock approaches the interface (i.e., from the light or heavy fluid side) and the initial growth of perturbations is linear in time. The resulting flow field can be attributed to the baroclinically generated vorticity resulting from the misalignment of the density gradient across the interface and the pressure gradients that occur during the shock interaction. The initial evolution of RM instabilities can be described in terms of vortex dynamics; Zabusky and others [Zab99, Lee06, Cot07] have discussed the crucial role vorticity plays in the early development of RM and other baroclinic instabilities. There is no general solution to this problem, but one can compare to linear stability analysis results [Ric60, Mes69], linear models [Haa91, Yan94] at early time, and to nonlinear models [Sad98] at intermediate and late times. Numerical solutions on very fine grids are used as fiducials for comparison.

1h. *Mach Reflection Problems** The archetypal problem in this family of 2-D compressible flow problems was set forth by Woodward & Colella [Woo84], who analyze the canonical problem of this family: the Mach 10 shock impinging on a 60^{o} wedge. There are numerous other problems that accompany the theory of the resulting wave structure, from regular reflection, single-, transitional-, and double-Mach reflection, etc. [Gla86]; Ben-Dor [Ben06, Ben07] provides a discussion of the current understanding

of these complex phenomena. Roughly speaking, depending on the angle of incidence of the shock and the Mach number, the particular solution structure (e.g., regular vs. Mach reflection) can be predicted and used to evaluate code performance, as described, e.g., by Chen and Trucano [Che02].

2. Dynamic Material Response

2a. *Hunter's Problem* Hunter [Hun57] treated a generalization of the problem of Blake [Bla52, Sha42] by considering the dynamic response of a spherically symmetric, semi-infinite, elastic-perfectly-plastic medium with a single inclusion centered at the origin. This problem is driven by a pressure boundary condition on the interior boundary; see also [Lun49, Hop60, Cha62, Hun68, Mor69] for discussions of spherical elastic-plastic wave propagation. By requiring that the velocity of the outward-propagating elastic-plastic boundary be constant, Hunter obtains a closed-form solution for the corresponding time-dependent interior driving pressure and, subsequently, the stress and velocity field throughout the entire medium. The closed-form expression for the time-dependent pressure of the interior cavity could be used to drive hydrocode simulations of this configuration, which would allow code-verification analyses to be conducted.

2b. *Bleich & Nelson's Plane-Wave Problem* Bleich and Nelson [Ble66] considered the case of 1-D plane waves in an elastic-perfectly-plastic half-space for arbitrary combinations of (uniform) step-function pressure (diagonal) and shear (off-diagonal) loads on the free surface. This behavior is perhaps the simplest case of dynamic elastic-plastic plane wave propagation. As shown in [Ble66], the time-dependent material response for this 1-D problem with compressive pressure and positive shear on the free surface can be expressed as combinations of elliptic integrals of the first, second, and third kinds. Moreover, the solution for this problem can assume characteristically different behavior depending on the values of the applied stresses and the material properties; for example, the existence and location of the elastic precursor relative to the plastic wave front varies as a function of these parameters.

2c. *The Verney Problem* Verney [Ver68] examined the case of finite-radius, spherical copper and uranium shells collapsing under a given loading; see also [How02, Weh05]. Motivated by experiments in which such shells were driven by high explosives, Verney constructed a simplified, approximate mathematical model of the problem, assuming incompressible, elastic-perfectly-plastic material response. In this model, which leads to closed-form solutions, the initial kinetic energy of the material dissipates via conversion to plastic work. The intermediate (time-dependent) results of the mathematical model can be compared against hydrocode results of the same configuration.

2d. *Enhanced Dynamic Sphere (EDS) Problem** The dynamic sphere problem [Wil05, Li05a, Kam08] possesses a closed-form solution for the dynamic, small-strain deformation of a hollow, finite-thickness sphere of linear elastic material, with arbitrary driving conditions on the interior and exterior boundaries. By virtue of the solution method described in [Wil05], the material response model can be generalized to include inelastic effects, such as perfect plasticity; additionally, both rate-dependent plasticity and

anisotropic material response are being developed and incorporated. Therefore, a suitable generalization of this problem—say, first to elastic-perfectly-plastic material with the driving conditions used in the linear elastic cases described in [Wil05]—provides an ideal test with which to verify hydrocode simulations of more complex material behavior in the small-strain limit for finite-thickness, spherically symmetric systems.

3. Transport Processes

3a. *Lowrie-Rauenzahn Equilibrium-Diffusion Radiative Shock Problem* This problem, described in [Low07a] provides a semi-analytic solution for planar radiative shock waves in the equilibrium diffusion (1-*T*) limit. In this approximation, the radiation in effect modifies the material EOS through addition of radiative pressure and radiation energy terms. The equilibrium diffusion case can also be approximated by other radiation models in the optically-thick limit; see [Dra07] for a discussion of radiative shocks in the optically-thick regime. The solution consists of initially quiescent flow that is processed by the shock, together with the post-shock flow, all of which can be solved for numerically via the solution of a high-order polynomial equation and a nonlinear ODE. For verification purposes, the initial conditions for the hydrocode are given by imposing a computed exact solution at the starting time and allowing that solution to evolve in time.

3b. *Lowrie Nonequilibrium-Diffusion Radiative Shock Problem* This problem, described in [Low07b,c] provides a semi-analytic solution for planar radiative shock waves in the grey nonequilibrium diffusion (2-*T*) limit. In this approximation, the independent internal energy densities of the material and the radiation allow that their respective temperatures may be out of equilibrium; the grey approximation admits cross-sections that are state-dependent but not frequency-dependent. The solution consists of initially quiescent flow that is processed, together with the post-compression flow. By virtue of the nonlinearities associated with the nonequilibrium assumption, a range of different solution behaviors can occur as a function of the Mach number. As in the equilibrium-diffusion variant, the exact solution is obtained via the solution of a high-order polynomial equation and a nonlinear ODE and this solution is used as the initial conditions for a hydrocode simulation.

3c. *Radiation-Acoustics Problem* This problem, described in [Vin62] is a linear perturbation analysis of a medium in which radiation is coupled to the hydrodynamics. The medium is in local thermodynamic equilibrium, and the analysis looks at small departures from this equilibrium. Two distinct solutions arise, one of which is a radiatively-modified acoustic wave and the other of which is a radiative diffusion wave. The radiation modifies the phase speed of the acoustic wave in some regions of parameter space and introduces a small amount of damping. The radiative diffusion wave is generally strongly damped, with a damping length on the order of the perturbation wavelength. The analytic solution is valid for both low and high energy density material. The primary assumptions for its validity are that departures from thermodynamic and hydrodynamic equilibrium be small and that scattering effects be negligible.

3d. *Top Hat/Crooked Pipe Problem** This problem, described in [Gra00, Gen01], models temperature-source driven radiative flow in a cylindrically symmetric domain consisting of a low density, optically thin material that embeds and is embedded by dense, optically thick material. There is no electron conduction, ion conduction, or scattering in this problem, which is used to test different transport methods and algorithms and focuses, in particular, on the material temperature at five points in the optically thin material.

3e. *Shestakov & Bolstad Problem** This problem, discussed in [She05], presents exact solutions for a linearization of a system modeling the multifrequency radiation diffusion and matter energy balance equations. Based on an approach similar to that in [Su97], this test problem incorporates more realistic assumptions regarding the opacity and the specific heat. Solutions are given for two special cases: (1) with no sources, an initially cold radiation field, and a localized matter energy profile; and (2) initially cold matter and radiation fields with a source of matter energy extending over finite space and time intervals.

3f. *Heat-conduction Problems** The problems posed and solved by Miller and Hutchens are concerned with pure heat conduction in spherically [Mil07a, Mil07b, Hut07] and cylindrically [Hut07] symmetric geometry. Using power-law forms for the specific heat and conduction coefficients, one may calculate closed-form representations for the temperature field throughout the domain of these problems.

We catalogue the proposed test problems in Table 2 below, according to the key physics processes of each problem.

Table 2. Identification of the *proposed* ASC Tri-Lab Test Suite problems and their corresponding physics models. Problems marked with an asterisk (*) are for reference only and do not have complete specifications provided in the appendix.

Test Problem	Gas Dynamics	Material Response	Radiation Transport	Heat Conduct.
1. Riemann	•			
2. Guderley	•			
3. Cook/Cabot	•			
4. Blast Wave	•			
5. Shu-Osher	•			
6. TGV	•			
7. RM	•			
8. RT*	•			
9. Mach Reflection*	•			
10. Hunter		•		
11. B&N		•		
12. Verney		•		
13. EDS*		•		
14. L&R EDRS	•		•[1]	
15. Lowrie NEDRS	•		•[2]	
16. Rad-Acoustics	•		•	
17. Top-hat*			•	
18. S&B*			•	
19. Miller/Hutchens*				•

1. Equilibrium-diffusion approximation
2. Nonequlibrium-diffusion approximation

Method of Manufactured Solutions Applied to the TLTS

The Method of Manufactured Solutions (MMS) presents another approach to devising problems for the TLTS. Although no MMS solutions are proposed in this document, we feel that this procedure is worth discussing, as it is a proven technique with which to verify the order-of-accuracy of software for numerical solution of ODEs and PDEs [Roa02]. When used to verify the order-of-accuracy, successful MMS results are used to bolster the claim that the code is free of order-impacting coding mistakes. In practice, MMS has also proven valuable for identifying algorithmic weaknesses and deficiencies. The great strength of MMS is that it can be successfully applied in cases where no exact analytic solution is known.

The MMS procedure consists of the following steps:

1. Determine the governing set of equations solved by the code and the formal or expected order-of-accuracy of the solution method;
2. Construct a manufactured solution for the equations and determine the source term associated with this solution;
3. Modify the software to include the appropriate source terms;
4. Run the modified code using input that is expected to generate the corresponding correct numerical solution;
5. Calculate the global discretization error;
6. Refine the grid and repeat steps 3 and 4 until the numerical solution appears to converge;
7. Calculate the observed order-of-accuracy from the set of numerical solutions, and compare it to the formal or expected order-of-accuracy.

If the trend in the observed order-of-accuracy agrees with the formal or expected order-of-accuracy, then the code is said to have passed the MMS verification test.

A major attraction of using MMS in Code Verification is that it can fill coverage gaps in testing, e.g., the interaction of algorithms for which no exact solutions are known and, thus, can be used to increase confidence in the code [Knu07]. This particularly attractive feature can be applied to the knotty problems associated with verification of multi-physics problems.

There are, however, some complications in applying MMS to the problems encountered in the Tri-Lab Test Suite. A practical obstacle is that manufactured solutions result in source terms being added to the interior equations, to the boundary conditions, or to both. This can sometimes be accomplished via input to the code; typically, however, simulation software requires "under the hood" code modifications to incorporate the necessary source terms. Thus, the matter of intrusive source terms is problematic but not insurmountable. A second issue is that the goal of traditional MMS differs from that of a typical test in the TLTS: the purpose of the former is usually to uncover coding mistakes and algorithmic deficiencies, while the intent of the latter is to address questions of code suitability and solution verification. While MMS can potentially be applied to the latter goals, it requires resolution of two difficulties to be described below.

One concern is that of the physically realistic nature of most tests in the TLTS. Manufactured solutions are, by construction, always mathematically correct solutions of the governing equations, but they are often physically unrealistic. Consequently, they might not stress the code in exactly the same way as physically realistic problems. A related difficulty is that MMS traditionally requires only smooth (i.e., sufficiently differentiable) manufactured solutions, whereas realistic physical problems—such as those in the TLTS—often involve non-smooth solutions, e.g., hydrodynamic shock waves or discontinuous stress waves.

To overcome these difficulties, we propose the following four approaches by which the MMS technique could be aligned with TLTS goals. (i) Take the analytic solutions in the TLTS that, strictly speaking, are not exact solutions to the governing equations (i.e., for which the equations reduce to solvable, but not closed-form, cases, e.g., the Sedov problem) and use those solutions to create truly exact solutions necessarily involving source terms; this approach may address the realism problem in some instances. (ii) Use manufactured solutions that have smooth-but-steep fronts to approximate shocks, to obviate the issue of discontinuous solutions. (iii) Apply MMS to physical problems in the TLTS by attempting to create realistic manufactured solutions from scratch. (iv) Take 1D solutions in the TLTS and manufacture 2D or 3D solutions from them. All of these approaches are properly characterized as research topics, but they are worthwhile pursuing in order to improve the code coverage within the TLTS and develop genuine (and elusive) multiphysics test problems.

Evaluating Computed Errors

To conduct quantitative code verification analysis, it is necessary that one evaluate the error in the computed solution. To gauge this error, one must have a reference solution that one takes as the "true" solution to the equations. In code verification, one seeks problems that have computable exact solutions; in practical terms, this means that the "true" solution is either (i) expressible to closed form or (ii) one for which the equations are reducible to forms that one can solve accurately, precisely, and confidently. An example of the former is the Noh problem [Noh87] with its algebraically simple solution, while examples of the latter include the shock tube problem (which involves a root-solve [Got88]), the Sedov problem [Sed59] (which involves numerical quadrature [Kam07]), and the Reinicke/Meyer-ter-Vehn problem [Rei91] (which involves the numerical solution of nonlinear ODEs [Kam00]). In the following discussion, we will use the term "reference solution" to indicate the computed exact solution.

How Computed Errors are Used

There are at least two ways computed errors are employed. The first use is to assess whether or not the numerical algorithm is implemented correctly. Evidence for this is obtained from the computed errors, which can be quantified in the measured convergence rate and compared with the formal rate derived from numerical analysis. Here, numerical analysis guides the choice of an error norm, whether cell-averaged or point values should be calculated, etc. If the evaluation used differs from that suggested by numerical analysis, then there should be no expectation that the computed error should behave in a manner consistent with theory and no rigorous statement about the correctness of the implementation of the algorithm can be made.

Other reasons for computing the errors include determining satisfactory performance for a specific physics regime, for particular phenomena, or for an application of interest. In these cases, the raison d'être is to identify algorithmic weaknesses, as opposed to problems (i.e., bugs) in the software implementation. For these purposes, the error

computation should account for how the simulation results are interpreted. Below (or in each problem description) we suggest error measures that highlight the objective of each test problem and allow results from different codes to be compared.

Error Norms

An accepted quantitative measure of error is the difference between computed and "true" solutions. This quantity is evaluated as the norm of the difference between these (discrete) functions over the computational mesh. The specific form of the norm is the L_p norm of functional analysis, e.g., given in 1-D for the function g as

$$\| g \|_p \equiv \left(\int_a^b |g(x)|^p \, dx \right)^{1/p} . \tag{1}$$

In particular, it is recommended that L_1, L_2, and L_∞ norms *all* be evaluated in the error analysis, where, following from the equation above,

$$\| g \|_\infty \equiv \max_{x \in [a,b]} |g(x)| . \tag{2}$$

In the following, we use the double-bar notation "||" without a subscript to denote any member of this family of norms. In particular, the use of the L_1 norm for shocks can clearly be linked to the works of Lax [Lax54, Lax72]; see also the discussion by Majda and Osher [Maj77].

Asymptotic Convergence Analysis

The axiomatic premise of asymptotic convergence analysis is that the computed difference between the reference and computed solutions can be expanded in a series based on some measure of the discretization of the underlying equations. Taking the spatial mesh as the obvious example, the ansatz for the error in a 1-D simulation is taken to be

$$\| g^{\text{ref}} - g^{\text{comp}} \| = A_0 + A_1(\Delta x)^\alpha + o\left((\Delta x)^\alpha\right) . \tag{3}$$

In this relation, g^{ref} is the reference solution, g^{comp} is the computed solution, Δx is some measure of the mesh-cell size, A_0 is the zero-th order error, A_1 is the first order error, and the notation "$o\left((\Delta x)^\alpha\right)$" denotes terms that approach zero faster than $(\Delta x)^\alpha$ as $\Delta x \to 0^+$. For consistent numerical solutions, A_0 should be identically zero; we take this to be the case in the following discussion. For a consistent solution, the exponent α of Δx is the convergence rate: $\alpha = 1$ implies first-order convergence, $\alpha = 2$ implies second order convergence, etc.

Assume that the calculation has been run on a "coarse" mesh (subscript *c*), characterized by Δx_c, which we hereafter also denote as Δx. The error ansatz implies:

$$\left\| g^{\text{ref}} - g_c^{\text{comp}} \right\| = A_1(\Delta x)^{\alpha} + \cdots . \tag{4}$$

We further assume that we have computational results on a "fine" mesh Δx_f (subscript *f*), where $0 < \Delta x_f < \Delta x_c$ with $\Delta x_c / \Delta x_f \equiv \sigma > 1$. In this case, the error anszatz implies:

$$\left\| g^{\text{ref}} - g_f^{\text{comp}} \right\| = \sigma^{-\alpha} A_1(\Delta x)^{\alpha} + \cdots . \tag{5}$$

Manipulation of these two equations leads to the following explicit expressions for the quantities α and A_1:

$$\alpha = \left[\log \left\| g^{\text{ref}} - g_c^{\text{comp}} \right\| - \log \left\| g^{\text{ref}} - g_f^{\text{comp}} \right\| \right] \Big/ \log \sigma \ , \tag{6}$$

$$A_1 = \left\| g^{\text{ref}} - g_c^{\text{comp}} \right\| \Big/ (\Delta x)^{\alpha} \ . \tag{7}$$

These two equalities are the workhorse relations that provide a direct approach to convergence analysis as a means to evaluating the order of accuracy for code verification.

In the case of calculation verification, one does not have an exact solution and, instead, turns to a finely zoned calculation to serve in place of the exact solution. In this case, the results for the convergence rate can be expressed as

$$\alpha = \left[\log \left\| g_f^{\text{comp}} - g_c^{\text{comp}} \right\| - \log \left\| g_f^{\text{comp}} - g_m^{\text{comp}} \right\| \right] \Big/ \log \sigma \ , \tag{8}$$

where the subscript *m* here denotes values on a "medium" mesh, i.e., one for which $0 < \Delta x_f < \Delta x_m < \Delta x_c$ with $\Delta x_c / \Delta x_m \equiv \sigma > 1$.

Issues in Error Computation

There are several subtle but important—and, in some cases, open—issues associated with the appropriate numerical estimation of the quantities mentioned above. While the general reader may find the following topics arcane, it is imperative that code analysts at least be aware of these issues.

• Nondimensionalization The above expressions for the error ansatz and the associated convergence parameters contain no assumptions regarding the dimensions of the associated variables. Consequently, parameters in the resulting scaling relations (e.g., Eq. 4) may have inconsistent units. One way to avoid this issue is to nondimensionalize all quantities prior to conducting such an analysis. For example, one can choose

representative quantities G and X with which to nondimensionalize the computed quantity g and the representative mesh scale Δx:

$$g' \equiv g/G \quad \text{and} \quad \Delta x' \equiv \Delta x/X \ . \tag{9}$$

The nondimensional error ansatz is posited to be

$$\left\| g'^{\text{ref}} - g_c'^{\text{comp}} \right\| = A_1(\Delta x')^{\alpha} + \cdots, \tag{10}$$

where all terms in this equation are now dimensionless. In this case, care must be taken to nondimensionalize consistently throughout the analysis, and to properly dimensionalize results, e.g., if one were to use this relation to estimate errors at another mesh size.

• Dimension For problems in multiple space dimensions (e.g., 2-D Cartesian (x,y)), the spatial convergence analysis described above can be assumed to carry over trivially, such that, e.g., the ansatz of Eq. 3 follows identically. That is, one typically does not assume separate convergence rates in separate coordinates. This seems to be a reasonable assumption in almost all cases; the exception is time-convergence, since the time-integration scheme for a PDE may be of different order than the spatial integrator. For a more thorough discussion and examples of combined space-time convergence, see [Hem05, Tim06a].

• Frame Spatial convergence analysis is idealized to refer to a fixed mesh, i.e., the Eulerian frame. Approaches have been taken to extend convergence analysis simplistically to the Lagrangian frame (e.g., [Kam03]). More sophisticated approaches, however, are needed; for example, since the fundamental Lagrangian equations are discretized with respect to *mass* and not *space*, an error ansatz analogous to Eq. 3 with Δx replaced by Δm would be appropriate.

• Non-uniform Meshes The intention behind the expression "Δx" in Eq. 3 is that it is a meaningful measure of the characteristic length-scale of mesh cells of the discretized eqations. If either adaptive mesh refinement (AMR) or an arbitrary Lagrangian-Eulerian (ALE) approach is used, however, such a quantity—if one exists—is likely to change during the course of a calculation. Again, straightforward approaches for non-uniform and AMR meshes have been examined (e.g., [Li05b]), but these are topics of open research.

• Norm Evaluation The expression for the norm in Eq. 1 is appropriate, e.g., for Cartesian geometries. This term must be appropriately modified for non-Cartesian geometries. For example, for 1-D spherically symmetric calculations, the integral of the norm is properly expressed as

$$\| g \|_p \equiv \left(\int_a^b |g(r)|^p \, dV(r) \right)^{1/p} = \left(\int_a^b |g(r)|^p \, 4\pi r^2 dr \right)^{1/p}. \tag{11}$$

In general, when evaluating the norm one must be mindful of the domain of the integral as well as any symmetries associated with the problem.

• Norm Evaluation & Exact Solutions The definition for the norm in Eq. 1 suggests a simple evaluation of this expression. In 1-D one might evaluate the norm as:

$$\left\| g^{\text{ref}} - g^{\text{comp}} \right\|_1 \equiv \int_a^b \left| g^{\text{ex}}(x) - g^{\text{comp}}(x) \right| dx \approx \sum_{i=1}^{N} \left| g^{\text{ex}}(x_i) - g^{\text{comp}}(x_i) \right| \Delta x_i \quad .(12)$$

Such an expression, while notionally correct, can obscure important aspects of the computational algorithm. Finite volume discretizations, which are used in many Eulerian and Lagrangian hydrodynamics algorithms, provide computed values $g^{\text{comp}}(x_i)$ that are *not* point values but are, in fact, *averages* over the computational cell. Despite the associated inaccuracy, one often uses point-values of the reference solution and cell-averaged computed values in numerical evaluation of expressions such as Eq. 12. Verification lore for the Riemann problem of 1-D hydrodynamics [Rid07] and numerical results with high-resolution numerical schemes for many calculations suggest that the discrepancy incurred by this assumption is small (say, that it does not affect the leading digit of the calculated convergence rate). Rigorous numerical evidence with such a numerical scheme for the Cog-8 problem is given by Timmes et al. [Tim06b], who show that the leading digit of the convergence rate is the same for both point values and cell-averaged values, consistent with anecdotal notions. It is reasonable to anticipate that such results (i.e., that this discrepancy is small) may depend on the particular numerical scheme used.

• Norm Evaluation & Interpolation The expression for the convergence rate α in the calculation verification (Eq. 8) implies a direct comparison of computed solutions on two different meshes. The analogous expression (Eq. 6) for code verification requires an indirect comparison of computed solutions on different meshes. To evaluate the differences of two calculations, a common mesh is required; this begs the immediate question, should one extrapolate (restrict) fine-mesh values to the coarse mesh, or interpolate (prolong) coarse-mesh values onto the fine mesh? Margolin & Shashkov [Mar08] provide a rationale for the former: "…by moving each of the simulation results to the coarsest mesh, we average out the smaller scales and eliminate them as a source of error in studying convergence, thus isolating the discretization error." The detailed manner by which one should move solutions between different meshes remains an open research area. Particular attention should be paid to accurately interpolating solutions near discontinuities.

Summary

Verification analysis seeks to generate quantitative evidence of consistency between the mathematical statements of the physics models (typically, partial differential equations) and the computed solutions of the discrete analogues of these equations, as implemented with numerical algorithms in the simulation codes. Therefore, verification represents a fundamental and necessary part of the development, assessment, and application of simulation software for physics and engineering. An agreed-upon set of seven problems [Bro06] used by the LANL, LLNL, and SNL forms a nominal basis for current, mutually undertaken verification purposes.

In this document, we suggest a wide range of problems with which to augment, both in quantity and quality, the existing Tri-Lab Verification Suite of verification test problems. The suggested problems are meant to contribute to the "next generation" Tri-Lab Verification Test Suite, the determination of which must include deliberation and consensus among experts from each institution. The problems we propose and for which we provide detailed initialization and evaluation information are the following:

- *Riemann Problems* [Got88] Several one-dimensional, inviscid, non-heat conducting, compressible gas Riemann problems for a polytropic gas, chosen for their ability to highlight particular numerical method pathologies or problematic physics regimes. This problem admits a closed-form self-similar solution for polytropic and stiffened gas EOSs. Nonconvex EOS problems could also be included.
- *Guderley Problem* [Gud42] One-dimensional, inviscid, non-heat conducting, compressible gas dynamics of a polytropic gas flowing inward in a spherically converging geometry. By the choice of a particular boundary condition, the entire flow-field can be expressed in closed-form.
- *Cook & Cabot's Problem* [Coo04]] One-dimensional, inviscid, non-heat conducting, compressible gas dynamics of a polytropic gas that gradually steepens into a shock wave. By virtue of the initial condition, this problem has an exact solution up to the time of shock formation.
- *Woodward-Colella Interacting Blast Wave Problem* [Woo84] Very strong one-dimensional shocks interacting in an inviscid, non-heat conducting, compressible polytropic gas.
- *Shu-Osher Problem* [Shu89] One-dimensional, inviscid, non-heat conducting, compressible gas dynamics of a polytropic gas interacting with a perturbed environment. This problem discriminates an algorithm's abilities to accurately resolve detailed flow structures in the presence of shock waves.
- *Taylor-Green Vortex (TGV) Problem* [Tay38] An initially uniform density with regular pattern of sinusoidal variation in x and y velocity and pressure, which evolves into a turbulent state. Although no late-time solution exists, the well-codified initial conditions and evaluation by many codes in the open literature (e.g., [Dri07]) make the TGV problem an ideal test-bed for the evaluation of multidimensional hydrodynamic simulation of disordered flows.

- *A Richtmyer-Meshkov (RM) Problem* [Mar57, Ric60, Mes69] The Richtmyer-Meshkov (RM) problem considers the stability of an impulsively accelerated interface separating two compressible or incompressible fluids of different density. We provide a specific set of initial conditions with which to generate this fundamental hydrodynamic instability in hydrocode simulations.
- *Bleich & Nelson's Plane-Wave Problem* [Ble66] Provides time-dependent material response in 1-D, slab geometry for elastic-perfectly-plastic material with step-function compressive pressure and positive shear on a free surface, in terms elliptic integrals of the first, second, and third kinds.
- *Hunter's Problem* [Hun57] A generalization of the problem of Blake [Bla52, Sha42], giving a closed-form solution for the dynamic response of a spherically symmetric, semi-infinite, elastic-perfectly-plastic medium with an inclusion.
- *The Verney Problem* [Ver68] This problem describes the collapse of finite-radius, spherical copper and uranium shells under external, radial loading, for which experimental data can be compared with both hydrocode results and the outcome of an idealized mathematical model.
- *Lowrie/Rauenzahn Equilibrium-Diffusion Radiation-Hydrodynamics Problem* [Low07a] Provides a semi-analytic solution for planar radiative shock waves in the equilibrium diffusion (1-*T*) limit, for which the radiation in effect modifies the material EOS through addition of radiative pressure and radiation energy terms.
- *Lowrie Nonequilibrium-Diffusion Radiation-Hydrodynamics Problem* [Low07b,c] Gives a semi-analytic solution for planar radiative shock waves in the grey nonequilibrium approximation, for which the independent internal energies densities of the material and the radiation allow their respective temperatures to be out of equilibrium with the grey approximation admitting cross-sections that are state-dependent but not frequency-dependent.
- *Radiation-Acoustics Problem* [Vin62] Provides an analytic solution, valid for both low and high energy density material, to a linear perturbation problem for small departures from thermodynamic equilibrium of a medium in which radiation is coupled to the hydrodynamics

The problems we suggest be considered for a future revision of this document and for which we do *not* provide detailed initialization/evaluation information are:

- *A Rayleigh-Taylor (RT) Problem* [Sha84] A Rayleigh-Taylor (RT) problem captures the instability that develops at the interface between two fluids of different densities, when the lighter fluid pushes against the heavier fluid.
- *Mach Reflection Problems* [Ben07] These problems occur when a shock wave in given medium obliquely encounters another medium with a different acoustic impedence. Depending on the angle of intersection of the shock with the interface, a host of different reflection configurations can occur.
- *Enhanced Dynamic Sphere (EDS) Problem* An extension of the dynamic sphere problem [Wil05, Li05a, Kam08] for the dynamic, small-strain deformation of a hollow, finite-thickness sphere of linear elastic material, with arbitrary driving conditions on the interior and exterior boundaries, to include inelastic effects,

such as perfect plasticity, rate-dependent plasticity, or anisotropic material response.

- *Top-hat/Crooked-pipe Problem* [Gra00, Gen01] A radiation problem in which a temperature source drives radiative flow down a cylinder of optically thin material and around a cylindrical section of dense, optically thick material.
- *Shestakov/Bolstad Problem* [She05] This problem presents exact solutions for a linearization of a system modeling the multifrequency radiation diffusion and matter energy balance equations.
- *Miller's Heat Conduction Problem* [Mil07] and *Hutchen's Heat Conduction Problem* [Hut07] Based on power-law forms for the specific heat and conduction coefficients, these spherical and cylindrical test problems possess closed-form solutions for the temperature field.

Acknowledgement

The authors acknowledge the support of their respective ASC V&V Program Managers and Project Leaders for their support of this activity: Scott Doebling and Mark Anderson at LANL; Joe Sefchik, Richard Klein, Frank Graziani, and Maurice AufderHeide at LLNL; Martin Pilch and Anthony Giunta at SNL. Additionally, the authors thank the following individuals for their input to early drafts of this document: Greg Hutchens and François Hemez at LANL; John Bolstad, David S. Miller, and Carol S. Woodward at LLNL; Curt Ober and John Niederhaus at SNL. This work was performed under the auspices of the National Nuclear Security Administration of the United States Department of Energy by three laboratories: Los Alamos National Laboratory, operated by Los Alamos National Security, LLC, under contract DE-AC52-06NA25396; Lawrence Livermore National Laboratory, operated by Lawrence Livermore National Security, LLC under contract DE-AC52-07NA27344; and Sandia National Laboratories, a multiprogram laboratory operated by Sandia Corporation, a Lockheed-Martin Company, under contract DE-AC-94AL85000.

References

[Arn89] Arnett, W.D., Bahcall, J.N., Kirshner, R.P., and Woosley, S.E., "Supernova 1987a," *Ann. Rev. Astron. Astrophys.* **27**, pp. 629–700 (1989).

[Ben06] Ben-Dor, G., "A state-of-the-knowledge review on pseudo-steady shock-wave reflections and their transition criteria," *Shock Waves* **15**, pp. 277–294 (2006).

[Ben07] Ben-Dor, G., *Shock Wave Reflection Phenomena*, 2nd Edition, Springer, Berlin (2007).

[Bla52] Blake, F.G., "Spherical Wave Propagation in Solid Media," *J. Acoust. Soc. Am.* **24**, pp. 211–215 (1952).

[Ble66] Bleich, H.H., and Nelson, I., "Plane Waves in an Elastic-Plastic Half-Space Due to Combined Surface Pressure and Shear," *J. Appl. Mech.* **33**, pp. 149–158 (1966).

[Bro06] Brock, J.S., Kamm, J., Rider, W.J., Brandon, S., Woodward, C., Knupp, P., and Trucano, T.G., *Verification Test Suite for Physics Simulation Codes*, Los Alamos National Laboratory report LA-UR-06-8421.

[Bur95] Burrows, A., Hayes, J., and Fryxell, B.A., "On the nature of core-collapse supernova explosions," *Astrophys. J.* **450**, pp. 830–850 (1995).

[Cha62] Chadwick, P., "Propagation of Spherical Plastic-Elastic Disturbances from an Expanded Cavity," *Quart. J. Mech. Appl. Math.* **15**, pp. 349–376 (1962).

[Che02] Chen, M., and Trucano, T., *ALEGRA Validation Studies for Regular, Mach, and Double Mach Shock Reflection in Gas Dynamics*, Sandia National Laboratories report SAND2002-2240 [2002].

[Cog91] Coggeshall, S.V., "Analytic Solutions of Hydrodynamics Equations," *Phys. Fluids A* **3**, pp. 757–769 (1991).

[Coo04] Cook, A.W., and Cabot, W.H., "A high-wavenumber viscosity for high-resolution numerical methods," *J. Comput. Phys.* **195**, pp. 594–601 (2004).

[Cot07] Cotrell, D.L., and Cook, A.W., "Scaling the incompressible Richtmyer-Meshkov instability," *Phys. Fluids* **19,** 078105 (2007).

[Cur96] Curran, E., Heiser, W., and Pratt, D., "Fluid phenomena in scram jet combustion systems," *Annu. Rev. Fluid Mech.* **28**, pp. 323–360 (1996).

[Dah05] Dahmen, W., Müller, S., and Voß, A., "Riemann Problem for the Euler Equation with Non-Convex Equation of State including Phase Transitions," *Analysis and Numerics for Conservation Laws*, ed. G. Warnecke, Springer, Heidelberg, pp. 137–162 (2005).

[Dra07] Drake, R.P., "Theory of radiative shocks in optically thick media," *Phys. Plasmas* **14**, pp. 043301-1–10 (2007).

[Dri07] Drikakis, D., Fureby, C., Grinstein, F., and Youngs, D., "Simulation of Transition and Turbulence Decay in the Taylor-Green Vortex," *J. Turbulence* **8**, pp. 1–12 (2007).

[Fic74] Fickett, W., and Rivard, W.C., *Test Problems for Hydrocodes*, Los Alamos Scientific Laboratory report LA-5479 (1974).

[Fic79] Fickett, W., and Davis, W.C., *Detonation*, University of California Press, Berkeley, CA (1979).

[Gen01] Gentile, N., "Implicit Monte Carlo Diffusion—An Acceleration Method for Monte Carlo Time-Dependent Radiative Transfer Simulations," *J. Comput. Phys.* **172**, pp. 543–571 (2001).

[Got88] Gottlieb, J.J., and Groth, C.P.T., "Assessment of Riemann Solvers for Unsteady One-Dimensional Inviscid Flows of Perfect Gases," *J. Comput. Phys.* **78**, pp. 437–458 (1988).

[Gla86] Glaz, H.M., Colella, P., Glass, I.I., and Deschambault, R.L., *A Detailed Numerical, Graphical, and Experimental Study of Oblique Shock Wave Reflections*, Defense Nuclear Agency report DNA-TR-86-356 (1986).

[Gra00] Graziani, F., and LeBlanc, J., *The Crooked Pipe Problem*, Lawrence Livermore National Laboratory report UCRL-MI-143393 (2000).

[Gud42] Guderley, G., "Starke kugelige und zylindrische Verdichtungsstöße in der Nähe des Kugelmittelpunktes bzw. der Zylinderachse," *Luftfahrtforschung* **19**, pp. 302–312 (1942).

[Haa91] Haan, S.W., "Weakly nonlinear hydrodynamic instabilities in inertial fusion," *Phys. Fluids B* **3**, pp. 2349-2355 (1991).

[Hem05] Hemez, F.M., *Non-Linear Error Ansatz Models for Solution Verification in Computational Physics*, Los Alamos National Laboratory report LA-UR-05-8228 (2005).

[Hir01] Hirschler, T., and Gretler, W., "On the eigenvalue problem of imploding shock waves," *Z. angew. Math. Phys.* **52**, pp. 151–166 (2001).

[Hop60] Hopkins, H.G., "Dynamic Expansion of Spherical Cavities in Metals," in *Progress in Solid Mechanics, Vol. 1*, eds. I. N. Sneddon and R. Hill, North Holland, Amsterdam, pp. 83–164 (1960).

[How02] Howell, B.P., and Ball, G.J. "A Free-Lagrange Augmented Godunov Method for the Simulation of Elastic–Plastic Solids," *J. Comput. Phys.* **175**, pp. 128–167 (2002).

[Hun57] Hunter, S.C., "The Propagation of Spherically Symmetric Disturbances in Ideally Plastic Materials," in *Proceedings of the Conference on Properties of Materials at High Rates of Strain, London 1957*, pp. 147–155 (1957).

[Hun68] Hunter, S.C., and Crozier, R.J.M., "Similarity Solution for the Rapid Uniform Expansion of a Spherical Cavity in a Compressible Elastic-Plastic Solid," *Quart. J. Mech. Appl. Math.* **21**, pp. 467–486 (1968).

[Hut07] Hutchens, G.J., *Heat Conduction Test Problems for Code Verification*, Los Alamos National Laboratory report LA-UR-07-5547 (2007).

[JAI07] JAIEG, *Joint Working Group (JOWOG) and Exchange of Information by Visit and Report (EIVR) Handbook, October 2007*, Joint Atomic Information Exchange Group, Ft. Belvoir, VA (2007).

[Joh99] Johnson, J.N., and Chéret, R., "Shock waves in solids: an evolutionary perspective," *Shock Waves* **9**, pp. 193–200 (1999).

[Kam00] Kamm, J., *Investigation of the Reinicke & Meyer-ter-Vehn Equations: I. The Strong Conduction Case*, Los Alamos National Laboratory report LA-UR-00-4304 (2000).

[Kam03] Kamm, J., Brock, J., Rousculp, C., and Rider, W., *Verification of an ASCI Shavano Project Hydrodynamics Algorithm*, Los Alamos National Laboratory report LA-UR-03-6999 (2003).

[Kam07] Kamm, J., Timmes, F., and Bolstad, J., "On Efficient Generation of Numerically Robust Sedov Solutions," submitted to *Astrophys. J. Suppl. Ser.*, in revision (2007).

[Kam08] Kamm, J., Williams, T., Brock, J., and Li, S., "Application of Gegenbauer Polynomial Expansions to Mitigate Gibbs Phenomenon in Fourier-Bessel Series Solutions of a Dynamic Sphere Problem," submitted to *Comm. Num. Meth. Engrng.*, in review (2008).

[Kho99] Khokhlov, A.M., Oran, E.S., and Thomas, G.O., "Numerical simulation of deflagration-to-detonation transition: The role of shock-flame interactions in turbulent flames," *Combustion and Flame* **117**, pp. 323–339 (1999).

[Knu03] Knupp, P., and Salari, K., *Verification of Computer Codes in Computational Science and Engineering*, Chapman & Hall/CRC, Boca Raton, FL (2003).

[Knu07] Knupp, P., Ober, C., and Bond, R., "Measuring Progress in Order-Verification within Software Development Projects," submitted to *Engrng. Comp.* (2007).

[Lax54] Lax, P.D., "Weak Solutions of Nonlinear Hyperbolic Equations and their Numerical Computation," *Comm. Pure Appl. Math.* **7**, pp. 159–193 (1954).

[Lax72] Lax, P.D., *Hyperbolic Systems of Conservation Laws and the Mathematical Theory of Shock Waves*, SIAM, Philadelphia, PA (1972).

[Laz81] Lazarus, R.B., "Self-similar solutions for converging shocks and collapsing cavities," *SIAM J. Numer. Anal.* **18**, pp. 316–371 (1981).

[Lee06] Lee, D.K., Peng, G., and Zabusky, N.J., "Circulation rate of change: A vortex approach for understanding accelerated inhomogeneous flows through intermediate times," *Phys. Fluids* **18**, 097102 (2006).

[Lin95] Lindl, J.D., "Development of the indirect-drive approach to inertial confinement fusion and the target physics basis for ignition and gain," *Phys. Plasmas* **2**, pp. 3933–4024 (1995).

[Li05a] Li, S., *Exact Eigenfunction Solutions for the Spherically Symmetric Dynamic Response of Spherical Shells: Code Implementation*, Los Alamos National Laboratory report LA-UR-05-5306 (2005).

[Li05b] Li, S., Rider, W.J., and Shashkov, M.J., "Two-Dimensional Convergence Study for Problems with Exact Solution: Uniform and Adaptive Grids," Los Alamos National Laboratory report LA-UR-05-7985 (2005).

[Low07a] Lowrie, R., and Rauenzan, R., "Radiative shock solutions in the equilibrium diffusion limit," *Shock Waves* **16**, pp. 445–453 (2007).

[Low07b] Lowrie, R., and Edwards, J.D., "Shock wave solutions for radiation hydrodynamics," in *Proceedings of the Joint International Topical Meeting on Mathematics & Computation and Supercomputing in Nuclear Applications* (M&C + SNA 2007), Monterey, CA, 15–19 April 2007, Los Alamos National Laboratory report LA-UR-07-1077 (2007).

[Low07c] Lowrie, R., "Radiative Shock Solutions," presentation at Numerical Methods for Multi-Material Fluid Flows, Prague, CZ, 10–14 September 2007, Los Alamos National Laboratory report LA-UR-07-5986 (2007), available at http://www-troja.fjfi.cvut.cz/~multimat07/presentations/tuesday/Lowrie.pdf

[Lun49] Luntz, Ya.L., "The Propagation of Spherical Waves in an Elastic-Plastic Medium," *Prikladnaya Matematika i Meckhanika* **XIII**, pp. 55–78 (1949), translated in *Spherical Wave Propagation in Isotropic Elasto-Plastic Medium*, University of California (Berkeley) Institute of Engineering Research Series No. 63, Issue 3, pp. 33–64 (1953).

[Maj77] Majda, A., and Osher, S., "Propagation of error into regions of smoothness for accurate difference approximations to hyperbolic equations," *Comm. Pure Appl. Math.* **30**, pp. 671–705 (1977).

[Mar57] Markstein, G.H., "Flow disturbances induced near a slightly wavy contact surface, or flame front, traversed by a shock wave," *J. Aero. Sci.* **24**, pp. 238–239 (1957).

[Mar08] Margolin, L.G., and Shashkov, M., "Finite volume methods and the equations of finite scale: A mimetic approach," *Int. J. Num. Meth. Fluids* **56**, pp. 991–1002 (2008).

[Men89] Menikoff, R., and Plohr, B.J., "The Riemann problem for fluid flow of real materials," *Rev. Mod. Phys.* **61**, pp. 75–130 (1989).

[Mes69] Meshkov, E.E., "Instibility of the interface of two gases accelerated by a shock wave," *Izv. Akad. Nauk SSSR, Mekh. Zhidk. Gaza* **4**, pp. 151–157 (1969).

[Mey82] Meyer-ter-Vehn, J., and Schalk, C., "Selfsimilar spherical compression waves in gas dynamics," *Z. Naturforsch. A* **37**, pp.955–969 (1982).

[Mil07a] Miller, D.S., *Spherical Heat Conduction Verification Problem*, Lawrence Livermore National Laboratory report UCRL-TR-231058 (2007).

[Mil07b] Miller, D.S., *Some Verification Problems with Possible Transport Applications*, Lawrence Livermore National Laboratory report UCRL-TR-233568 (2007).

[Mor69] Morland, L.W., "Spherical Wave Propagation in Elastic-Plastic Work-Hardening Materials," *J. Mech. Phys. Solids* **17**, pp. 371–385 (1969).

[Mül06] Müller, S., and Voß, A., "The Riemann Problem for the Euler Equations with Nonconvex and Nonsmooth Equations of State: Construction of Wave Curves," *SIAM J. Sci. Comput.* **28**, pp. 651–681 (2006).

[Nie03] Niederhaus, C.E., and Jacobs, J.W., "Experimental study of the Richtmyer-Meshkov instability of incompressible fluids," *J. Fluid Mech.* **485**, pp. 243–277 (2003).

[Noh87] Noh, W.F., "Errors for Calculations of Strong Shocks Using an Artificial Viscosity and an Artificial Heat-Flux," *J. Comput. Phys.* **72**, pp. 78–120 (1987).

[Plo88] Plohr, B., "Shockless Acceleration of Thin Plates Modeled by a Tracked Random Choice Method," *AIAA J.* **26**, pp. 470–478 (1988).

[Pon06] Ponchaut, N.F., Hornung, H.G., Pullin, D.I., and Mouton, C.A., "On imploding cylindrical and spherical shock waves in a perfect gas," *J. Fluid Mech.* **560**, pp. 103–122 (2006).

[Ram08] Ramsey, S., *Evaluation of the Guderley Converging Shock Wave Standard Solution Mode*, Los Alamos National Laboratory report LA-UR-08-05442 (2008).

[Rei91] Reinicke, P., and Meyer-ter-Vehn, J., "The Point Explosion with Heat Conduction," *Phys. Fluids A* **3**, pp. 1807–1818 (1991).

[Ric60] Richtmyer, R.D., "Taylor instability in shock acceleration of compressible fluids," *Commun. Pure Appl. Math.* **13**, pp. 297–319 (1960).

[Rid07] Rider, W., private communication.

[Roa02] Roache, P., "Code Verification by the Method of Manufactured Solutions," *J. Fluids Engrng* **124**, pp. 4–10 (2002).

[Roa04] Roache, P., "Building PDE Codes to be Verifiable and Validatable," *Comput. Sci. Engrng.* **6**, pp. 30–38 (2004).

[Sad98] Sadot, O., Erez, L., Alon, U., Oron, D., Levin, L.A., Erez, G. Ben-Dor, G., and Shvarts, D., "Study of nonlinear evolution of single-mode and two-bubble interaction under Richtmyer-Meshkov instability," *Phys. Rev. Lett.* **80**, pp. 1654–1657 (1998).

[Sal04] Saltelli, A., Tarantola, S., Campolongo, F., and Ratto, M., *Sensitivity Analysis in Practice*, John Wiley & Sons, Chichester, UK (2004).

[Sau99] Saurel, R., and Abgrall, R., "A Multiphase Godunov Method for Compressible Multifluid and Multiphase Flows," *J. Comput. Phys.* **150**, 425–467 (1999).

[Sau01] Saurel, R., and Le Metayer, O., "A multiphase model for compressible flows with interfaces, shocks, detonation waves and cavitation," *J. Fluid Mech.* **431**, 239–271 (2001).

[Sed59] Sedov, L.I., *Similarity and Dimensional Methods in Mechanics*, Academic Press, New York, NY, p. 146 ff. (1959).

[Sha42] Sharpe, J.A., "The Production of Elastic Waves by Explosion Pressures. I. Theory and Empirical Field Observations," *Geophysics*, **7**, pp. 144–154 (1942).

[Sha84] Sharp, D.H., "An overview of Rayleigh-Taylor instability," *Physica D* **12**, pp. 3–18 (1984).

[She05] Shestakov, A.I., and Bolstad, J.H., "An exact solution for the linearized multifrequency radiation diffusion equation," *J. Quant. Spect. Rad. Trans.* **91**, pp. 133–153 (2005).

[Shu89] Shu, C.-W., and S. Osher, S., "Efficient Implementation of Essentially Non-oscillatory Shock-Capturing Schemes, II," *J. Comput. Phys.* **83**, 32–78 (1989).

[Soo03] Sood, A., Forster, R.A., and Parsons, D.K., "Analytical Benchmark Test Set for Criticality Code Verification," *Prog. Nucl. Energy* **42**, pp. 55–106 (2003).

[Su96] Su, B., and Olson, G.L., "Benchmark Results for the Non-Equilibrium Marshak Diffusion Problem," *J. Quant. Spectrosc. Radiat. Transfer* **56**, pp. 337–351 (1996).

[Su97] Su, B., and Olson, G.L., "An analytical benchmark for non-equlibrium radiative transfer in an isotropically scattering medium," *Ann. Nucl. Energy* **24**, pp. 1035–1055 (1997).

[Swe90] Swegle, J.W., "Irreversible phase transitions and wave propagation in silicate geologic materials," *J. Appl. Phys.* **68**, pp. 1563–1579 (1990).

[Tay37] Taylor, G.I., and Green, A.E., "Mechanism of the Production of Small Eddies from Large Ones," *Proc. Roy. Soc. Lond. A* **158**, pp. 499–521 (1937).

[Tim06a] Timmes, F.X., Fryxell, B., and Hrbek, G.M., *Spatial-Temporal Convergence Properties of the Tri-Lab Verification Test Suite in 1D for Code Project A*, Los Alamos National Laboratory report LA-UR-06-6444.

[Tim06b] Timmes, F.X., Fryxell, B., and Hrbek, G.M., *Two- and Three-Dimensional Properties of the Tri-Lab Verification Test Suite for Code Project A*, Los Alamos National Laboratory report LA-UR-06-6697.

[Tru06] Trucano, T.G., Swiler, L.P., Igusa, T., Oberkampf, W.L., and Pilch, M., "Calibration, validation, and sensitivity analysis: What's what," *Reliab. Engrng. Syst. Safety* **92**, pp. 1331–1357 (2006).

[Tor99] Toro, E.F., *Riemann Solvers and Numerical Methods for Fluid Dynamics*, Springer, Berlin (1999).

[Ver68] Verney, D., "Évaluation de la Limite Élastique du Cuivre et de l'Uranium par des Expèriences d'Implosion «Lente»," in *Behavior of Dense Media under High Dynamic Pressures, Symposium, H.D.P.*, IUTAM, Paris 1967, Gordon & Breach, New York, pp. 293–303 (1968).

[Vin62] Vincenti, W.G., and Baldwin, B.S., "Effect of thermal radiation on propagation of plane acoustic waves," *J. Fluid Mech.* **12**, pp. 449–477 (1962).

[Weh05] Weseloh, W., et al., *PAGOSA Sample Problems*, Los Alamos National Laboratory report LA-UR-05-6514 (2005).

[Whi74] Whitham, G.B., *Linear and Nonlinear Waves*, Wiley, New York, NY (1974).

[Wil05] Williams, T.O., Li, S., Brock, J.S., and Kamm, J.R., *Spherical Shell Analysis for Material Modeling*, Los Alamos National Laboratory report LA-UR-05-8038 (2005).

[Woo84] Woodward, P., and Colella, P., "The Numerical Simulation of Two-Dimensional Fluid Flow with Shocks," *J. Comput. Phys.* **54**, pp. 115–173 (1984).

[Yan93] Yang, J., Kubota, T., and Zukoski, E.E., "Applications of shock-induced mixing to supersonic combustion," *AIAA J.* **31**, pp. 854–862 (1993).

[Yan94] Yang, Y., Zhang, Q., and Sharp, D.H., "Small amplitude theory of Richtmyer-Meshkov instability," *Phys. Fluids A* **6**, pp. 1856–1873 (1994).

[Zab99] Zabusky, N.J., "Vortex paradigm for accelerated inhomogeneous: Visiometrics for the Rayleigh-Taylor and Richtmyer-Meshkov environments," *Ann. Rev. Fluid Mech.* **31**, pp. 495–536 (1999).

Appendix: Problem Descriptions

In this appendix, we provide descriptions for several of the proposed test problems mentioned in this text. These problem descriptions contain much of the information suggested by Oberkampf & Trucano [Obe07] in their explanation of "strong-sense" verification benchmarks. Given the complexity of hydrocodes and problem specification, however, the descriptions we provide are not definitive, i.e., there remain unspecified choices in problem set-up that the code analyst must make. These descriptions provide the starting points for setting up these problem as well as a touchstone against which descriptions of the "identical" problem, run by different analysts or with different simulation codes, can be compared. In any written analysis of these problems, it is imperative that researchers describe *as thoroughly as possible* the complete specification and set-up of the problem (up to including the code input deck in the written report). The provided descriptions of the following problems are intended to be largely self-contained.

1. *1-D Riemann Problems*
2. *The Guderley Problem*
3. *The Cook-Cabot Riemann Invariant Problem*
4. *The Woodward-Colella Blast Wave Problem*
5. *The Shu-Osher Entropy WaveProblem*
6. *The Taylor-Green Vortex (TGV) Problem*
7. *A Richtmyer-Meshkov (RM) Problem*
8. *Bleich & Nelson's Plane-Wave Problem*
9. *Hunter's Problem*
10. *The Verney Problem*
11. *Vincenti & Baldwin Radiation-Acoustics Problem*
12. *Lowrie/Rauenzahn Equilibrium-Diffusion Radiative Shock Problem*
13. *Lowrie Nonequilibrium-Diffusion Radiative Shock Problem*

The following problems are proposed for future versions of this document. We believe that these problems would substantially augment the physics coverage provided by those in this appendix. As further problems are considered, we encourage others to use similar procedures in the problem descriptions, i.e., to follow the guidance contained in [Obe07].

1. *A Rayleigh-Taylor (RT) Problem*
2. *Mach Reflection Problems*
3. *Enhanced Dynamic Sphere (EDS) Problems*
4. *Shestakov & Bolstad Problem*
5. *Top Hat/Crooked Pipe Problem*
6. *Miller's or Hutchens' Heat Conduction Problems*

References

[Obe07] Oberkampf, W.L., and Trucano, T.G., "Verification and Validation Benchmarks," *Nuclear Design and Engineering* **23**, pp. 716–743 (2007); also available as Sandia National Laboratories report SAND2007-0853 (2007).

I. **Name**: The 1-D Riemann Problem

II. **Conceptual Description**

General: Riemann Problems consist of a 1-D, slab geometry consisting of two materials separated by an idealized (massless/perfect) interface. The interface is removed at the initial time so that the materials on either side are allowed to dynamically interact. Exact solutions for this class of problems can be computed for a variety of material models. The most popular solutions obey strength-free, inviscid, non-heat conducting polytropic and "stiffened-gas" equations of state. Solutions exist for other material models as well, including some that contain non-zero stress deviators (i.e., exhibit strength). At the initial time of the problem (t=0), the two materials are assigned constant, uniform states. Under the conservation of mass, momentum, and energy, the materials evolve compression (shock) and rarefaction waves. The proposed problems have revealed a number of algorithmic pathologies as standard methods for testing a variety of shock-capturing methods. They cover a significant portion of the planar 1-D "phenomenology space" for ideal, polytropic gases, and some interesting cases modeled by stiffened gases.

For convex EOSs, five fundamentally different solutions structures exist for this problem, based on the initial conditions. Based on the wave structure (from left to right in 1-D), these solutions are:

1. Rarefaction-Contact-Shock or Shock-Contact-Rarefaction
2. Shock-Contact-Shock
3. Rarefaction-Contact-Rarefaction
4. Rarefaction-Contact-Vacuum or Vacuum-Contact-Rarefaction
5. Rarefaction-Contact-Vacuum-Contact-Rarefaction

It is straightforward to devise initial conditions that lead to each of these states. Such problems are particularly convenient for code verification as (i) they are easy to set-up for Eulerian, Lagrangian, and ALE codes, (ii) the simulations run quickly, (iii) the exact solution allows unambiguous code verification analysis.

Processes modeled: The problems described here test the integration of the conservation laws for the flow of strength-free, inviscid, non-heat conducting, compressible gas in 1-D planar geometry.

Initial conditions: Uniform and constant material density, pressure, and velocity on each side of the initial interface.

Boundary conditions: The initial conditions are maintained on the boundaries of the mesh. (The boundaries should not interact with the interior wave evolution.)

Benchmark type: The idealized case reduces to a non-closed-form solution that requires the solution of one nonlinear equation (type 3 of [Obe07]), converged to either machine accuracy or a clearly stated tolerance.

Principal code features tested:

1. Basic compressible hydrodynamics, including single-, and multiple-material EOS calls.
2. Specific problems are designed to test specific code features or physics regimes, as listed below.

III. **Mathematical Description**

A theoretical overview of the mathematics underlying the Riemann problem is given in [Smi79] (and can be found as well in a variety of modern texts on hyperbolic equations), while a deep review of the physics is given in [Men89]. A practical description of solution approaches for the polytropic gas case is contained in [Got88] and more broadly, [Tor99]; the stiffened gas case is described in [Plo88]. We restrict the test problems to these two EOSs, references for others are listed in the Additional User Information section. In the following, all quantities are in consistent cgs units.

The governing equations are the 1-D Euler equations in Cartesian coordinates:

$$\begin{aligned} \frac{\partial \rho}{\partial t} + \frac{\partial (\rho u)}{\partial x} &= 0 \\ \frac{\partial (\rho u)}{\partial t} + \frac{\partial (\rho u^2 + p)}{\partial x} &= 0 \\ \frac{\partial (\rho E)}{\partial t} + \frac{\partial [(\rho E + p) u]}{\partial x} &= 0 \end{aligned}$$

where ρ is the mass density, u is the velocity, p is the pressure, $E = e + u^2/2$ is the total energy per unit mass, and e is the internal energy per unit mass.

The equation of state (EOS) relates the pressure, density, and internal energy. For the polytropic (ideal gas) EOS, $p = (\gamma - 1)\rho e$, where γ is the (constant) ratio of specific heats. For the stiffened gas EOS, $p = (\gamma - 1)\rho e - \gamma \pi$, where π is a constant.

The system response quantities of interest include:

i. Snapshots of density, velocity, pressure, SIE as a function of position
ii. Time-histories of density, velocity, pressure, and SIE at specified positions
iii. Total energy, kinetic energy, internal energy as a function of time

Descriptions of the specific tests follow. The descriptions include the initial left and right states, the domain, the initial interface location, x_i, and the final solution time, t_f. Unless otherwise noted, the left and right materials are polytropic gases and $\gamma_l = \gamma_r = \gamma = 7/5$. The features of the solution and the particular reasons it is useful to code developers are also described. Although the Riemann problem is scale invariant in space-time, we will present our problem statements in dimensional terms using the cgs system.

The Sod Problem The Sod problem [Sod79] is the canonical Riemann problem; see also [Gre04]. The wave structure consists of a shock moving to the right, a contact moving to the right, and a rarefaction moving to the left. It is not a severe test, but quickly identifies problems resolving the wave structure.

Sod Problem Parameters			
	ρ [g/cm^3]	u [cm/s]	p [dyn/cm^2]
Left	1.0	0.0	1.0
Right	0.125	0.0	0.1
$0 \le x \le 1$ cm; $x_i = 0.5$ cm; $t_f = 0.25$ s			

The Modified Sod Problem The modified Sod problem [Tor99] differs from the original Sod problem in that the rarefaction wave is transonic: an eigenvalue of the flux Jacobian changes sign inside the rarefaction fan. Several early shock-capturing methods produced noticeable jumps or "glitches" at the sonic point, and this pathology is revealed by this test. The initial interface location should be $x_i = 0.3$cm.

Modified Sod Problem Parameters			
	ρ [g/cm^3]	u [cm/s]	p [dyn/cm^2]
Left	1.0	0.75	1.0
Right	0.125	0.0	0.1
$0 \le x \le 1$ cm; $x_i = 0.3$ cm; $t_f = 0.2$ s			

The Einfeldt Problem The solution of the Einfeldt problem [Ein91] consists of two strong rarefaction waves. Between the rarefactions the density and pressure drop very low, nearly to vacuum conditions. The original purpose of this problem was to test Riemann solvers (as part of Euler solvers) at near-vacuum conditions. The test is also useful for the probing the regime where the internal energy is dominated by the kinetic energy. Numerical methods that conserve total energy often show large errors in the internal energy field for this test, sometimes called the 1-2-3 problem.

Einfeldt Problem Parameters			
	ρ [g/cm^3]	u [cm/s]	p [dyn/cm^2]
Left	1.0	-2.0	0.4
Right	1.0	2.0	0.4
$0 \le x \le 1$ cm; $x_i = 0.5$ cm; $t_f = 0.15$ s			

RCVCR Problem This modified version of the Einfeldt Problem tests the ability of a code to handle the formation of a vacuum state.

RCVCR Problem Parameters			
	ρ [g/cm^3]	u [cm/s]	p [dyn/cm^2]
Left	1.0	-4.0	0.4
Right	1.0	4.0	0.4
$0 \le x \le 1$ cm; $x_i = 0.5$ cm; $t_f = 0.15$ s			

The Vacuum Expansion Problem The Vacuum Expansion Problem has vacuum conditions as the left state, and the material on the right undergoes a free expansion. The wave structure consists of a strong, transonic right rarefaction. The problem tests the handling of vacuum conditions and the prediction of the speed of the tail (left edge) of the rarefaction wave. On a Lagrangian mesh, the problem can be set up with the interface on the domain boundary (with void outside the domain) to test the boundary conditions in a code. The problem is the same as a piston problem described in [Lan59], which has an analytic solution, depending on the speed of the piston.

Vacuum Expansion Problem Parameters			
	ρ [g/cm^3]	u [cm/s]	p [dyn/cm^2]
Left	0.0	0.0	0.0
Right	1.0	0.0	1.0
$-5 \le x \le 1$ cm; $x_i = 0.0$ cm; $t_f = 0.75$ s			

The Stream Collision Problem The Stream Collision Problem consists of a left shock, a trivial contact, and a right shock [Tor99]. The key feature of the solution is that when the two shocks form at the initial time, errors in all field variables are produced and are not dissipated as the solution evolves. In particular, the density is underpredicted and the energy (and temperature) are overpredicted near the initial discontinuity, a problem referred to as “overheating” in the literature. In applications, overheating is often observed when shocks reflect from a wall boundary. This problem is a similar to the planar version of the Noh problem, but the shocks are weaker.

Stream Collision Problem Parameters			
	ρ [g/cm^3]	u [cm/s]	p [dyn/cm^2]
Left	1.0	+2.0	0.1
Right	1.0	-2.0	0.1
$0 \le x \le 1$ cm; $x_i = 0.5$ cm; $t_f = 0.8$ s			

The LeBlanc Problem The LeBlanc Problem is a test of the robustness of the numerical method. It consists of a strong shock moving to the right, a contact moving to the right, and a strong, transonic rarefaction. For this problem, $\gamma = 5/3$.

LeBlanc Problem Parameters			
	ρ [g/cm^3]	u [cm/s]	p [dyn/cm^2]
Left	1.0	0.0	$(2/3)\times10^{-1}$
Right	10^{-3}	0.0	$(2/3)\times10^{-10}$
$0 \le x \le 1$ cm; $x_i = 0.3$ cm; $t_f = 0.5$ s			

The Peak Problem The peak problem is also a robustness test [Lis03, Gre04]. The domain is [0.1, 0.6] and the initial interface location is $x_i = 0.5$cm. It consists of a strong shock moving to the right, followed closely by a contact surface, and a left-moving rarefaction. The density peak between the shock and the contact is difficult to capture.

Peak Problem Parameters			
	ρ [g/cm^3]	u [cm/s]	p [dyn/cm^2]
Left	0.1261192	8.9047029	782.92899
Right	6.591493	2.2654207	3.1544874
$0.1 \le x \le 0.6$ cm; $x_i = 0.5$cm; $t_f = 3.9\times10^{-3}$ s			

Slow Shock Problem The Slow Shock problem is described in [Jin96]; various similar versions are presented in [Col84, Rob90, Qui94]. The solution consists of a Mach 3 shock wave moving to the right at approximately 0.109648 cm/s; the other waves are infinitely weak. Many shock-capturing methods produce long wavelength oscillations behind the shock. The origin of the oscillations is complicated, but understood, as described in [Kar97] and the references therein.

Slow Shock Problem Parameters			
	ρ [g/cm^3]	u [cm/s]	p [dyn/cm^2]
Left	3.857143	-0.810631	10.33333
Right	1.0	-3.44	1.0
$0 \le x \le 1$ cm; $x_i = 0.5$ cm; $t_f = 30.0$ s			

The Stationary Contact Problem The stationary contact problem consists of a strong shock wave moving to the right, a stationary contact, and a strong rarefaction moving to the left [Tor99]. The conditions are actually the left part of the Woodward-Colella blast waves problem [Woo84], with the velocity shifted to make the contact stationary. For many shock-capturing methods, contact discontinuities are the most difficult waves to compute; they are continually damped by the method over the course of the simulation, and unlike shocks, have no natural steepening mechanism to counteract this damping. The smearing of the contact surface is often an indicator of the amount of damping of the numerical method. Some methods do not damp stationary contacts, but this can give a false sense of the numerical dissipation; the same methods do damp slowly moving contacts.

Stationary Contact Problem Parameters			
	ρ [g/cm^3]	u [cm/s]	p [dyn/cm^2]
Left	1.0	-19.59745	10^3
Right	1.0	-19.59745	10^{-2}
$0 \le x \le 1$ cm; $x_i = 0.8$ cm; $t_f = 0.012$ s			

The Water-Air Shock Tube Problem This is a two-material, water-air shock tube problem [Sau99, Sau01], widely used by the multiple-material hydrodynamics community to evaluate algorithm performance. The water is modeled by the stiffened gas EOS while the air is a polytropic gas.

Water-Air Shock Tube Problem Parameters					
	ρ [g/cm^3]	u [cm/s]	p [dyn/cm^2]	γ	π [dyn/cm^2]
Left (water)	1.0	0.0	10^{10}	4.4	6×10^9
Right (air)	0.5	0.0	10^6	1.4	0.0
$0 \le x \le 100$ cm; $x_i = 70$ cm; $t_f = 229\times10^{-6}$ s					

IV. **Accuracy Assessment**

i. Calculations will be run on a nominal mesh, which is to include 100 zones in the specified domain (400 zones for the peak problem). Calculations will be run also at mesh resolutions of two, four, and eight times the nominal resolution.
ii. Exact solutions for the density, velocity, pressure, and SIE will be generated at the positions corresponding to the center of each mesh cell, for each zone in the specified domain 1.
iii. Values of the L_1, L_2, and L_∞ norm of the difference between the computed and exact density, velocity, pressure, and SIE are to be evaluated for each mesh resolution at its native resolution. Plots of error versus mesh resolution are to be generated. Inferred convergence properties are to be evaluated both (i) interpolated over all mesh resolutions and (ii) interpolated between each two adjacent mesh resolutions.
iv. Values of the L_1, L_2, and L_∞ norm of the difference between the computed and exact density, velocity, pressure are to be evaluated for each mesh resolution coarsened onto the coarsest (nominal) mesh. Plots of error versus mesh resolution are to be generated. Inferred convergence properties are to be evaluated both (i) interpolated over all mesh resolutions and (ii) interpolated between each two adjacent mesh resolutions.
v. The total energy, kinetic energy, and internal energy as functions of time are to be plotted.

V. **Additional User Information**

The focus of the above proposed tests is on single-material, polytropic gas and two-material, stiffened gas configurations. With increasing interest in multimaterial problems and more complex material descriptions, however, we anticipate the scope will expand. For the ambitious reader we provide the following references.

Solution techniques for nonpolytropic but ideal gases is given by [Col85], and for more general convex EOSs by [Qua03]. Additionally, it is possible to examine phenomena that arise with non-convex EOSs [Men89, Mül06]. Using the appropriate tabular or analytic non-convex EOS, one can formulate shock tube initial conditions that lead to non-classical structures such as rarefaction shocks and compression fans, which are associated, e.g., with polymorphic phase transitions exhibited by certain metals [Joh99] and geologic materials [Swe90]. Numerical schemes that correctly resolve the wave patterns for convex EOSs may fail dramatically for non-convex EOSs. Consequently, this case provides a demanding test of hydrodynamics algorithm robustness for atypical (but not unheard-of) material behavior.

VI. **References**

[Col84] Colella, P., and Woodward, P.M., "The Piecewise Parabolic Method (PPM) for Gas-Dynamical Simulations," *J. Comput. Phys.* **54**, pp. 174–201 (1984).

[Col85] Colella, P., and Glaz, H.M., "Efficient Solution Algorithms for the Riemann Problem for Real Gases," *J. Comput. Phys.* **59**, pp. 264–289 (1985).

[Ein91] Einfeldt, B., Munz, C. D., Roe, P.L., and Sjögreen, B., "On Godunov-Type Methods near Low Densities," *J. Comput. Phys.* **92**, pp. 273–295 (1991).

[Got88] Gottlieb, J.J., and Groth, C.P.T., "Assessment of Riemann Solvers for Unsteady One-Dimensional Inviscid Flows of Perfect Gases," *J. Comput. Phys.* **78**, pp. 437–458 (1988).

[Gre04] Greenough, J.A., and Rider, W.J., "A quantitative comparison of numerical methods for the compressible Euler equations: fifth-order WENO and piecewise-linear Godunov," *J. Comput. Phys.* **196**, pp. 259–281 (2004).

[Joh99] Johnson, J.N., and Chéret, R., "Shock waves in solids: an evolutionary perspective," *Shock Waves* **9**, pp. 193–200 (1999).

[Kar97] Karni, S., and Canic, S., "Computations of Slowly Moving Shocks," *J. Comput. Phys.* **136**, pp. 132–139 (1997).

[Lan59] Landau, L.D., and Lifshitz, E.M., *Fluid Mechanics*, p. 358, Pergamon Press, 1959.

[Lis03] Liska, R., and Wendroff, B., "Comparison of Several Difference Schemes on 1D and 2D Test Problems for the Euler Equations," *SIAM J. Sci. Comput.* **25**, 995–1017 (2003), http://www-troja.fjfi.cvut.cz/~liska/CompareEuler/compare8/

[Men89] Menikoff, R., and Plohr, B.J., "The Riemann problem for fluid flow of real materials," *Rev. Mod. Phys.* **61**, pp. 75–130 (1989).

[Mül06] Müller, S., and Voß, A., "The Riemann Problem for the Euler Equations with Nonconvex and Nonsmooth Equations of State: Construction of Wave Curves," *SIAM J. Sci. Comput.* **28**, pp. 651–681 (2006).

[Obe07] Oberkampf, W.L., and Trucano, T.G., *Verification and Validation Benchmarks*, Sandia National Laboratories report SAND2007-0853 (2007).

[Plo88] Plohr, B., "Shockless Acceleration of Thin Plates Modeled by a Tracked Random Choice Method," *AIAA J.* **26**, pp. 470–478 (1988).

[Qua03] Quartapelle, L., Castelletti, L., Guardone, A., and Quaranta, G., "Solution of the Riemann problem of classical gasdynamics," *J. Comput. Phys.* **190**, pp. 118–140 (2003).

[Qui94] Quirk, J.J., "A Contribution to the Great Riemann Solver Debate," *Int. J. Num. Meth. Fluids* **18**, pp. 555–574 (1994).

[Rob90] Roberts, T.W., "The Behavior of Flux Difference Splitting Schemes near Slowly Moving Shock Waves," *J. Comput. Phys.* **90**, 141–160 (1999).

[Sau99] Saurel, R., and Abgrall, R., "A Multiphase Godunov Method for Compressible Multifluid and Multiphase Flows," *J. Comput. Phys.* **150**, 425–467 (1999).

[Sau01] Saurel, R., and Le Metayer, O., "A multiphase model for compressible flows with interfaces, shocks, detonation waves and cavitation," *J. Fluid Mech.* **431**, 239–271 (2001).

[Smi79] Smith, R.G., "The Riemann problem in gasdynamics," *Trans. Am. Math. Soc.* **249**, pp. 1–50 (1979).

[Sod78] Sod, G.A., "A Survey of Several Finite Difference Methods for Systems of Nonlinear Hyperbolic Conservation Laws," *J. Comput. Phys.* **27**, 1–31 (1978).

[Swe90] Swegle, J.W., "Irreversible phase transitions and wave propagation in silicate geologic materials," *J. Appl. Phys.* **68**, pp. 1563–1579 (1990).

[Tor99] Toro, E.F., *Riemann Solvers and Numerical Methods for Fluid Dynamics, A Practical Introduction*, 2nd ed., Springer, Berlin, 1999.

[Woo84] Woodward, P., and Colella, P., "The Numerical Simulation of Two-Dimensional Fluid Flow with Strong Shocks," *J. Comput. Phys.* **54**, pp. 115–173 (1984).

I. **Name**: The Guderley Problem

II. **Conceptual Description**

General: The Guderley Problem consists of a 1-D, spherical geometry consisting of a single, inviscid, non-heat conducting polytropic gas with a shockwave converging through quiescent, zero-pressure material toward the origin. Using Lie group methods, one can reduce the partial differential equations for the dynamically evolving flow field describing a converging, infinite-strength shock in terms of a set of coupled, nonlinear ordinary differential equations (ODEs), involving a nonlinear eigenvalue, for the nondimensional similarity variables. Under the conservation of mass, momentum, and energy, the shock wave converges onto the origin. The post-"bounce" state, with finite-strength outgoing shock, is obtained as the solution to related set of ODEs and constraints that constitute a separate nonlinear eigenvalue problem. Together, these solutions provide a complete description of the spherically convergent, self-similar flow: from inflow (pre-"bounce"), through convergence ("bounce"), to outflow (post-"bounce").

Processes modeled: This problem tests the integration of the conservation laws for converging-then-diverging flow of strength-free, inviscid, non-heat conducting, compressible gas in spherical geometry.

Initial conditions: Pre-shock (near-origin): uniform and constant material density, pressure, and velocity; post-shock (far-field): must be assigned using a numerical solution of the related ODEs (to a specified accuracy) for the nondimensional similarity variables.

Boundary conditions: (i) Lagrangian: applied velocity at an initially-specified radial location, or (ii) Eulerian: either (iia) specified velocity and pressure at a fixed radial location or (iib) constant velocity and pressure at a fixed, far-field radial boundary location (so that boundary-condition induced waves do not affect the solution in the domain of interest).

Benchmark type: This problem has a non-closed-form solution that requires a numerical procedure involving the solution of ODEs to a specified accuracy (type 3 of [Obe07]).

Principal code features tested:

1. Basic compressible shock-hydrodynamics of converging-then-diverging flow in spherical geometry.
2. Application of boundary forcing function (if the solution is so driven).

III. **Mathematical Description**

This problem was originally described in the seminal paper by Guderley [Gud42]. Subsequent general treatments of this problem are presented in [But54, Sta60,

Whi74, Laz77, Rod78, Laz81, Mey82], with specific aspects discussed more recently by [Hir01, Pon06, Ram07, Hor08]. While the initial state of the problem is conceptually simple, the ODEs describing the dynamic solution and the techniques used to solve those ODEs are complicated; the interested reader is referred to [Laz77, Laz81, Pon06, Ram07] for details.

The form of the 1-D compressible flow equations amenable to analysis for this problem is given as:

$$\begin{aligned} \frac{\partial \rho}{\partial t} + \frac{\partial (\rho u)}{\partial r} &= -(m-1)\frac{\rho u}{r} \\ \frac{\partial u}{\partial t} + u\frac{\partial u}{\partial r} &= -\frac{1}{\rho}\frac{\partial p}{\partial r} \\ \frac{\partial S}{\partial t} + u\frac{\partial S}{\partial r} &= 0 \end{aligned}$$

where ρ is the mass density, u is the velocity, $p = (\gamma\text{-}1)\rho e$ is the pressure, S is the thermodynamic entropy, and m is an integer identifying the geometry, with m=3 for spherically symmetric flow.

A Lie group analysis of these equations (see [Ram07]) reveals the existence of a set of dimensionless similarity variables that reduce the above PDEs to a set of coupled, nonlinear ODEs. For the incoming shock problem, the independent variable for this set of ODEs is the similarity variable

$$\xi = r/(kt^{\alpha})$$

where the similarity exponent α must be solved for. Approximate formulae with which to estimate α are given, e.g., in [Sta60]; a robust numerical technique with which to evaluate α is given in [Hir01]. Using these methods, a complete solution of the ODEs for the incoming shock problem can be obtained. It can be shown [Ram07] that the identical similarity exponent satisfies the required constraints for the outgoing shock problem. Due to the finite-strength shock of the outgoing phase, however, the forms of the equations and of the constraints to be satisfied differ from those of the incoming solution; as described in detail in [Laz81, Ram07], the solution method for those equations differs, as well.

The transformation between the similarity solution (which is obtained from numerical integration of the appropriate ODEs and numerical solution of the corresponding nonlinear eigenvalue problems) and the physical variables remains, in a sense, ambiguous. This is due to the dependence of this transformation on the parameter k in the definition of the independent similarity variable, given above. This parameter is related to the initial energy and density of the process that generates the incoming shock, to quote Ramsey [Ram07], “from an infinitely weak state, at infinity, infinitely long ago.”

Therefore, the problem we propose is related to the similarity solution given by Lazarus [Laz81] and depicted by Ramsey [Ram07]. These solutions are shown in Figs. 1 and 2.

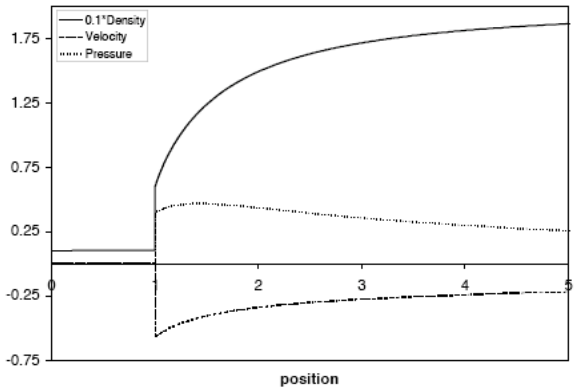

Figure 1. Incoming-flow solution for density, velocity, and pressure for the Guderley problem for the case $m = 3$, $k = 1$, $\gamma = 1.4$, $t = -1$, corresponding to Fig. 5.9 of [Ram07] and Figs. 8.8, 8.10, and 8.12 of [Laz81].

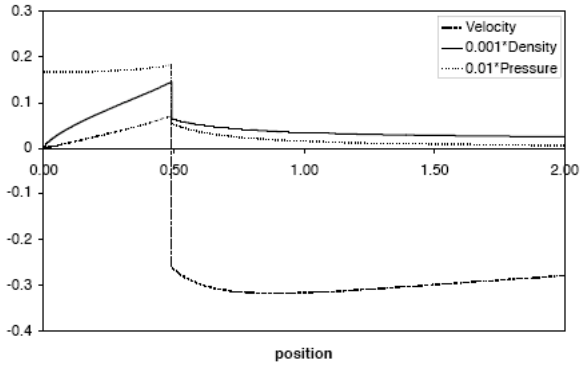

Figure 2. Outgoing-flow solution for density, velocity, and pressure for the Guderley problem for the case $m = 3$, $k = 1$, $\gamma = 1.4$, $t = +1$, corresponding to Fig. 5.12 of [Ram07] and Figs. 8.26, 8.28, and 8.30 of [Laz81].

In the following, all quantities are in consistent cgs units.

The system response quantities of interest include:

i. Snapshots of density, velocity, pressure, SIE as a function of position
ii. Time-histories of density, velocity, pressure, and SIE at specified positions
iii. Total energy, kinetic energy, internal energy as a function of time

Configuration #1: 1-D (r) Spherical Incoming Shock [Laz81, Ram08]

Left computational boundary $= r_L = 0.0$ cm

Right computational boundary $= r_R = 3.0$ cm

Left analysis boundary	$= r_L = 0.0$ cm
Right analysis boundary	$= r_R = 2.0$ cm
Adiabatic index	$= \gamma = 3$
Scaling parameter	$= k = 1$
Initial time	$= t_{\text{init}} = -1.0$ s
Final times	$= t_{\text{fin}} =$ -0.1 s, +0.1 s, +0.5 s

IV. **Accuracy Assessment**

i. Calculations will be run on a nominal mesh, which is to include 150 zones in the entire computational domain. Calculations will be run also at mesh resolutions of two, four, and eight times the nominal resolution.
ii. Exact solutions for the density, velocity, pressure, and SIE will be generated at the positions corresponding to the center of each mesh cell or for the appropriate cell-averaged quantity (for finite volume codes), for each zone in the specified domain.
iii. The values at $t_{\text{init}} = -1.0$ s will be mapped onto the computational mesh to be used as the initial condition for the subsequent calculation. For this configuration, erroneous values propagating in to the computational mesh from the right boundary should not influence the computed solution on the analysis domain (which is a strict subset of the computational domain)
iv. Values of the L_1, L_2, and L_∞ norm of the difference between the computed and exact density, velocity, pressure, and SIE are to be evaluated for each mesh resolution at its native resolution on the analysis domain. Plots of error versus mesh resolution are to be generated. Inferred convergence properties are to be evaluated both (i) interpolated over all mesh resolutions and (ii) interpolated between each two adjacent mesh resolutions.
v. Values of the L_1, L_2, and L_∞ norm of the difference between the computed and exact density, velocity, pressure are to be evaluated for each mesh resolution coarsened onto the coarsest (nominal) mesh. Plots of error versus mesh resolution are to be generated. Inferred convergence properties are to be evaluated both (i) interpolated over all mesh resolutions and (ii) interpolated between each two adjacent mesh resolutions.
vi. The total energy, kinetic energy, and internal energy as functions of time are to be plotted.

V. **Additional User Information**

The idealized zero-pressure state near the origin for the incoming shock phase corresponds to the case of an infinitely strong shock; this assumption simplifies the jump conditions that must be satisfied at the incoming shock (see [Pon06] for an asymptotic analysis in the case of a finite-strength incoming shock). In the corresponding hydrocode simulations, however, the near-origin pressure must be set to a non-zero value that is small, i.e., several orders of magnitude smaller than the post-shock pressure. The suggested value to be used is 10^{-4} dyn cm^{-2}. The effect on verification analyses of this small initial pressure has not been quantified, but is anticipated to be minimal.

VI. **References**

[But54] Butler, D.S., *Converging Spherical and Cylindrical Shocks*, U.K. Ministry of Supply Armament Research Establishment report 54/54 (Theoretical Research Report 12/54), Fort Halstead, Kent, UK (1954).

[Gud42] Guderley, G., "Starke kugelige und zylindrische Verdichtungsstöße in der Nähe des Kugelmittelpunktes bzw. der Zylinderachse," *Luftfahrtforschung* **19**, pp. 302–312 (1942); contact J. Kamm (kammj@lanl.gov) for the original or an English-language translation.

[Hir01] Hirschler, T., and Gretler, W., "On the eigenvalue problem of imploding shock waves," *Z. angew. Math. Phys.* **52**, pp. 151–166 (2001).

[Hor08] Hornung, H., Pullin, D., and Ponchaut, N., "On the question of universality of imploding shock waves," submitted to *Zeit. angew. Math. Mech.*, in review (2008).

[Laz77] Lazarus, R.B., and Richtmyer, R.D., *Similarity solutions for converging shocks*, Los Alamos Scientific Laboratory report LA-6823-MS (1977).

[Laz81] Lazarus, R.B., "Self-similar solutions for converging shocks and collapsing cavities," *SIAM J. Numer. Anal.* **18**, pp. 316–371 (1981).

[Mey82] Meyer-ter-Vehn, J., and Schalk, C., "Selfsimilar spherical compression waves in gas dynamics," *Z. Naturforsch. A* **37**, pp. 955–969 (1982).

[Obe07] Oberkampf, W.L., and Trucano, T.G., *Verification and Validation Benchmarks*, Sandia National Laboratories report SAND2007-0853 (2007).

[Pon06] Ponchaut, N.F., Hornung, H.G., Pullin, D.I., and Mouton, C.A., "On imploding cylindrical and spherical shock waves in a perfect gas," *J. Fluid Mech.* **560**, pp. 103–122 (2006).

[Ram07] Ramsey, S., *A Rigorous Investigation of the Self-Similar Converging-Reflected Shock Wave Standard Solution Mode*, Los Alamos National Laboratory report LA-UR-07-5261 (2007).

[Ram08] Ramsey, S., *Evaluation of the Guderley Converging Shock Wave Standard Solution Mode*, Los Alamos National Laboratory report LA-UR-08-05442 (2008).

[Rod78] Rodríguez, M., and Liñán, A., *Implosiones autosemejantes isentropicas y no isentropicas*, Junta de Energia Nuclear Report J.E.N. 405, Madrid, Spain (1978).

[Sta60] Stanyukovich, K.P., *Unsteady Motion of Continuous Media*, Pergamon Press, London (1960).

[Whi74] Whitham, G.B., *Linear and Nonlinear Waves*, Wiley, New York, NY (1974).

I. **Name**: The Cook & Cabot Problem

II. **Conceptual Description**

General: The Cook & Cabot Problem [Coo04; see also Lan87] consists of a compressible, breaking wave for the 1-D Euler equations of gas dynamics. For the specified initial conditions and up to a specified time, two of the three characteristic fields are constant and only the third characteristic field evolves dynamically. In particular, this temporally evolving characteristic satisfies an equation similar to Burgers' equation (see, e.g., [Whi74]): with the given initial conditions, the solution remains smooth up until the time at which the third field "breaks," i.e., a shock forms and the solution becomes discontinuous. Therefore, this problem provides a rigorous and quantitative test of the resolution of planar, 1-D compressible hydrodynamics algorithms on a smooth, nonlinear problem. In particular, this problem can be used to quantify how well the spectral content of the computed solution compares with the exact solution for smooth flows that transition into discontinuous flows.

Processes modeled: This problem tests the integration of the conservation laws for the flow of strength-free, inviscid, non-heat conducting, compressible gas in 1-D planar geometry, up to the point of wave-breaking.

Initial conditions: Sinusoidally-varying material density, pressure, and velocity on the unit interval; the formulae for these variables are given below.

Boundary conditions: Periodic boundary conditions.

Benchmark type: The idealized case reduces to a closed-form solution that requires the solution of one nonlinear equation (type 1 of [Obe07]), converged to either machine accuracy or a clearly stated tolerance.

Principal code features tested:

1. Basic compressible hydrodynamics, including strongly nonlinear interactions for a single material.

III. **Mathematical Description**

A brief mathematical description of the problem is given in [Coo04]. In that paper, sufficient information is provided to derive the entire solution up to the point of shock formation. The salient points are discussed below.

The system response quantities of interest include:

i. Snapshots of density, velocity, pressure, and specific internal energy (SIE) as a function of position.
ii. Time-histories of density, velocity, pressure, and SIE at specified positions.
iii. Total energy, kinetic energy, and internal energy as a function of time.

Configuration #1: [Coo04]

Left boundary	$= x_L = 0.0$ cm
Right boundary	$= x_R = 1.0$ cm
Adiabatic index	$= \gamma = 5/3$
Initial density	$= \rho = \rho_0 [1 + \varepsilon \sin(2\pi x/\lambda)]$
Reference density	$= \rho_0 = 10^{-3}$ g cm^{-3}
Initial pressure	$= p = p_0 (\rho/\rho_0)^{\gamma}$
Reference pressure	$= p_0 = 10^6$ dyn cm^{-2}
Initial sound speed	$= c = c_0 (\rho/\rho_0)^{(\gamma-1)/2}$
Ref. sound speed	$= c_0 = (\gamma p_0/\rho_0)^{1/2} \approx 4.0824829\times10^4$ cm s^{-1}
Initial velocity	$= u = 2(c_0 - c)/(\gamma-1)$
Initial perturbation	$= \varepsilon = 0.1$
Initial wavelength	$= \lambda = N \Delta x$, where N = number of gridpoints on [0,1]
Final time	$= t_{\rm fin} = t_{\rm break}$, which is given for a point initially at x by:

$$t_{\rm break} = \frac{\lambda}{(\gamma+1)\pi\varepsilon c_0} \frac{[1+\varepsilon\sin(2\pi x/\lambda)]^{(3-\gamma)/2}}{\cos(2\pi x/\lambda)}$$

The exact solution at time $t > 0$ is the initial profile modified in such a way that each point is advected with velocity $u - c$, i.e., so that points on the profile at time t have moved from their initial (t=0) position x to the location $\xi = x + (u - c)\, t$. This exact solution is valid, for a given x, up to the point in time given by $t_{\rm break}$ above. The earliest time at which any point on the unit interval arrives at its breaking time is given by:

$$t_{\rm break,\ min} \approx \frac{\lambda}{(\gamma+1)\pi\varepsilon c_0} [1 + O(\varepsilon^3)]$$

which is the last time for which the exact solution (described above) is valid over the entire interval. A later time for calculation verification studies is given by the time at which the peaks of the initial sinusoidal profile (at $\pm\lambda/4$ from the central zero of the density profile) reach the breaking point. This time is given by

$$t_{\rm p} \approx \frac{(\gamma-1)(x_b - x_p)}{(\gamma+1)(c_b - c_p)} \approx \frac{\lambda}{2(\gamma+1)\varepsilon c_0} \approx (\pi/2) t_{\rm break,\ min}$$

Comparison of the (code) convergence results at $t < t_{\rm break,\ min}$ with (calculation) convergence results at $t > t_{\rm break,\ min}$ reveals differences in the hydrodynamics algorithm for smooth and discontinuous flows.

IV. **Accuracy Assessment**

i. Calculations will be run on a nominal mesh, which is to include 100 zones in the specified domain. Calculations will be run also at mesh resolutions of two, four, and eight times the nominal resolution, with appropriate modifications of the initial conditions (e.g., in the initial wavelength of the perturbation).
ii. Exact solutions for the density, velocity, pressure, and SIE will be generated at the positions corresponding to the center of each mesh cell, for each zone in the specified domain 1.
iii. Values of the L_1, L_2, and L_∞ norm of the difference between the computed and exact density, velocity, pressure, and SIE are to be evaluated for each mesh resolution at its native resolution. Plots of error versus mesh resolution are to be generated. Inferred convergence properties are to be evaluated both (i) interpolated over all mesh resolutions and (ii) interpolated between each two adjacent mesh resolutions.
iv. Values of the L_1, L_2, and L_∞ norm of the difference between the computed and exact density, velocity, pressure are to be evaluated for each mesh resolution coarsened onto the coarsest (nominal) mesh. Plots of error versus mesh resolution are to be generated. Inferred convergence properties are to be evaluated both (i) interpolated over all mesh resolutions and (ii) interpolated between each two adjacent mesh resolutions.
v. The total energy, kinetic energy, and internal energy as functions of time are to be plotted.
vi. The power spectrum (computed by Fourier transform) of the solution is to be graphically compared with that of the analytical solution.

V. **Additional User Information**

VI. **References**

[Coo04] Cook, A.W., and Cabot, W.H., "A high-wavenumber viscosity for high-resolution numerical methods," *J. Comput. Phys.* **195**, pp. 594–601 (2004).
[Lan87] Landau, L.D., and Lifschitz, E.M., *Fluid Mechanics*, Pergammon Press, London, UK (1987).
[Obe07] Oberkampf, W.L., and Trucano, T.G., *Verification and Validation Benchmarks*, Sandia National Laboratories report SAND2007-0853 (2007).
[Whi74] Whitham, G.B., *Linear and Nonlinear Waves*, Ch. 4, Wiley, New York, NY (1974).

I. **Name**: The Woodward-Colella Interacting Blast Waves Problem

II. **Conceptual Description**

General: The Woodward-Colella Blast Waves Problem is a one-dimensional (planar) test for robust shock capturing, strong shock interactions, and tracking contact surfaces [Woo84]. The governing equations are the Euler equations, so the problem is inviscid and there are no explicit diffusive effects; the ideal (polytropic) gas equation of state is used. The domain of the problem is a shock tube with two (virtual) diaphragms, dividing the tube into two short sections near the ends and a longer section between them. The short sections are at (different) high pressures, and the center section is at low pressure; initially the density is constant and the velocity is zero in all three regions. At the starting time the diaphragms are broken, sending two strong shocks into the center section and rarefactions towards the ends of the tube. The problem is not symmetric: since the left and right sections have different initial pressures, the strengths of the left and right rarefactions and shocks are different. Complex wave interactions develop as the rarefactions reflect off the reflective boundaries, as the rarefactions catch up to the shocks, and as the shocks interact with each other and with contact surfaces. There is no known analytic solution.

Processes modeled: This problem tests the ability of the numerical method to provide robust, nonoscillatory solutions in the presence of strong shocks and complex wave interactions for an inviscid, compressible gas in planar geometry.

Initial conditions: Everywhere: constant density and zero velocity. Left (10%): constant high pressure. Center (80%): constant low pressure. Right (10%): constant high pressure. Other properties can be determined from the ideal gas equation of state.

Boundary conditions: Left and right: wall (or reflective) boundary conditions.

Benchmark type: There is no known analytic solution past an early time when the expansion wave on the left reflects from the left wall. Numerical simulations on very fine grids, however, are accepted as fiducials for comparison purposes (type 4 of [Obe07]).

Principal code features tested:

1. Nonoscillatory shock capturing.
2. Conservation of mass, momentum, and energy through the correct wave speeds.
3. Numerical dissipation for compressible fluid dynamics.
4. Accuracy in the presence of strong interacting shocks.

III. **Mathematical Description**

This problem was originally described in a paper by Woodward and Colella, [Woo84]; see also [Gre04]. The governing equations are the Euler equations in 1D, Cartesian coordinates:

$$\begin{aligned} \frac{\partial \rho}{\partial t} + \frac{\partial (\rho u)}{\partial x} &= 0 \\ \frac{\partial (\rho u)}{\partial t} + \frac{\partial (\rho u^2 + p)}{\partial x} &= 0 \\ \frac{\partial (\rho E)}{\partial t} + \frac{\partial [(\rho E + p)u]}{\partial x} &= 0 \end{aligned}$$

where ρ is the mass density, u is the velocity, p is the pressure, $E = e + u^2/2$ is the total energy per unit mass, and e is the internal energy per unit mass. The ideal gas law relates the pressure, density, and internal energy: $p = (\gamma - 1)\rho e$ where $\gamma = 7/5$ is the ratio of specific heats.

The problem domain is $0 \le x \le 1$ cm. Initially, the density is $\rho = 1.0$ g/cm^3 and the velocity is $u = 0.0$ cm/s. The left diaphragm is at $x = 0.1$ cm and the right diaphragm is at $x = 0.9$ cm. The pressures in the left, center, and right sections are $p = 10^3$ dyn/cm^2, $p = 10^{-2}$ dyn/cm^2, and $p = 10^2$ dyn/cm^2, respectively. The final time of the simulation is $t_{fin} = 0.038$ s.

The system response quantities of interest include snapshots of density, velocity, and pressure as a function of position, as well as time-histories of the total, internal, and kinetic energies.

IV. **Accuracy Assessment**

Calculations will be run on a series of uniform meshes, having 200, 400, and 800 zones covering the specified domain. Plots of density, velocity, and pressure, as functions of position should be produced at the final time. The density from a 5th order AMP scheme on a 6400 cell mesh is shown below.

This test is usually compared at t=0.038, a time after the strong shocks have interacted and passed through each other. The right-going shock is at $x \approx 0.865$ cm, followed by the larger of the two peak values at x≈0.78 with a converged value of approximately 6.45 g/cm^3. Moving to the left, the local minimum between these two peaks at x≈0.745 cm with a density of approximately 3.20 g/cm^3. The second lower peak is at x≈0.65 cm with a density of approximately 5.30 g/cm^3. The final important feature is the contact discontinuity at x≈0.59 cm; this contact is embedded in an expansion, which can cause the contact to spread excessively.

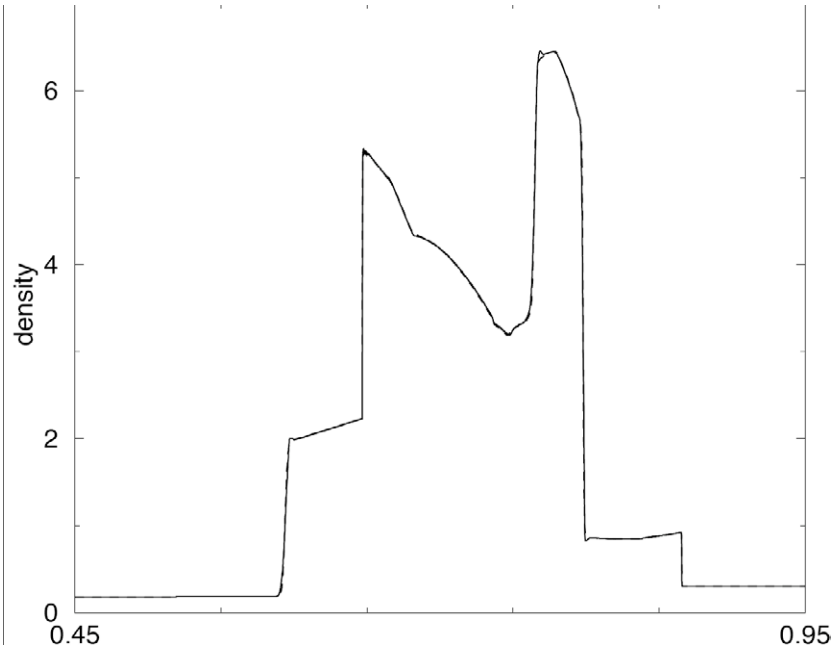

Figure 1. Density as a function of position at the final time for the Woodward-Colella Interacting Blast Waves problem described in the text.

The principal value of this problem is to determine how well the simulation code resolves flow features. Features of the solution that, if not captured, are considered failures include the following:

i. Inability to run to the final time.
ii. Inability to correctly calculate the shock locations.
iii. The presence of oscillations at the Nyquist frequency near shocks and contacts.

V. **Additional User Information**

VI. **References**

[Gre04] Greenough, J.A., and Rider, W.J., "A quantitative comparison of numerical methods for the compressible Euler equations: fifth-order WENO and piecewise-linear Godunov," *J. Comput. Phys.* **196**, pp. 259–281 (2004).

[Obe07] Oberkampf, W.L., and Trucano, T.G., *Verification and Validation Benchmarks*, Sandia National Laboratories report SAND2007-0853 (2007).

[Woo84] Woodward, P., and Colella, P., "The Numerical Simulation of Two-Dimensional Fluid Flow with Strong Shocks," *J. Comput. Phys.* **54**, pp. 115–173 (1984).

I. **Name**: The Shu-Osher Problem

II. **Conceptual Description**

General: The Shu-Osher Problem [Shu89] is a one-dimensional (planar) test for accurately computing complex flow structures in the presence of a shock wave. The governing equations are the Euler equations, so the problem is inviscid and there are no explicit diffusive effects; the ideal (polytropic) gas equation of state is used. In the problem, a shock wave propagates into a quiescent, constant pressure field with a sinusoidal density profile. After passing through the shock, the density profile has two components. One is at approximately the same frequency and amplitude as the initial profile, and compression waves associated with it eventually steepen into shock waves in a classical "N-wave" pattern. The second component is at a higher frequency and larger amplitude that follows the shock more closely. The test is the ability of the method to resolve these higher frequency features without spurious oscillations and excessive dissipation. There is no known analytic solution.

Processes modeled: This problem tests the ability of the numerical method to provide nonoscillatory solutions in the presence of shocks and to accurately resolve fine scale flow structures for an inviscid, compressible gas in planar geometry.

Initial conditions: Pre-shock (right): zero velocity, constant pressure, sinusoidal density. Post-shock (left): uniform density, pressure, and velocity determined from the nominal pre-shock state by the Rankine-Hugoniot jump conditions.

Boundary conditions: Left: in the Eulerian reference frame, subsonic inflow, which maintains the nominal post-shock state. In the Lagrangian reference frame, constant pressure and velocity at nominal post-shock values. Right: fixed at initial state. *Note*: As no waves reach the boundaries during the simulation and the boundary conditions are not the focus of the test, other boundary specifications are allowable as long as they do not disrupt the interior of the domain.

Benchmark type: There is no known analytic solution; however, numerical simulations on very fine grids are accepted as fiducials for comparison (type 4 of [Obe07]).

Principal code features tested:

1. Nonoscillatory shock capturing.
2. Numerical dissipation for compressible fluid dynamics.
3. Accuracy and resolving power in the presence of shocks.

III. **Mathematical Description**

This problem was originally described in a paper by Shu & Osher [Shu89]. The governing equations are the Euler equations in 1D, Cartesian coordinates:

$$\frac{\partial \rho}{\partial t} + \frac{\partial \rho u}{\partial x} = 0$$
$$\frac{\partial \rho u}{\partial t} + \frac{\partial (\rho u^2 + p)}{\partial x} = 0$$
$$\frac{\partial \rho E}{\partial t} + \frac{\partial ((\rho E + p)u)}{\partial x} = 0$$

where ρ is the density, u is the velocity, p is the pressure, $E = e + u^2/2$ is the total energy per unit mass, and e is the internal energy per unit mass. The ideal gas law relates the pressure, density, and internal energy: $p = (\gamma - 1)\rho e$ where $\gamma = 7/5$ is the ratio of specific heats.

The domain is [-4.5cm, 4.5cm], and the initial location of the shock wave is at $x = -4.0$ cm. To the right of the shock, $u = 0$ and $p = 1.0$ dyn/cm^2, and the density is sinusoidal, $\rho = 1 + \varepsilon \sin(\lambda x)$ g/cm^3, where $\varepsilon = 0.2$ and $\lambda = 5$. The jump conditions for a Mach 3 shock specify the state to the left of the shock; approximate values are $\rho = 3.857143$ g/cm^3, $u = 2.629369$ cm/s, and $p = 10.33333$ dyn/cm^2. The final time of the simulation is $t_{fin} = 1.8$ s.

The system response quantities of interest include snapshots of density, velocity, and pressure as a function of position.

Although the description above is an Eulerian one, the problem can also be solved by Lagrangian or Arbitrary Lagrangian Eulerian (ALE) methods. The only adjustments needed are to ensure that initially, the left boundary extends past $x = -7.75$ cm, and that the initial, post-shock pressure and velocity are maintained at the left boundary.

IV. **Accuracy Assessment**

Calculations will be run on a series of uniform meshes, the coarsest having 200 zones covering the specified domain. For each additional mesh, double the number of zones each time. Plots of density, velocity, and pressure, as functions of position should be produced at the final time. The density from a 7th-order Weighted ENO scheme on a 1600 cell mesh is shown below.

The solution features of principal interest are the fine scale density perturbations behind the shock. On a 200 cell uniform Eulerian mesh, they are represented by about 7.5 points per wavelength; on 400 cells, about 15 points per wavelength. Most high-order (higher than second) shock-capturing methods capture the first peak behind the shock with minimal dissipation on the 400 cell mesh; following peaks are often slightly damped. On the 200 cell mesh, the first peak is well resolved but damped, some of the following peaks are clearly discernable but others may be damped beyond recognition. Generally, second-order TVD methods fail to resolve the fine scale perturbations on 200 or 400 cell meshes; even on 800 cells, they are

damped significantly. See the work of Greenough and Rider [Gre04] for a further discussion.

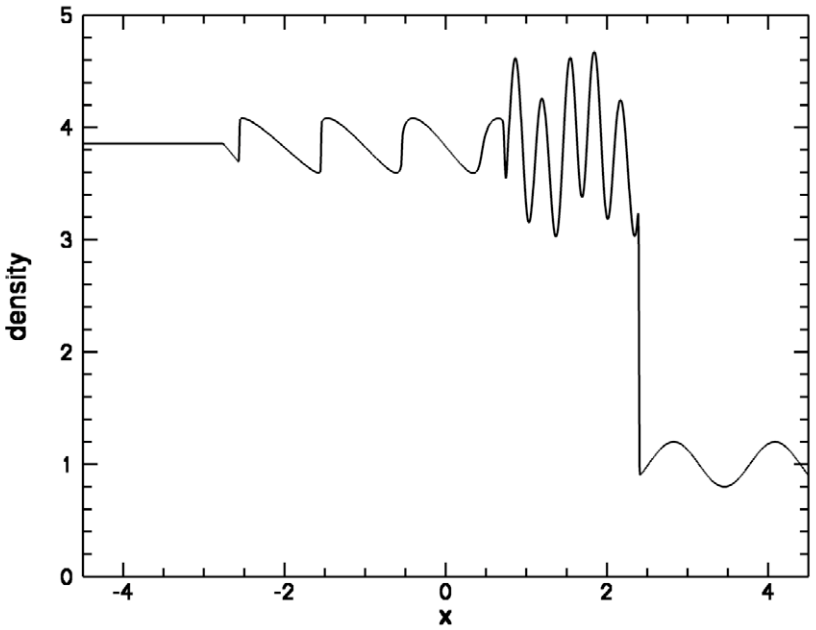

Figure 1. Density as a function of position at the final time for the Shu-Osher problem described in the text.

The principal value of the test is to determine how accurately the simulation code resolves flow features. Features of the solution that, if not captured, are considered failures include the following:

i. Inability to preserve the initial conditions upstream of the shock constitutes failure.
ii. Inability to correctly predict the shock location is a failure.
iii. The presence of oscillations at the Nyquist frequency near the main shock, or the near the compression waves that develop into shocks behind it, constitute failure.
iv. Inability to find a mesh resolution at which the fine scale features are captured constitutes failure.

V. **Additional User Information**

The problem was initially motivated by weak wave interactions with shocks [McK68], in particular a weak entropy wave with a shock and the resultant entropy, vorticity, and acoustic waves produced in the interaction. In that paper linearized estimates for the amplitude of these post-shock waves were derived. A similar test problem defined in Jiang & Shu [Jia96] specifies much smaller initial density fluctuations in the spirit of [McK68].

Another popular variant is to set $\lambda = 5\pi$ in the initial density. This variant is more challenging because the initial frequency is higher, and the effective simulation time is longer.

VI. **References**

[Gre04] Greenough, J.A., and Rider, W.J., "A quantitative comparison of numerical methods for the compressible Euler equations: fifth-order WENO and piecewise-linear Godunov," *J. Comput. Phys.* **196**, pp. 259–281 (2004).

[Jia96] Jiang, G.S., and Shu, C.-W., "Efficient implementation of weighted ENO schemes," *J. Comput. Phys.* **126**, pp. 202–228 (1996).

[McK68] McKenzie, J.F., and Westphal, K.O., "Interaction of Linear Waves with Oblique Shock Waves," *Phys. Fluids* **11**, pp. 2350–2362 (1968).

[Obe07] Oberkampf, W.L., and Trucano, T.G., *Verification and Validation Benchmarks*, Sandia National Laboratories report SAND2007-0853 (2007).

[Shu89] Shu, C.-W., and Osher, S., "Efficient Implementation of Essentially Non-oscillatory Shock-Capturing Schemes, II," *J. Comput. Phys.* **83**, pp. 32–78 (1989).

I. **Name**: The Taylor-Green Vortex Problem

II. **Conceptual Description**

General: The Taylor-Green Vortex (TGV) Problem harks back to Taylor [Tay38] and has been revisited since by many researchers (see, e.g., [Dri07]) as a model problem with which to examine the transition to turbulence from a well-characterized initial state. Although closed-form (infinite series) asymptotic solutions to this configuration exist for an incompressible fluid at early time [Tay38], no closed-form solution is known for the compressible case. At initial time of the problem (t=0), there is a regular pattern of sinusoidal variation in velocity, with the pressure having sinusoidal variations about a fixed value P_0 and the initial density assuming a constant value. This regular initial configuration evolves through a phase where it is (nearly) singular into a complex, disordered state.

Processes modeled: This problem tests the integration of the conservation laws for the flow of strength-free, inviscid, non-heat conducting, compressible gas in 3-D Cartesian geometry. In particular, this problem can be applied to evaluate codes that are used to simulate large-scale turbulence without resorting to Reynolds averaging (or analogous closure approaches), i.e., to codes that employ (implicit) large eddy simulation.

Initial conditions: Specific initial conditions for this 3-D configuration are given below in Section III.

Boundary conditions: Periodic boundaries on the exterior of the mesh.

Benchmark type: While the idealized incompressible case has an asymptotic series solution for early time, the compressible case considered here has no known analytic solution. Numerical simulations on very fine grids, however, are widely accepted as fiducials (albeit of unknown accuracy) for comparison (type 4 of [Obe07]).

Primary code features tested:

1. Basic compressible, multi-dimensional hydrodynamics of disordered flow of a polytropic gas.

III. **Mathematical Description**

The seminal paper in which this problem was proposed is [Tay38]; modern considerations of this problem include [Bra83, Hic06]. A discussion of the particular problem we consider is given in [Dri07]. In the following, all quantities are in consistent cgs units.

The system response quantities of interest include:

i. Fourier spectra of velocity as a function of wavenumber for the following non-dimensional times: t^*=0, 2.2, 6.7, 8.9, 14.7, 36.3, 49.4, and 62.8, where

the non-dimensional time is defined as $t^* \equiv k\, U_0$, where the reference velocity U_0 is defined below and the wavenumber k is unity for the mesh specified below; see Fig. 1 for a depiction of the flowfield at these times.

ii. Snapshots of density, velocity, pressure, and vorticity at the above times.

iii. Total energy, kinetic energy, internal energy as a function of time.

Configuration #1: 3-D Taylor Green Vortex [Dri07]

Left boundary	$= x_L = 0.0$ cm
Right boundary	$= x_R = 2\pi$ cm
Bottom boundary	$= x_B = 0.0$ cm
Top boundary	$= x_T = 2\pi$ cm
Aft boundary	$= x_A = 0.0$ cm
Fore boundary	$= x_F = 2\pi$ cm
Adiabatic index	$= \gamma = 1.4$
Density	$= \rho = 1.178\times10^{-3}$ g cm^{-3}
x-velocity	$= u = U_0 \sin(x) \cos(y) \cos(z)$
y-velocity	$= v = -U_0 \cos(x) \sin(y) \cos(z)$
z-velocity	$= w = 0$
Reference velocity	$= U_0 = 10^4$ cm s^{-1}
Pressure	$= p = P_0 + (1/8)\, \rho\, U_0^2\, [1 + \cos(2z)]\, [\cos(2x) + \cos(2y)]$
Reference pressure	$= P_0 = 1.07\times10^5$ Pa
Final time	$= t_{fin}$ = given by the nondimensional times above

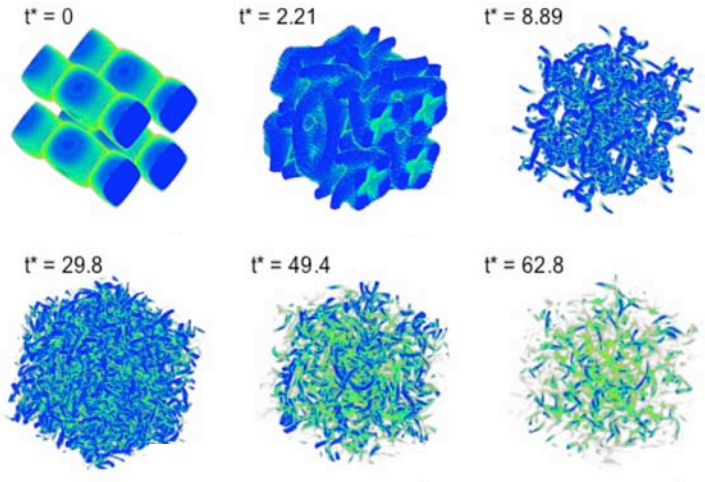

Figure 1. Volume renderings of the largest eigenvalue of the velocity gradient tensor $\partial u_i/\partial x_j$ for the TGV flow at the indicated nondimensional times [Dri07].

IV. **Accuracy Assessment**

i. Calculations will be run on a nominal mesh, which is to include 64 zones in each direction of the specified domain. Calculations will be run also at mesh resolutions of two and four eight times the nominal resolution.
ii. Plot of the Fourier spectrum of the velocity versus wavenumber are to be plotted at the nondimensional times given above.
iii. Values of the L_1, L_2, and L_∞ norm of the difference between the computed and finest-mesh values of the density, velocity, pressure, and vorticity are to be evaluated for each mesh resolution at its native resolution. Plots of error versus mesh resolution are to be generated. Inferred convergence properties are to be evaluated both (i) interpolated over all mesh resolutions and (ii) interpolated between each two adjacent mesh resolutions.
iv. Values of the L_1, L_2, and L_∞ norm of the difference between the computed and finest-mesh density, velocity, pressure are to be evaluated for each mesh resolution coarsened onto the coarsest (nominal) mesh. Plots of error versus mesh resolution are to be generated. Inferred convergence properties are to be evaluated both (i) interpolated over all mesh resolutions and (ii) interpolated between each two adjacent mesh resolutions.
v. The total energy, kinetic energy, and internal energy as functions of time are to be plotted.

V. **Additional User Information**

VI. **References**

[Bra83] Brachet, M.E., Meiron, D.I., Orszag, S.A., Nickel, B.G., Morg, R.H., and Frisch, U., "Small-scale structure of the Taylor-Green vortex," *J. Fluid Mech.* **130**, pp. 411–452 (1983).

[Dri07] Drikakis, D., Fureby, C., Grinstein, F., and Youngs, D., "Simulation of Transition and Turbulence Decay in the Taylor-Green Vortex," *J. Turbulence* **8**, pp. 1–12 (2007).

[Hic06] Hickel, S., Adams, N.A., and Domaradzki, J.A., "An adaptive local deconvolution method for implicit LES," *J. Comput. Phys.* **213**, pp. 413–436 (2006).

[Obe07] Oberkampf, W.L., and Trucano, T.G., *Verification and Validation Benchmarks*, Sandia National Laboratories report SAND2007-0853 (2007).

[Tay37] Taylor, G.I., and Green, A.E., "Mechanism of the Production of Small Eddies from Large Ones," *Proc. Roy. Soc. Lond. A* **158**, pp. 499–521 (1937).

I. **Name**: A Richtmyer-Meshkov Problem

II. **Conceptual Description**

General: The Richtmyer-Meshkov (RM) problem considers the stability of an impulsively accelerated interface separating two compressible or incompressible fluids of different density [Mar57, Ric60, Mes69]. This instability is of fundamental importance in a variety of applications, spanning a wide range of length scales. At large scales RM instability generates mixing in supernovae [Arn89, Bur95]; at smaller scales it plays an important role in deflagration-to-detonation transition [Kho99] and enhances mixing in ramjet engines [Yan93, Cur96]; at even smaller scales it initiates shell break-up in inertial confinement fusion capsules [Lin95, Nie03]. The RM instability is often referred to as the impulsive or shock-induced Rayleigh-Taylor (RT) instability. Unlike RT, where the instability takes place only when the light fluid accelerates into the heavy fluid and the initial growth of perturbations is exponential in time, RM is unstable no matter which direction the shock approaches the interface from (i.e., from either the light or heavy fluid side) and the initial growth of perturbations is linear in time. The resulting flow field can be attributed to the baroclinically generated vorticity resulting from the misalignment of the density gradient across the interface and the pressure gradients that occur during the shock interaction. Indeed, compressible linear theory [Fra86, Mik94] implies that baroclinic vorticity can be deposited by a shock at an interface initially without a density gradient because shock refraction at the interface subsequently modifies the initial density gradient. The initial evolution of RM instabilities can be described in terms of vortex dynamics, where Zabusky and others [Zab99, Lee06, Cot07] have discussed the crucial role vorticity plays in the early development of RM and other baroclinic instabilities.

Processes modeled: This problem tests the ability of codes to model multiple fluid interactions in the presence of shocks and to capture the large and fine scale dynamics of the mixing layer (e.g., mixing layer amplitude, displacement, roll-up, and secondary instabilities).

Initial conditions: The initial conditions for this problem are quiescent fluids at a given temperature and pressure (e.g., air and SF_6) with either a single mode sinusoidal perturbation at the interface between the gases or a multimode disturbance with a well characterized spectrum [Coo04]. Computationally, the interface disturbance can either be sharp or smeared depending on what numerical method is being used. Similarly, the way the shock is generated depends on the numerical method being employed. For example, for an Eulerian code one might use as the initial condition one-dimensional analytic results to set up a shock of specified strength upstream of the interface. On the other hand, for a Lagrangian code one would most likely allow the upstream wall to translate normal to the interface with constant velocity (i.e., acting as a piston driving a shock of constant strength). How one deals with the details of shock generation or the initial interface are assumed to only have a small effect in most cases (e.g., different codes give similar amplitude

and displacement results even though those codes are based on very different numerical methods), although amplitude results can be sensitive to how the mixing layer width is calculated (e.g., the common "spike" and "bubble" threshold definitions or the more recent entrainment length ideas [Coo04]).

Boundary conditions: For Lagrangian methods, the shock is most likely formed by an impulsively accelerated boundary to a constant velocity (i.e., a piston) on either side of the interface. For Eulerian methods, the computational domain is usually taken to be of fixed shape and size with the shock being generated by using the one-dimensional analytic results to set it up. For the most part, previous results show that amplitude and growth rates are only slightly affected by the details of the boundary conditions employed (e.g., periodic or symmetry). For example, boundary conditions may be no-slip and non-reflecting at the ends (i.e., at z_{min} and z_{max}), and zero normal velocity at the bottom (i.e., $y=y_{min}$), top (i.e., $y=y_{max}$), and both sides (i.e., $x=x_{min}$ and x_{max}).

Benchmark type: There is no general solution to this problem, but one can compare to linear stability analysis results [Ric60, Mes69], linear models [Haa91, Yan94] at early time, and to nonlinear models [Sad98] at intermediate times.

Principal code features tested:

1. Ability to maintain planar shocks.
2. Model the interaction of multiple fluids in the presence of shocks.
3. Ability to converge large scale details of the mixing layer (e.g., mixing layer amplitude and displacement).
4. Ability to converge fine scale details of the mixing layer (e.g., roll-up and secondary instabilities).
5. Numerical dissipation for compressible fluid dynamics.
6. Test interface reconstruction algorithms.
7. Test particle tracking methods.

III. **Mathematical Description**

The dynamics of the RM instability are governed by conservation of mass, conservation of momentum, and conservation of energy (for each fluid)

$$\frac{\partial \rho}{\partial t} + \nabla \cdot (\rho \mathbf{v}) = 0$$

$$\frac{\partial (\rho \mathbf{v})}{\partial t} + \nabla \cdot (\rho \mathbf{v}\mathbf{v}) + \nabla p + \nabla \cdot \overline{\overline{\tau}} = 0$$

$$\frac{\partial (\rho E)}{\partial t} + \nabla \cdot [(\rho E + p)\mathbf{v}] + \nabla \cdot \mathbf{q} + \overline{\overline{\tau}} : \nabla \mathbf{v} = 0 \quad ,$$

where boundary conditions (e.g., velocity, stress, temperature, mass conservation, and thermodynamic equilibrium) at the interface couple the two systems together. Here, ρ denotes the density, $\boldsymbol{v}$ is the velocity vector, p is the pressure, $\overline{\overline{\tau}}$ is the stress

tensor, E is the total energy, and $\boldsymbol{q}$ is the heat flux vector. The above system of equations is closed by using an equation of state to relate temperature and pressure such as the ideal gas law

$$p = \rho RT \quad ,$$

where R is the gas constant and T is the temperature.

The linear stability of this problem was first considered in detail by Richtmyer [Ric60] who followed Taylor's [Tay50] formulation and modeled gravity as a Dirac delta function. The growth rate of the impulsively accelerated instability was found to be

$$\frac{d\varepsilon}{dt} = kAV\varepsilon_0 \quad ,$$

where V is the interface velocity, $k = 2\pi/\lambda$ is the wavenumber of the initial interface modulation, ε is the amplitude, and ε_0 is its initial value. The Atwood number, A, is defined as

$$A = \frac{\rho_h - \rho_l}{\rho_h + \rho_l} \quad ,$$

where ρ_l and ρ_h are the densities of the light and heavy fluids, respectively. The linear growth stage [Ale88, Gro93] described by Richtmyer's [Ric60] result lasts as long as the perturbation amplitude is sufficiently small (i.e., is much less than the wavelength). The impulsive formulations give good results for small amplitudes and weak shocks, when compressibility effects following the initial shock interaction are not important. When the amplitude becomes comparable to the wavelength, the growth rate decreases owing to the influence of the nonlinearity of the governing equations.

The effects of weak nonlinearity can be incorporated by developing a solution in the form of an asymptotic expansion using the perturbation amplitude [Haa91], however, these solutions have the weakness that when truncated they produce results that quickly diverge from the exact solution when the amplitude reaches moderate size. Others [Zha97] have found a solution to this problem by posing their series solution as a Pade approximant, which significantly extends its validity; however, the solution of Zhang & Sohn [Zha97] does not possess the generally accepted asymptotic behavior as time approaches infinity. This weakness has been addressed by Sadot et al. [Sad98], who present a model that captures the initial weakly nonlinear behavior yet also provides the correct late-time asymptotic form.

Although the description above is an Eulerian one, the problem can also be solved by Lagrangian or Arbitrary Lagrangian Eulerian (ALE) methods.

Figure 1 shows mixing layer amplitude results from linear and non-linear semi-analytic models [Haa91, Yan94, Zha97, Sad98] together with computational results from two very different codes, as well as experimental shock tube results [Col02]. The parameters used to generate theses results are those given in the experimental shock tube work of Jacobs [Col02], where the fluids are air and SF_6, the initial temperature is 292.5 K, the pressure is 9.269×10^5 g cm^{-2}, the single mode sinusoidal interface disturbance wavelength is 5.93 cm, the amplitude is 0.3 cm,[2] the Atwood number is about 0.6, and the fluids are taken to be polytropic gases with gamma being 1.276 for air and 1.093 for SF_6. Initial densities are calculated using the ideal gas equation of state. For the case of the ALE code, the shock is generated by translating the air side boundary at constant velocity (i.e., the "piston" velocity is set to 1.405×10^4 cm s^{-1}), while in the Eulerian code the initial condition is set up using one-dimensional analytic results to produce a shock of specified strength upstream of the interface. In either case, the initial shock strength is set to be comparable with the experimental interface translation speed of 9.7×10^3 cm s^{-1}. The boundary conditions are assumed to be periodic in the crossstream direction and no slip at the ends (if this is being set up in 3D the resulting third dimension boundaries are taken to be free). Also, the computational results shown here have about 300 points per wavelength in the crossstream direction and whatever resolution is needed to get converged results in the streamwise direction.

IV. **Accuracy Assessment**

i. Calculations will be run on a series of meshes with increasing resolution in order to judge grid convergence (domain convergence is not an issue for this problem). Values of the L_1, L_2, and L_∞ norm of the difference between the computed and finest-mesh values of the mixing layer amplitude, displacement, and growth rate are to be evaluated for each mesh resolution considered. Plots of error versus mesh resolution are to be generated. Inferred convergence properties are to be evaluated both (i) interpolated over all mesh resolutions and (ii) interpolated between each two adjacent mesh resolutions.

ii. Once convergence has been established, computations can be compared to linear stability analysis results [Mes69, Ric60].

iii. Also, at early and intermediate times one may compare to linear [Yan94] and weakly-nonlinear [Haa91, Zha97, Sad98] semi-analytical results. If desired, one may curve fit the analytic solutions and then calculate the L_1, L_2, and L_∞ norm of the difference between the computed and semi-analytic results.

[2] In the computations, an initial amplitude slightly larger than reported in the experiments is used so that the layer amplitude at its minimum value after the initial compression (this time is then taken to be t=0 for comparison to experiment and other computations and calculations) is similar in magnitude to the first experimental point. For a pure verification study, such agreement between simulation and experiment is not required, however, as it is irrelevant to verification purposes.

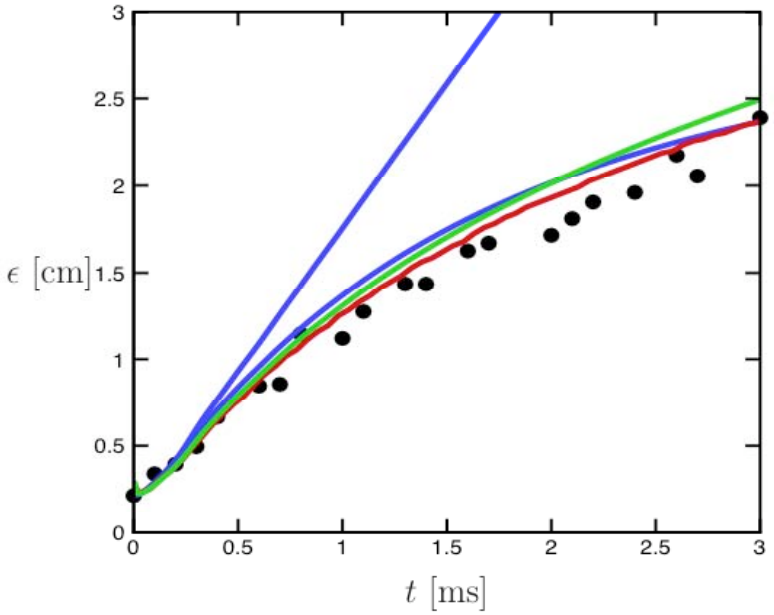

Figure 1. Mixing layer amplitude versus time, where the black dots correspond to Jacobs single shock tube data [Col02], the blue curves correspond to linear and non-linear semi-analytic results [Haa91, Yan94, Zha97, Sad98], the red curve corresponds to converged results from an Eulerian code, and the green curve corresponds to converged results from an ALE code. We note that computations are within about 4% of each other.

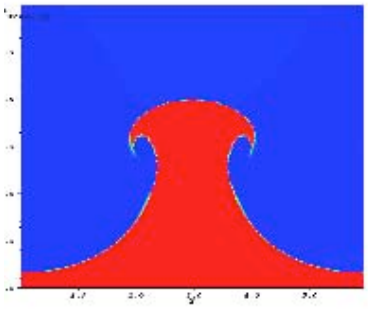

Figure 2. Density results from the ALE code [Col02] for a time of about 1.7 ms after the shock hits the interface disturbance. We note that the amplitude and mushroom width from the ALE code are approximately 1.8 cm and 2.2 cm, respectively.

V. **Additional User Information**

One can set up the computational RM problems to approximate shock tube experiments (e.g., [Col02, Tom08]). Current experimental shock tube techniques allow one to set up a moderately well characterized single mode disturbance of small amplitude confined to a limited range of wavelengths, some multimode generation scheme, the exact spectrum of which may not be known, or more general geometries. Results for the mixing layer amplitude, displacement, and growth rate as well as qualitative and quantitative measure of the layer structure can be compared to experimental shock tube results (e.g., [Col02]). The ability of simulations to capture important experiment features rightly falls within the purview of *validation*, which presents different issues from verification; see, e.g., [AIA98, ASM06, Bab04, Obe04, Sor07] for general discussions of validation and [Obe02] for a discussion of validation experiments.

VI. **References**

[AIA98] AIAA, *Guide for the Verification and Validation of Computational Fluid Dynamics Simulations*, American Institute of Aeronautics and Astronautics, AIAA G-077-1998 (1998).

[Ale88] Aleshin, A.N., Gamalii, E.G., Zaitsev, S.G., Lazareva, E.V., Lebo, I.G., and Rozanov, V.B., "Nonlinear and transitional states in the onset of the Richtmyer-Meshkov instability," *Sov. Tech. Phys. Lett.* **14**, pp. 466-468 (1988).

[Arn89] Arnett, W.D., Bahcall, J.N., Kirshner, R.P., and Woosley, S.E., "Supernova 1987a," *Annu. Rev. Astron. Astrophys.* **27**, pp. 629-700 (1989).

[ASM06] ASME, *V&V 10-2006 Guide for Verification and Validation in Computational Solid Mechanics*, American Society of Mechanical Engineers (2006).

[Bab04] Babuska, I., and Oden, J.T., "Verification and validation in computational engineering and science: Basic concepts," *Comput. Methods Appl. Mech. Engrng.* **193**, pp. 4057–4066 (2004).

[Bur95] Burrows, A., Hayes, J., and Fryxell, B.A., "On the nature of core-collapse supernova explosions," *Astrophys. J.* **450**, pp. 830-850 (1995).

[Col02] Collins, B.D., and Jacobs, J.W., "PLIF flow visualization and measurements of the Richtmyer-Meshkov instability of an air/SF6 interface," *J. Fluid Mech.* **464**, pp. 113-136 (2002).

[Coo04] Cook, A.W., Cabot, W. and Miller, P.L., "The mixing transition in Rayleigh-Taylor instability," *J. Fluid Mech.* **511**, pp. 333-362 (2004).

[Cot07] Cotrell, D.L., and Cook, A.W., "Scaling the incompressible Richtmyer-Meshkov instability," *Phys. Fluids* **19,** 078105 (2007).

[Cur96] Curran, E., Heiser, W., and Pratt, D., "Fluid phenomena in scram jet combustion systems," *Annu. Rev. Fluid Mech.* **28**, pp. 323-360 (1996).

[Dra06] Drake, R.P., *High-Energy-Density Physics*, Springer, Berlin, 2006.

[Fra86] Fraley, G., "Rayleigh-Taylor stability for a normal shock-wave density discontinuity," *Phys. Fluids* **29**, pp. 376-386 (1986).

[Gro93] Grove, J.W., Holmes, R., Sharp, D.H., Yang, Y., and Zhang, Q., "Quantitative theory of Richtmyer-Meshkov instability," *Physical Rev. Lett.* **71**, pp. 3473-3476 (1993).

[Haa91] Haan, S.W., "Weakly nonlinear hydrodynamic instabilities in inertial fusion," *Phys. Fluids B* **3**, pp. 2349-2355 (1991).

[Kho99] Khokhlov, A.M., Oran, E.S., and Thomas, G.O., "Numerical simulation of deflagration-to-detonation transition: The role of shock-flame interactions in turbulent flames," *Combustion and Flame* **117**, pp. 323-339 (1999).

[Lee06] Lee, D.K., Peng, G., and Zabusky, N.J., "Circulation rate of change: A vortex approach for understanding accelerated inhomogeneous flows through intermediate times," *Phys. Fluids* **18**, 097102 (2006).

[Lin95] Lindl, J.D., "Development of the indirect-drive approach to inertial confinement fusion and the target physics basis for ignition and gain," *Phys. Plasmas* **2**, pp. 3933-4024 (1995).

[Mar57] Markstein, G.H., "Flow disturbances induced near a slightly wavy contact surface, or flame front, traversed by a shock wave," *J. Aeronautical Sciences* **24**, pp. 238-239 (1957).

[Mes69] Meshkov, E.E., "Instibility of the interface of two gases accelerated by a shock wave," *Izv. Akad. Nauk SSSR, Mekh. Zhidk. Gaza* **4**, pp. 151-157 (1969).

[Mik94] Mikaelian, K.O., "Freeze-out and the effects of compressibility in the Richtmyer-Meshkov instability," *Phys. Fluids* **6**, pp. 356-368 (1994).

[Nie03] Niederhaus, C.E., and Jacobs, J.W., "Experimental study of the Richtmyer-Meshkov instability of incompressible fluids," *J. Fluid Mech.* **485**, pp. 243-277 (2003).

[Obe04] Oberkampf, W.L., Trucano, T.G., and Hirsch, C., "Verification, validation, and predictive capability in computational engineering and physics," *Appl. Mech. Rev.* **57**, pp. 345–384 (2004).

[Obe02] Oberkampf, W.L., "What are Validation Experiments?" *Experimental Techniques* **25**, pp. 35–40 (2002).

[Ric60] Richtmyer, R.D., "Taylor instability in shock acceleration of compressible fluids," *Commun. Pure Appl. Math.* **13**, pp. 297-319 (1960).

[Sad98] Sadot, O., Erez, L., Alon, U., Oron, D. Levin, L.A., Erez, G., Ben-Dor, G., and Shvarts, D., "Study of nonlinear evolution of single-mode and two-bubble interaction under Richtmyer-Meshkov instability," *Phys. Rev. Lett.* **80**, pp. 1654-1657 (1998).

[Sor07] Sornette, D., Davis, A.B., Ide, K., Vixie, K.R., Pisarenko, V., and Kamm, J.R., "Algorithm for model validation: Theory and applications," *Proc. Nat. Acad. Sci. USA* **104**, pp. 6562–6567 (2007).

[Tay50] Taylor, G.I., "The instability of liquid surfaces when accelerated in a direction perpendicular to their planes. I.," *Proc. Roy. Soc. Lond. A* **201**, pp. 192-196 (1950).

[Tom08] Tomkins, C., Kumar, S., Orlicz, G., and Prestridge, K., "An experimental investigation of mixing mechanisms in shock-accelerated flow," *J. Fluid Mech.* **611**, pp. 131–150 (2008).

[Yan93] Yang, J., Kubota, T., and Zukoski, E.E., "Applications of shock-induced mixing to supersonic combustion," *AIAA J.* **31**, pp. 854-862 (1993).

[Yan94] Yang, Y., Zhang, Q., and Sharp, D.H., "Small amplitude theory of Richtmyer-Meshkov instability," *Phys. Fluids A* **6**, pp. 1856-1873 (1994).

[Zab99] Zabusky, N.J., "Vortex paradigm for accelerated inhomogeneous flows: Visiometrics for the Rayleigh-Taylor and Richtmyer-Meshkov environments," *Annu. Rev. Fluid Mech.* **31**, pp. 495-536 (1999).

[Zha97] Zhang, Q., and Sohn, S., "Non-linear theory of unstable fluid mixing driven by shock wave," *Phys. Fluids* **9**, pp. 1106-1124 (1997).

I. **Name**: Bleich & Nelson's Plane EPP Problem

II. **Conceptual Description**

General: Bleich and Nelson [Ble66] consider the case of 1-D plane waves in an elastic-perfectly-plastic half-space for arbitrary combinations of (uniform) step-function normal (diagonal) and shear (off-diagonal) stress loads on the free surface. This behavior is perhaps the simplest case of dynamic elastic-plastic plane wave propagation. The time-dependent solution for this 1-D, slab-geometry problem with uniform, constant step-function-in-time compressive pressure and positive shear on the free surface can be expressed in terms of elliptic integrals of the first, second, and third kinds and, thus, can be evaluated numerically with high precision. Moreover, the material response for this problem can assume characteristically different behavior depending on the combination of the applied stresses and the material properties; for example, the existence and location of the elastic precursor relative to the plastic wave front varies as a function of these parameters.

Processes modeled: This problem tests 1-D plane elastic-plastic wave propagation generated from free-surface loading. This includes the interaction between elastic and plastic states at the elastic-plastic boundary, as well as the dissipation of energy through plastic work.

Initial conditions: Uniform, constant, zero-velocity EPP material state.

Boundary conditions: Normal and shear stresses applied at the free surface at x=0. This driving stress vanishes for $t < 0$ and is constant for $t \geq 0$. The far-field boundary is ignored, as the final time is chosen to be before any outgoing wave interacts with the finite computational outer boundary.

Benchmark type: This is a closed-form, analytical solution (type 2 of [Obe07]).

Principal code features tested:

1. Basic hydrodynamics, including single-material EOS calls
2. Unidirectional, planar elastic-perfectly-plastic stress wave propagation
3. Time-dependent stress boundary condition implementation

III. **Mathematical Description**

The governing equations are those for standard infinitesimal strain in an EPP medium. These equations reduce to the conservation of momentum together with the constitutive relations relating stress and strain and a plastic yield condition. The interested reader is referred to the complete mathematical description of this problem given in [Ble66]; see also [Cri67] for further background.

The system response quantities of interest include:

i. Snapshots of density, velocity, pressure, normal stress σ_{xx}, tangential stress σ_{yy}, and shear stress σ_{xy} as a function of position.
ii. Snapshots of nondimensional normal stress and nondimensional shear stress, consistent with this in Figs. 5, 6, and 7 of [Ble66].
iii. Time-histories of density, velocity, pressure, normal stress σ_{xx}, tangential stress σ_{yy}, and shear stress σ_{xy} at specified locations.
iv. Total energy as a function of time.

We propose to develop dimensional initial and boundary conditions to generate the three fundamentally different EPP solutions presented in [Ble66]. All three lead to plastic yielding, with the first and third exhibiting elastic precursor behavior in the shear stress while the second does not. Figure 1, corresponding to the first of these configurations, shows Fig. 5 of [Ble66] with the computed solution for the nondimensional normal and shear stresses as a function of the nondimensional similarity variable. Figure 2, corresponding to the second configuration, shows Fig. 6 of [Ble66] and depicts the same variables for another solution.

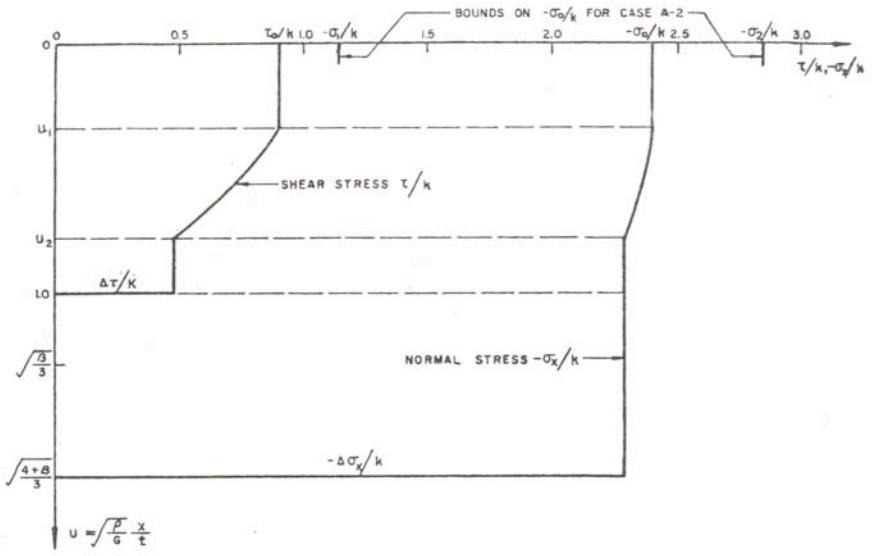

Figure 1. Plot of the nondimensional normal and shear stresses (along the abscissa) as functions of the nondimensional similarity variable (along the ordinate) for one of the Bleich & Nelson solutions; taken from Fig. 5 of [Ble66].

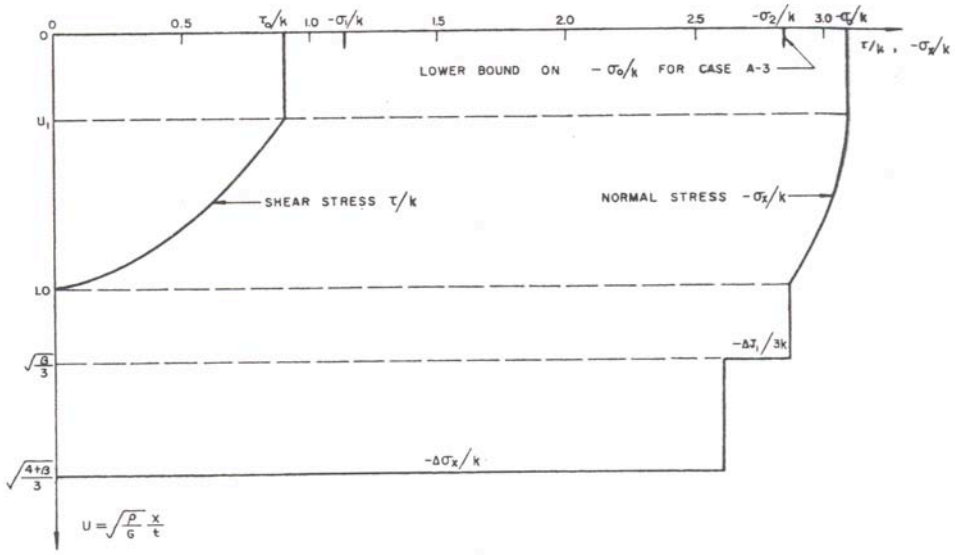

Figure 2. Plot of the nondimensional normal and shear stresses (along the abscissa) as functions of the nondimensional similarity variable (along the ordinate) for another Bleich & Nelson solutions; taken from Fig. 6 of [Ble66].

The proposed configurations are as follows, where ν is Poisson's ratio, Y is the yield stress in simple shear, and $\mathcal{H}(t)$ is the Heaviside function:

Configuration #1: To be consistent with Fig. 5 of [Ble66], with $\nu = 0.25$ and driving normal stress $\sigma_{xx} = -2.4Y\,\mathcal{H}(t)$ and driving shear stress $\sigma_{xy} = 0.9Y\,\mathcal{H}(t)$.

Configuration #2: To be consistent with Fig. 6 of [Ble66], $\nu = 0.25$ and driving normal stress $\sigma_{xx} = -3.1Y\,\mathcal{H}(t)$ and driving shear stress $\sigma_{xy} = 0.9Y\,\mathcal{H}(t)$.

Configuration #3: To be consistent with Fig. 8 of [Ble66], $\nu = 0$ and driving normal stress $\sigma_{xx} = -2.55Y\,\mathcal{H}(t)$ and driving shear stress $\sigma_{xy} = 0.9Y\,\mathcal{H}(t)$.

IV. **Accuracy Assessment**

i. Calculations will be run on a nominal mesh, which is to include ≥100 zones in the range between the left boundary and the right boundary. Calculations will also be run at mesh resolutions of two, four, and eight times the nominal resolution.

ii. Exact solutions for the density, velocity, pressure, normal stress deviator σ_{xx}, tangential stress deviator σ_{yy}, and shear stress deviator σ_{xy} will be generated at the positions corresponding to the center of each mesh cell, for each zone in the computational domain.

iii. Values of the L_1, L_2, and L_∞ norm of the difference between the computed and exact density, velocity, pressure, normal stress deviator σ_{xx}, tangential stress

deviator σ_{yy}, and shear stress deviator σ_{xy} are to be evaluated for each mesh resolution at its native resolution. Plots of error versus mesh resolution are to be generated. Inferred convergence properties are to be evaluated both (i) interpolated over all mesh resolutions and (ii) interpolated between each two adjacent mesh resolutions.

iv. Values of the L_1, L_2, and L_∞ norm of the difference between the computed and exact density, velocity, pressure, normal stress deviator σ_{xx}, tangential stress deviator σ_{yy}, and shear stress deviator σ_{xy} are to be evaluated for each mesh resolution coarsened onto the coarsest (nominal) mesh. Plots of error versus mesh resolution are to be generated. Inferred convergence properties are to be evaluated both (i) interpolated over all mesh resolutions and (ii) interpolated between each two adjacent mesh resolutions.

V. **Additional User Information**

VI. **References**

[Ble66] Bleich, H.H., and Nelson, I., "Plane Waves in an Elastic-Plastic Half-Space Due to Combined Surface Pressure and Shear," *J. Appl. Mech.* **33**, pp. 149–158 (1966).

[Cri67] Cristescu, N., *Dynamic Plasticity*, North-Holland Publishing Co., Amsterdam (1967).

[Obe07] Oberkampf, W.L., and Trucano, T.G., *Verification and Validation Benchmarks*, Sandia National Laboratories report SAND2007-0853 (2007).

I. **Name**: Hunter's Problem

II. **Conceptual Description**

General: Hunter's Problem consists of an infinite, uniform, elastic-perfectly-plastic (EPP) medium, containing a spherical inclusion of radius a about the origin. At initial time (t=0) the boundary of the inclusion (r=a) is subject to a specified, time-dependent driving pressure $\mathcal{P}$; this driving pressure has a complicated but closed form, given in [Hun57], which can be evaluated numerically and used to drive a hydrocode simulation. The specified driving pressure generates elastic-plastic waves such that the boundary between elastic and plastic deformation moves outward from the cavity wall with constant radial velocity. This problem is, in some sense, a generalized EPP analogue of the Blake problem [Bla52]. The phenomena associated with spherical wave propagation in EPP materials are discussed, e.g., by [Lun49, Hop60, Cha62, Hun68, Mor69].

Processes modeled: This problem tests outgoing, spherically divergent elastic-plastic wave propagation in the absence of boundary reflections. This includes the interaction between elastic and plastic states at the elastic-plastic boundary, as well as the dissipation of energy through plastic work.

Initial conditions: Uniform, constant, zero-velocity EPP material with a vacuum cavity.

Boundary conditions: Pressure $\mathcal{P}$ applied at the inner surface boundary r=a. This driving pressure has a complicated albeit closed form, given in [Hun57]. The far-field boundary is ignored, as the final time is chosen to be before any outgoing wave interacts with the finite computational outer boundary.

Benchmark type: This is a closed-form, analytical solution (type 2 of [Obe07]).

Principal code features tested:

1. Basic hydrodynamics, including single-material EOS calls.
2. Coupling of hydrodynamics with small-strain elastic-plastic dynamic material response.
3. Unidirectional, spherical elastic-perfectly-plastic stress wave propagation.
4. Time-dependent pressure boundary condition implementation.

III. **Mathematical Description**

A complete mathematical description of this problem is given in the references cited below, in particular [Hun57]. In the following, all quantities are in consistent cgs units, if not explicitly stated otherwise.

The system response quantities of interest include:

i. Snapshots of pressure, radial stress deviator σ_{rr}, and hoop stress deviator $\sigma_{\theta\theta}$, as functions of radius.
ii. Time-histories of pressure, radial stress deviator σ_{rr}, and hoop stress deviator $\sigma_{\theta\theta}$ at specified radii.
iii. Total energy as a function of time.

Configuration #1: [Kam08]

Cavity boundary	= a = 100 cm	= 1 m
Density	= ρ = 1.0 g cm^{-3}	= 10^3 kg m^{-3}
Bulk modulus	= K = 10^{10} dyn cm^{-2}	= 1 GPa
Poisson ratio	= 1/3	
→ Lame constant	= λ = 7.5×10^9 dyn cm^{-2}	= 0.75 GPa
→ Shear modulus	= μ = 3.75×10^9 dyn cm^{-2}	= 0.375 GPa
→ Long. wave speed	= c_L = 1.2247×10^5 cm s^{-1}	= 1.2247×10^3 m s^{-1}
→ Shear wave speed	= c_S = 6.1237×10^5 cm s^{-1}	= 6.1237×10^3 m s^{-1}
→ Plastic wave speed	= c_P = 10^5 cm s^{-1}	= 10^3 m s^{-1}
→ EP interface spd	= c_{EP} = 2.4495×10^4 cm s^{-1}	= 2.4495×10^2 m s^{-1}
Yield strength	= Y = 10^9 dyn cm^{-2}	= 0.1 GPa
Driving pressure	= $\mathcal{P}(t)$ = Evaluated by exact solution code	
Final time	= t_{fin} = 10^{-3} s	
Max. mesh radius	= $r_{\max}$ = 300 cm	= 3 m

Figure 1 shows the associated driving pressure $\mathcal{P}$ on the cavity wall as a function of time for this configuration. Figure 2 contains snapshots, at $t = 10^{-3}$ s, of the pressure (p), the (full) radial (σ_{rr}) stress, and (full) hoop ($\sigma_{\theta\theta}$) stress.

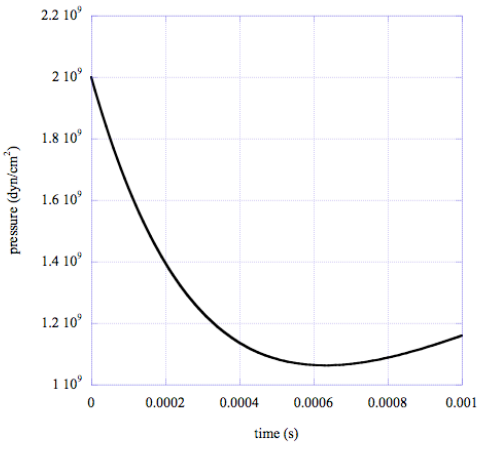

Figure 1. Driving pressure on cavity wall for the Hunter problem discussed in the text.

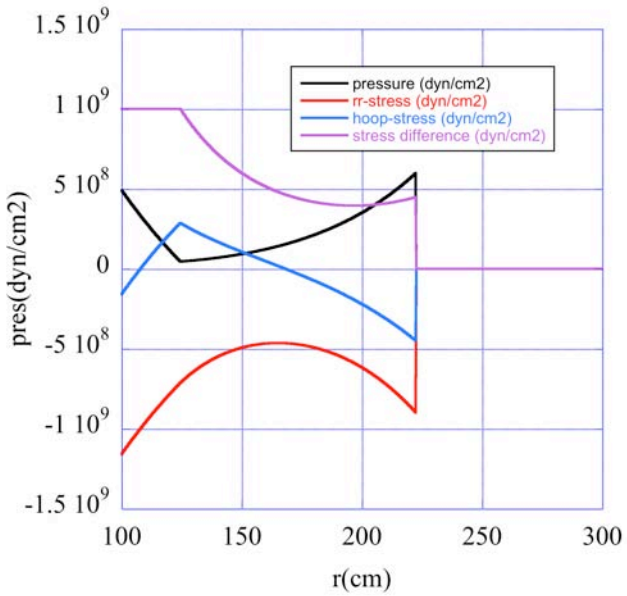

Figure 2. Snapshots, at $t = 10^{-3}$ s, of the pressure (p), the (full) radial (σ_{rr}) stress, and the full hoop ($\sigma_{\theta\theta}$) stress, relative to the original (undisplaced) position, for the Hunter problem discussed in the text. The region of plastic deformation extends from the original cavity boundary at r=100 cm out to an original position of $r \approx 125$ cm.

The driving pressure for this particular problem is sufficiently high, relative to the EPP material properties, that the displacement of the stresswave-processed material is appreciable at the final time. This aspect complicates the comparison of the exact solution with the computed results, since the values given by the exact solution formulae are relative to the initial (reference) positions. Therefore, those results must be transformed to the displaced positions and then interpolated to locations corresponding to the hydrocode mesh. This interpolation process will contribute to the overall error budget of the comparison between the exact solution and computed results. In the quantitative accuracy assessment, the values denoted as "exact" results are those quantities obtained by interpolating the (Lagrangian) Hunter results to the (Eulerian) hydrocode mesh positions.

IV. **Accuracy Assessment**

i. Calculations will be run on a nominal mesh, which is to include 100 zones in the mesh between cavity boundary (a) and the maximum radius of the calculation ($r_{\max}$). Calculations will also be run at mesh resolutions of two, four, and eight times the nominal resolution.

ii. Exact solutions for the pressure, radial stress deviator σ_{rr}, and hoop stress deviator $\sigma_{\theta\theta}$ will be generated at the radial positions corresponding to the center of each mesh cell, for each zone in the initial (undisplaced) domain $a \leq r \leq r_{\max}$.

iii. Values of the L_1, L_2, and L_∞ norm of the difference between the computed and exact pressure, radial stress deviator σ_{rr}, and hoop stress deviator $\sigma_{\theta\theta}$ are to be evaluated for each mesh resolution at its native resolution. Plots of error versus mesh resolution are to be generated. Inferred convergence properties are to be evaluated both (i) interpolated over all mesh resolutions and (ii) interpolated between each two adjacent mesh resolutions.

iv. Values of the L_1, L_2, and L_∞ norm of the difference between the computed and exact pressure, radial stress deviator σ_{rr}, and hoop stress deviator $\sigma_{\theta\theta}$ are to be evaluated for each mesh resolution coarsened onto the coarsest (nominal) mesh. Plots of error versus mesh resolution are to be generated. Inferred convergence properties are to be evaluated both (i) interpolated over all mesh resolutions and (ii) interpolated between each two adjacent mesh resolutions.

V. **Additional User Information**

VI. **References**

[Bla52] Blake, Jr., F.G., "Spherical wave propagation in solid media," *J. Acous. Soc. Am.* **24**, 211–215 (1952).

[Cha62] Chadwick, P., "Propagation of Spherical Plastic-Elastic Disturbances from an Expanded Cavity," *Quart. J. Mech. Appl. Math.* **15**, pp. 349–376 (1962).

[Hop60] Hopkins, H.G., "Dynamic Expansion of Spherical Cavities in Metals," in *Progress in Solid Mechanics, Vol. 1* (eds. I. N. Sneddon and R. Hill), North Holland, Amsterdam, pp. 83–164 (1960).

[Hun57] Hunter, S.C., "The Propagation of Spherically Symmetric Disturbances in Ideally Plastic Materials," in *Proceedings of the Conference on Properties of Materials at High Rates of Strain, London 1957*, pp. 147–155 (1957).

[Hun68] Hunter, S.C., and Crozier, R.J.M., "Similarity Solution for the Rapid Uniform Expansion of a Spherical Cavity in a Compressible Elastic-Plastic Solid," *Quart. J. Mech. Appl. Math.* **21**, pp. 467–486 (1968).

[Kam08] Kamm, J., *Analysis of the Blake and Hunter Problems with the SAGE Code*, Los Alamos National Laboratory report, LA-UR-08-06050 (2008).

[Lun49] Luntz, Ya.L., "The Propagation of Spherical Waves in an Elastic-Plastic Medium," *Prikladnaya Matematika i Meckhanika* **XIII**, pp. 55–78 (1949); translated in *Spherical Wave Propagation in Isotropic Elasto-Plastic Medium*, University of California (Berkeley) Institute of Engineering Research Series No. 63, Issue 3, pp. 33–64 (1953).

[Mor69] Morland, L.W., "Spherical Wave Propagation in Elastic-Plastic Work-Hardening Materials," *J. Mech. Phys. Solids* **17**, pp. 371–385 (1969).

[Obe07] Oberkampf, W.L., and Trucano, T.G., *Verification and Validation Benchmarks*, Sandia National Laboratories report SAND2007-0853 (2007).

I. **Name**: The Verney Problem

II. **Conceptual Description**

General: Verney [Ver68] discusses finite-radius, spherical copper and uranium shells collapsing under a given loading. Motivated by the experimental results for such shells driven by high explosives, Verney constructed a simplified, approximate mathematical model of the problem, assuming incompressible, elastic-perfectly material response. In this model, the initial kinetic energy of the material dissipates via conversion to plastic work, which leads to closed-form solutions for the final shell radius and the total plastic work. The final (time-independent) results of the mathematical model for shell dimensions and plastic work can be compared against hydrocode results of the same configuration. Moreover, for the copper and uranium cases, the experimental data can be compared with the (static) final state for the closed-form solution and hydrocode results. As described by Howell & Ball [How02] and Weseloh et al. [Weh05], this problem has been extended to the case of an idealized beryllium shell.

Processes modeled: This problem tests the integration of the conservation laws for converging flow of incompressible, elastic-perfectly-plastic material response. In particular, the dissipation of kinetic energy by plastic work is a key process in this problem.

Initial conditions: The initial material density and pressure are uniform and constant. The initial radial velocity, however, is not uniform: it is described by the inverse-square relation

$$u_r(r,t=0) = U_0 \left(R_0 / r \right)^2 ,$$

where R_0 is the initial inner radius of the spherical annulus and the constant U_0 is the initial radial velocity at the inner surface. The value of U_0 is given in terms of the material properties and initial configuration as:

$$U_0 = \sqrt{\frac{4Y}{3\rho} \frac{R_1}{\Delta} F_\alpha(\lambda)} ,$$

where, using the common notation of [Ver68, Weh05],

Y = yield strength
ρ = density
R_1 = initial outer radius of the spherical annulus
Δ = $R_1 - R_0$
λ = r_0 / R_0 with r_0 = final inner radius
$F_\alpha(\lambda)$ = $(1+\alpha)^3 \log(1+\alpha) + \lambda^3 \log(\lambda) - (1/3)\ \beta\ \log(\beta)$,
with $\alpha \equiv \Delta / R_0$ and $\beta \equiv \lambda^3 + \alpha^3 + 3\alpha^2 + 3\alpha$

Boundary conditions: The far-field boundary conditions are a constant, quiescent state. Any further boundary conditions depend on the symmetry of the problem: for example, if half of the problem is run in 2-D (r,z) geometry, then the appropriate symmetry boundary condition must be applied along z=0; similarly, if one octant of the problem is run in 3-D (x,y,z) geometry, then symmetry boundary conditions must be applied along the coordinate planes.

Benchmark type: This problem has a non-closed-form solution that requires numerical solution of ODEs to a specified accuracy (type 3 of [Obe07]).

Principal code features tested:

1. Incompressible elastic-plastic material response in converging geometry.
2. Energy conservation, including the dissipation of kinetic energy through plastic work.

III. **Mathematical Description**

This problem was originally described in the paper by Verney [Ver68]. A more thorough treatment is given by Weseloh et al. [Weh05], who obtain analytic expressions for the entire solution. The interested reader is referred these works for details.

In the following, all quantities are in consistent cgs units.

The system response quantities of interest include:

i. Snapshots of density, velocity, pressure, SIE as a function of position.
ii. Time-histories of density, velocity, pressure, and SIE at specified positions.
iii. Total energy, kinetic energy, internal energy as a function of time.

Configuration #1: 2-D (r,z) Spherical Cu, case "F" [Ver68]

Left boundary	$= z_L = 0.0$ cm
Right boundary	$= z_R = 12.0$ cm
Bottom boundary	$= r_L = 0.0$ cm
Top boundary	$= r_R = 12.0$ cm
Initial inner radius	$= R_0 = 5.0$ cm
Initial outer radius	$= R_1 = 10.0$ cm
Initial shell width	$= \Delta = 5.0$ cm
Initial non-dim. radius	$= \alpha = \Delta / R_0 = 1.0$
Non-dim. inner radius	$= \lambda = r_0 / R_0 = 0.55$
Initial density	$= \rho = 9.30333$ g cm^{-3}
Initial mass	$= M = 32150$ g
Bulk modulus	$= K = 1.38\times10^{12}$ dyn cm^{-2}
Shear modulus	$= G = 4.8\times10^{11}$ dyn cm^{-2}
Yield strength	$= Y = 1.2\times10^{9}$ dyn cm^{-2}
Inner/outer pressure	$= p_{I/O}$ = VOID (10^{-12} dyn cm^{-2}) ($0\le r<R_0$, $r>R_1$)

Inner/outer density = $\rho_{I/O}$ = VOID (10^{-6} g cm^{-3}) ($0 \le r < R_0$, $r > R_1$)
Inner/Outer Velocity = $u_{I/O}$ = 0.0 cm s^{-1}
Non-dim. parameter = $\beta = \lambda^3 + \alpha^3 + 3\alpha^2 + 3\alpha = 7.166375$
Energy dissipation function = $F_\alpha(\lambda) = 10.1502$
Initial inner radius velocity = $U_0 = 9.61\times10^4$ cm s^{-1}
Final time = $t_{fin} = 1.0\times10^{-4}$ s
Final inner radius = $r_0 = 2.75$ cm

Configuration #2: 2-D (r,z) Spherical Be [Weh05]

Left boundary = $z_L = 0.0$ cm
Right boundary = $z_R = 12.0$ cm
Bottom boundary = $r_L = 0.0$ cm
Top boundary = $r_R = 12.0$ cm
Initial inner radius = $R_0 = 8.0$ cm
Initial outer radius = $R_1 = 10.0$ cm
Initial shell width = $\Delta = 2.0$ cm
Initial non-dim. radius = $\alpha = \Delta / R_0 = 0.25$
Initial density = $\rho = 1.845$ g cm^{-3}
Initial mass = $M = 3771.42$ g
Bulk modulus = $K = 1.10\times10^{12}$ dyn cm^{-2}
Shear modulus = $G = 1.51\times10^{12}$ dyn cm^{-2}
Yield strength = $Y = 3.3\times10^9$ dyn cm^{-2}
Inner/outer pressure = $p_{I/O}$ = VOID (10^{-12} dyn cm^{-2}) ($0 \le r < R_0$, $r > R_1$)
Inner/outer density = $\rho_{I/O}$ = VOID (10^{-6} g cm^{-3}) ($0 \le r < R_0$, $r > R_1$)
Inner/Outer Velocity = $u_{I/O}$ = 0.0 cm s^{-1}
Final time = $t_{fin} = 1.0\times10^{-4}$ s
Final inner radius = $r_0 = 3.0$ cm
Non-dim. inner radius = $\lambda = r_0 / R_0 = 0.375$
Non-dim. parameter = $\beta = \lambda^3 + \alpha^3 + 3\alpha^2 + 3\alpha = 1.005859375$
Energy dissipation function = $F_\alpha(\lambda) = 0.382145$
Initial inner radius velocity = $U_0 = 6.75036\times10^5$ cm s^{-1}

IV. **Accuracy Assessment**

i. Calculations will be run on a nominal mesh, which is to include 120 zones along the coordinate axes. Calculations will be run also at mesh resolutions of two, four, and eight times the nominal resolution.
ii. Exact solutions of the model equations for the density, velocity, pressure, and SIE will be generated at the positions corresponding to the center of each mesh cell, for each zone in the specified domain 1.
iii. Values of the L_1, L_2, and L_∞ norm of the difference between the computed and exact density, velocity, pressure, and SIE are to be evaluated for each mesh resolution at its native resolution. Plots of error versus mesh resolution are to be

generated. Inferred convergence properties are to be evaluated both (i) interpolated over all mesh resolutions and (ii) interpolated between each two adjacent mesh resolutions.

iv. Values of the L_1, L_2, and L_∞ norm of the difference between the computed and finest-mesh calculated values of density, velocity, pressure, and SIE are to be evaluated for the lower mesh resolutions at their native resolution. Plots of this difference versus mesh resolution are to be generated. Inferred calculation convergence properties are to be evaluated both (i) interpolated over all mesh resolutions and (ii) interpolated between each two adjacent mesh resolutions.

v. Values of the L_1, L_2, and L_∞ norm of the difference between the computed and exact density, velocity, pressure are to be evaluated for each mesh resolution coarsened onto the coarsest (nominal) mesh. Plots of error versus mesh resolution are to be generated. Inferred convergence properties are to be evaluated both (i) interpolated over all mesh resolutions and (ii) interpolated between each two adjacent mesh resolutions.

vi. Values of the L_1, L_2, and L_∞ norm of the difference between the computed and finest-mesh calculated values of density, velocity, pressure are to be evaluated for each mesh resolution coarsened onto the coarsest (nominal) mesh. Plots of this difference versus mesh resolution are to be generated. Inferred convergence properties are to be evaluated both (i) interpolated over all mesh resolutions and (ii) interpolated between each two adjacent mesh resolutions.

vii. The total energy, kinetic energy, and internal energy as functions of time are to be plotted.

V. **Additional User Information**

The late-time, (static) final state for the closed-form solution and hydrocode results can be compared with the experimental data.

VI. **References**

[Ver68] Verney, D., "Évaluation de la Limite Élastique du Cuivre et de l'Uranium par des Expèriences d'Implosion «Lente»," in *Behavior of Dense Media under High Dynamic Pressures, Symposium, H.D.P.*, IUTAM, Paris 1967, Gordon & Breach, New York, pp. 293–303 (1968).

[How02] Howell, B.P., and Ball, G.J., "A Free-Lagrange Augmented Godunov Method for the Simulation of Elastic–Plastic Solids," *J. Comput. Phys.* **175**, pp. 128–167 (2002).

[Wes05] Weseloh, W., et al., *PAGOSA Sample Problems*, Los Alamos National Laboratory report LA-UR-05-6514 (2005).

I. **Name**: Lowrie-Rauenzahn Equilibrium-Diffusion Radiation-Hydrodynamics Problem

II. **Conceptual Description**

General: The Lowrie-Rauenzahn Equilibrium-Diffusion Radiation-Hydrodynamics Problem [Low07] provides a semi-analytic solution for planar radiative shock waves in the equilibrium diffusion (1-*T*) limit. [Mih99, Zel02] provide general background on radiative shocks, which are in the high-energy density regime, i.e., for which the ratio of radiation energy (pressure) to material energy (pressure) is sufficiently high for the radiation-related terms to have a significant impact on the dynamics. The equilibrium diffusion case can also be approximated by other radiation models in the optically-thick limit; see [Dra07] for a discussion of radiative shocks in the optically-thick regime. The solution consists of initially quiescent flow that is processed by the shock, together with the post-shock flow. In the regime of interest, the compressed post-density-jump material radiates, thereby heating the flow in front of the shock (generating an upstream radiation precursor) and cooling immediately behind the shock (a downstream cooling region).

Processes modeled: This problem tests planar radiation-hydrodynamics in the equilibrium-diffusion (1-*T*) limit. The assumed nonlinear coupling between the hydrodynamics and the radiative transfer is exercised for the case of a planar radiative shock wave. This coupling occurs through additional radiative source terms in the energy equation as well as the radiative contributions to the overall pressure and energy. In the equilibrium-diffusion model, it is assumed that the material temperature and radiation temperature remain in equilibrium, so that the radiation modifies the material EOS through addition of radiative pressure and radiation energy terms.

Initial conditions: The initial conditions to this problem are given by imposing a computed exact solution at the starting time and allowing that solution to evolve. The necessary equations and their relation to the physical variables required to initialize the problem are given in [Low07].

Boundary conditions: Uniform boundary conditions are applied at the ends of the computational mesh, which are taken to be sufficiently far from the computed shock structure so that they do not influence the solution.

Benchmark type: This is a non-closed-form solution that requires the numerical solution of both polynomial equations and a nonlinear ordinary differential equation (type 3 of [Obe07]).

Principal code features tested:

1. Basic hydrodynamics, including single-material, polytropic-gas EOS calls.
2. The equilibrium-diffusion (1-*T*) limit of radiative transfer.
3. The propagation of planar radiative shock waves.

III. **Mathematical Description**

A complete mathematical description of this problem is given in [Low07]; see also [Bou00]. The overall, *nondimensional* governing equations are given by:

$$\begin{aligned}
\frac{\partial \rho}{\partial t} &+ \frac{\partial(\rho u)}{\partial x} &&= 0 \\
\frac{\partial(\rho u)}{\partial t} &+ \frac{\partial(\rho u^2 + p^*)}{\partial x} &&= 0 \\
\frac{\partial(\rho E^*)}{\partial t} &+ \frac{\partial((\rho E^* + p^*)u)}{\partial x} &&= \frac{\partial}{\partial x}\left(\kappa \frac{\partial(T^4)}{\partial x}\right)
\end{aligned}$$

where the radiation modifies the pressure, specific internal energy density, and total energy density, respectively, as

$$p^* = p + \tfrac{1}{3} P_0 T^4 \ , \ e^* = e + (P_0 T^4)/\rho \ , \text{ and } E^* = e^* + \tfrac{1}{2} u^2 .$$

In these equations, ρ is the mass density, u is the velocity, p is the material pressure, T is the temperature, $E = e + u^2/2$ is the total energy per unit mass, and P_0 is the non-dimensional ratio of the radiation pressure to the material pressure (equivalently, of the radiation energy to the material energy) given by

$$P_0 = \left(\tilde{a}_R \tilde{T}_0^4\right)/\left(\tilde{\rho}_0 \tilde{a}_0^2\right) ,$$

where the tilde-quantities are the *dimensional* values of: $\tilde{a}_R$, the radiation constant; T_0, the upstream temperature; $\tilde{\rho}_0$, the upstream mass density; and $\tilde{a}_0$, the upstream sound speed.

The necessary reduced equations, which must be solved numerically, are described in [Low07] and [Bou00]. In the following, all quantities are in consistent cgs units.

The system response quantities of interest include:

i. Snapshots of density, velocity, pressure, and temperature as a function of position on the entire domain
ii. Total energy as a function of time

Configuration #1: Dimensional units consistent with [Low07]:

Left boundary = $x_{\min} = 0.0$ cm
Right boundary = $x_{\max} = 1.0$ cm
Pre-shock density = $\rho_0 = 1.0$ g cm^{-3}
Pre-shock temperature = $T_0 = 100$ eV
Adiabatic index = $\gamma = 5/3$
Pre-shock sound speed = $a_0 = 1.1713314 \times 10^7$ cm s^{-1}

Speed of light = $c = 2.99792458 \times 10^{10}$ cm s^{-1}
Radiation constant = $a_R = 137.20172$ erg cm^{-4} eV^{-4}
Total radiation cross-section = $\sigma_t = 853.13875$ cm^{-1}
Gradient length scale = $L = 1.0$ cm
Shock Mach number = $\mathcal{M}_0 = 10$
Pressure ratio = $\mathcal{P}_0 \equiv a_R T_0^4 / (\rho_0 a_0^2) = 0.0001$
Nondimensional thermal diffusion = $\kappa \equiv a_R T_0^4 c / (3 \sigma_t L \rho_0 a_0^3) = 0.0001$,
Initial shock position = $x_{s,0} = 0.9$ cm
Final time = $t_{fin} = 5.12237621763 \times 10^{-9}$ s

IV. **Accuracy Assessment**

i. Calculations will be run on a nominal mesh, which is to include ≥100 zones on the Cartesian domain $[x_{min}, x_{max}]$. Calculations will also be run at mesh resolutions of two, four, and eight times the nominal resolution.
ii. Exact solutions for the density and temperature will be generated for the case with the initial shock position at x=0.9 cm; this solution will be used to initialize the solution on the computational mesh. Note: for the Cartesian geometry considered, the point-wise value of the solution equals the volume-averaged solution.
iii. Values of the L_1, L_2, and L_∞ norm of the difference between the computed and exact density and temperature are to be evaluated for each mesh resolution at its native resolution. Plots of error versus mesh resolution are to be generated. Inferred convergence properties are to be evaluated both (i) interpolated over all mesh resolutions and (ii) interpolated between each two adjacent mesh resolutions.
iv. Values of the L_1, L_2, and L_∞ norm of the difference between the computed and exact density and temperature are to be evaluated for each mesh resolution coarsened onto the coarsest (nominal) mesh. Plots of error versus mesh resolution are to be generated. Inferred convergence properties are to be evaluated both (i) interpolated over all mesh resolutions and (ii) interpolated between each two adjacent mesh resolutions.

V. **Additional User Information**

VI. **References**

[Bou00] Bouquet, S., Teyssier, R., and Chieze, J.P., "Analytical study and structure of a stationary radiative shock," *Astrophys. J. Suppl. Ser.* **127**, pp. 245–252 (2000).
[Dra07] Drake, R.P., "Theory of radiative shocks in optically thick media," *Phys. Plasmas* **14**, pp. 043301-1–10 (2007).
[Low07] Lowrie, R., and Rauenzahn, R., "Radiative shock solutions in the equilibrium diffusion limit," *Shock Waves* **16**, pp. 445–453 (2007).
[Mih99] Mihalas, D., and Weibel-Mihalas, B.W., *Foundations of Radiation Hydrodynamics*, Dover, Mineola, NY (1999).

[Obe07] Oberkampf, W.L., and Trucano, T.G., *Verification and Validation Benchmarks*, Sandia National Laboratories report SAND2007-0853 (2007).

[Zel02] Zel´dovich, Y.B., and Raizer, Y.P., *Physics of Shock Waves and High-Temperature Hydrodynamic Phenomena*, Dover, Mineola, NY (2002).

I. **Name**: Lowrie Nonequilibrium-Diffusion Radiation-Hydrodynamics Problem

II. **Conceptual Description**

General: The Lowrie Nonequilibrium-Diffusion Radiation-Hydrodynamics Problem [Low07a,b] provides a semi-analytic solution for planar radiative shock waves using a grey nonequilibrium diffusion radiation model (2-*T*). [Mih99, Zel02] provide general background on radiative shocks, which are in the high-energy density regime, i.e., for which the ratio of radiation energy (pressure) to material energy (pressure) is sufficiently high for the radiation-related terms to have a significant impact on the material dynamics. In the nonequilibrium-diffusion approximation, the independent internal energies densities of the material and the radiation admit that their respective temperatures may be out of equilibrium; the grey approximation admits cross-sections that are state-dependent but not frequency-dependent. The solution consists of initially quiescent flow that is processed, together with the post-compression flow. In the regime of interest, the compressed post-density-jump material radiates, affecting the flow on either side of the compression: generating an upstream radiation precursor in front and modifying the downstream region behind. For a given polytropic gas material EOS and pre-shock conditions, the solution structure can be characterized by the shock Mach number: for very low Mach number, the solution is smooth; as the Mach number increases, an embedded hydrodynamic shock appears; as the Mach number increases further, the well-known Zel´dovich spike appears; at still higher Mach number, the temperature maximum of the Zel´dovich spike occurs downstream of the shock, while at *very* high Mach number, the solution is again smooth [Low07b].

Processes modeled: This problem tests planar radiation-hydrodynamics in the grey nonequilibrium-diffusion limit. In particular, the nonlinear coupling between the hydrodynamics and the radiative transfer is exercised for the case of a planar radiative shock wave. This coupling occurs through an additional equation for the radiation energy density as well as radiative coupling terms in the energy equations.

Initial conditions: The initial conditions to this problem are given by imposing a computed exact solution at the starting time and allowing that solution to evolve. The necessary equations and their relation to the physical variables required to initialize the problem are given in [Low07a].

Boundary conditions: Uniform boundary conditions are applied at the ends of the computational mesh, which are taken to be sufficiently far from the computed shock structure so that they do not influence the solution.

Benchmark type: This is a non-closed-form solution that requires the numerical solution of both polynomial equations and a nonlinear ordinary differential equation (type 3 of [Obe07]).

Principal code features tested:

1. Basic hydrodynamics, including single-material, polytropic-gas EOS calls.
2. The grey nonequilibrium-diffusion limit of radiative transfer.
3. The propagation of planar radiative shock waves.

III. **Mathematical Description**

A complete mathematical description of this problem is given in [Low07a], with further details summarized in [Low07b]; see also [Bou00]. The overall, *nondimensional* governing equations are given by:

$$\begin{aligned}
\frac{\partial \rho}{\partial t} &+ \frac{\partial(\rho u)}{\partial x} &&= 0 \\
\frac{\partial(\rho u)}{\partial t} &+ \frac{\partial(\rho u^2 + p + (1/3)P_0\phi)}{\partial x} &&= 0 \\
\frac{\partial(\rho E)}{\partial t} &+ \frac{\partial((\rho E + p)u)}{\partial x} &&= P_0\sigma_a\left(\phi - T^4\right) - \frac{1}{3}P_0 u\frac{\partial \phi}{\partial x} \\
\frac{\partial \phi}{\partial t} &+ \frac{\partial}{\partial x}\left(\frac{4}{3}u\phi - \kappa\frac{\partial \phi}{\partial x}\right) &&= -\sigma_a\left(\phi - T^4\right) + \frac{1}{3}u\frac{\partial \phi}{\partial x}
\end{aligned}$$

In these equations, ρ is the mass density, u is the velocity, p is the material pressure, T is the material temperature, e is the material internal energy per unit mass, $E = e + u^2/2$ is the total material energy per unit mass, ϕ is the radiation energy density, and σ_a is the absorption cross section. P_0 is the non-dimensional ratio of the radiation pressure to the material pressure (equivalently, of the radiation energy to the material energy) given by

$$P_0 = \left(\tilde{a}_R \tilde{T}_0^4\right) / \left(\tilde{\rho}_0 \tilde{a}_0^2\right),$$

where the quantities with tildes are the *dimensional* values of: $\tilde{a}_R$, the radiation constant; T_0, the upstream temperature; $\tilde{\rho}_0$, the upstream mass density; and $\tilde{a}_0$, the upstream sound speed. The value of κ is given by

$$\kappa = \tilde{c} / \left(3\sigma_t \tilde{a}_0 L\right),$$

where $\tilde{c}$ is the dimensional speed of light and $\tilde{\sigma}_t$ is the dimensional total cross section.

The necessary reduced equations, which must be solved numerically, are described in the references. In the following, all quantities are in consistent cgs units.

The system response quantities of interest include:

i. Snapshots of non-dimensional density and product of the non-dimensional density and one minus the nondimenstional material temperature on the same plot.
ii. Snapshots of the non-dimensional material temperature, non-dimensional radiation temperature, and the product of the non-dimensional material temperature and one minus this same quantity on the same plot, as functions of position over the entire domain and in the immediate vicinity of the compression; for the close-up plots, use the same abscissa limits—which vary with the Mach number—as in [Low07b].
iii. Total energy, material energy, and radiation energy as functions of time.

Configuration #1: $\mathcal{M}_0 = 1.2$, subcritical, no branch-point shock

Dimensional units consistent with [Low07b]:
Left boundary = $x_{\min} = 0.0$ cm
Right boundary = $x_{\max} = 1.0$ cm
Pre-shock density = $\rho_0 = 1.0$ g cm^{-3}
Pre-shock material temperature = $T_0 = 100$ eV
Pre-shock radiation temperature = $\theta_0 = 100$ eV
Adiabatic index = $\gamma = 5/3$
Pre-shock sound speed = $a_0 = 1.1713314\times10^{7}$ cm s^{-1}
Speed of light = $c = 2.99792458\times10^{10}$ cm s^{-1}
Radiation constant = $a_R = 137.20172$ erg cm^{-4} eV^{-4}
Absorption radiation cross-section = $\sigma_a = 1\times10^{6}$ cm^{-1}
Gradient length scale = $L = 1.0$ cm
Shock Mach number = $\mathcal{M}_0 = 1.2$
Pressure ratio = $\mathcal{P}_0 \equiv a_R T_0^{4} / (\rho_0 a_0^{2}) = 0.0001$
Nondimensional diffusion coefficient = $\kappa \equiv c / (3\sigma_t L\ a_0) = 1.0$,
Initial shock position = $x_{s,0} = 0.9$ cm
Final time = $t_{\text{fin}} = 5.12237621763\times10^{-9}$ s

Configuration #2: $\mathcal{M}_0 = 2$, subcritical, branch-point at shock

Dimensional units consistent with [Low07b];
Same conditions as Configuration #1 with flow velocity assigned such that:
Shock Mach number = $\mathcal{M}_0 = 2$
Final time = $t_{\text{fin}} = 5.12237621763\times10^{-9}$ s

Configuration #3: $\mathcal{M}_0 = 3$, subcritical, branch-point downstream of shock

Dimensional units consistent with [Low07b];
Same conditions as Configuration #1 with flow velocity assigned such that:
Shock Mach number = $\mathcal{M}_0 = 3$
Final time = $t_{\text{fin}} = 5.12237621763\times10^{-9}$ s

Configuration #4: $\mathcal{M}_0 = 5$, supercritical, branch-point downstream of shock
Dimensional units consistent with [Low07b];
Same conditions as Configuration #1 with flow velocity assigned such that:
Shock Mach number = $\mathcal{M}_0 = 5$
Final time = $t_{fin} = 5.12237621763 \times 10^{-9}$ s

Configuration #5: $\mathcal{M}_0 = 27$, supercritical, branch-point downstream of shock
Dimensional units consistent with [Low07b];
Same conditions as Configuration #1 with flow velocity assigned such that:
Shock Mach number = $\mathcal{M}_0 = 27$
Final time = $t_{fin} = 5.12237621763 \times 10^{-9}$ s

Configuration #6: $\mathcal{M}_0 = 30$, supercritical, branch-point but no shock
Dimensional units consistent with [Low07b];
Same conditions as Configuration #1 with flow velocity assigned such that:
Shock Mach number = $\mathcal{M}_0 = 30$
Final time = $t_{fin} = 5.12237621763 \times 10^{-9}$ s

Configuration #7: $\mathcal{M}_0 = 50$, supercritical, no branch-point, no shock
Dimensional units consistent with [Low07b];
Same conditions as Configuration #1 with flow velocity assigned such that:
Shock Mach number = $\mathcal{M}_0 = 50$
Final time = $t_{fin} = 5.12237621763 \times 10^{-9}$ s

IV. **Accuracy Assessment**

i. Calculations will be run on a nominal mesh, which is to include ≥100 zones on the Cartesian domain $[x_{min}, x_{max}]$. Calculations will also be run at mesh resolutions of two, four, and eight times the nominal resolution. Very high mesh resolutions will likely be required to resolve the Zel´dovich spike structure in the higher Mach number cases.
ii. The closed-form solutions for the density and temperature will be evaluated numerically; this solution will be used to initialize the solution on the computational mesh. Note: for the Cartesian geometry considered, the point-wise value of the solution equals the volume-averaged solution.
iii. Values of the L_1, L_2, and L_∞ norm of the difference between the computed and exact density and temperature are to be evaluated for each mesh resolution at its native resolution. Plots of error versus mesh resolution are to be generated. Inferred convergence properties are to be evaluated both (i) interpolated over all mesh resolutions and (ii) interpolated between each two adjacent mesh resolutions.
iv. Values of the L_1, L_2, and L_∞ norm of the difference between the computed and exact density and temperature are to be evaluated for each mesh resolution coarsened onto the coarsest (nominal) mesh. Plots of error versus mesh resolution are to be generated. Inferred convergence properties are to

be evaluated both (i) interpolated over all mesh resolutions and (ii) interpolated between each two adjacent mesh resolutions.

V. **Additional User Information**

VI. **References**

[Bou00] Bouquet, S., Teyssier, R., and Chieze, J.P., "Analytical study and structure of a stationary radiative shock," *Astrophys. J. Suppl. Ser.* **127**, pp. 245–252 (2000).

[Low07a] Lowrie, R., and Edwards, J.D., "Shock wave solutions for radiation hydrodynamics," in *Proceedings of the Joint International Topical Meeting on Mathematics & Computation and Supercomputing in Nuclear Applications* (M&C + SNA 2007), Monterey, CA, 15–19 April 2007, Los Alamos National Laboratory report LA-UR-07-1077 (2007).

[Low07b] Lowrie, R., "Radiative Shock Solutions," presentation at Numerical Methods for Multi-Material Fluid Flows, Prague, CZ, 10–14 September 2007, Los Alamos National Laboratory report LA-UR-07-5986 (2007), available at http://www-troja.fjfi.cvut.cz/~multimat07/presentations/tuesday/Lowrie.pdf

[Mih99] Mihalas, D., and Weibel-Mihalas, B.W., *Foundations of Radiation Hydrodynamics*, Dover, Mineola, NY (1999).

[Obe07] Oberkampf, W.L., and Trucano, T.G., *Verification and Validation Benchmarks*, Sandia National Laboratories report SAND2007-0853 (2007).

[Zel02] Zel´dovich, Y.B., and Raizer, Y.P., *Physics of Shock Waves and High-Temperature Hydrodynamic Phenomena*, Dover, Mineola, NY (2002).

I. **Name**: Radiation-Acoustics Problem

II. **Conceptual Description**

General: The Radiation-Acoustics Problem possesses a closed-form analytic solution for planar waves in a radiating fluid. The assumptions are that the waves are small perturbations on a gray medium with constant mean temperature and density, and that the radiation is in the diffusion limit. The material is at a single temperature and the radiation is in local thermodynamic equilibrium (LTE) with the material. The material and radiation temperature perturbations differ, however, so that the assumption of LTE only applies to the background state. Deviations from a constant opacity are neglected since they arise at higher order in the perturbation amplitude, and scattering is neglected. The waves are driven at one boundary of a Cartesian mesh and their phase speeds and damping lengths are parameterized by the ratio of the speed of sound to the speed of light, the ratio of the radiation energy density to the material energy density, and the driving frequency at the boundary. The solution applies to both the low- and high-energy density regimes.

Processes modeled: This problem tests planar radiation-hydrodynamics in the grey nonequilibrium-diffusion limit. In particular, the linear coupling between the hydrodynamics and the radiative transfer is exercised for the case of a planar radiative wave.

Initial conditions: The initial conditions to this problem are a constant background density and temperature. Due to the assumption of LTE, the background radiation and material temperatures are equal.

Boundary conditions: Sinusoidal time-dependent velocity and radiation temperature perturbations are applied at one boundary of the mesh. The velocity and radiation temperatures are related through the eigenvectors of the analytical solution. A Milne boundary condition is applied to the radiation at the other end of the mesh. The hydrodynamic boundary condition at the other end is irrelevant as long as the simulation stops before the wave reaches the boundary. Longer simulation times can result in wave reflections that corrupt the results. Transverse boundary conditions in a multi-dimensional calculation are unimportant as the problem is one-dimensional.

Benchmark type: This is a closed-form solution that requires the algebraic solution of a dispersion relation (type 1 of [Obe07]).

Principal code features tested:

1. Basic hydrodynamics, including single-material, polytropic-gas EOS calls.
2. The grey nonequilibrium-diffusion limit of radiative transfer.
3. The propagation of planar radiative waves.

III. **Mathematical Description**

A complete mathematical description of this problem is given in [Vin62,Mih83, Mih99, Bog96]. The governing equations are those of radiation hydrodynamics in the diffusion limit. The material and radiation quantities are taken to be small-amplitude plane wave perturbations about an equilibrium state. The equilibrium solution is a constant material temperature T_0 and density ρ_0 and a radiative source function equal to the Planck function. The equilibrium radiation temperature is T_0, but the material and radiation temperature perturbations are allowed to differ. The equilibrium velocity and radiative flux are both assumed to be zero. The perturbation quantities satisfy the following set of equations:

$$
\begin{aligned}
\frac{\partial \rho}{\partial t} &+ \frac{\partial u}{\partial x} &&= 0 \\
\frac{\partial u}{\partial t} &+ a_0^2 \frac{\partial([\rho + T_m]/\gamma + 4rT_r/3)}{\partial x} &&= 0 \\
\frac{\partial T_m}{\partial t} &+ (\gamma-1)\frac{\partial u}{\partial x} &&= 4\gamma(\gamma-1)rc\chi\left(T_r - T_m\right) \\
\frac{\partial T_r}{\partial t} &+ \frac{1}{3}\frac{\partial}{\partial x}\left(u - \frac{c}{\chi}\frac{\partial T_r}{\partial x}\right) &&= -c\chi\left(T_r - T_m\right)
\end{aligned}
$$

In these equations, ρ is the mass density perturbation in units of ρ_0, u is the velocity, and T_m and T_r are the material and radiation temperature perturbations in units of T_0. The quantity r is the dimensionless ratio of the radiation pressure to the material pressure (equivalently, of the radiation energy to the material energy), given by

$$r = \frac{a_R T_0^4}{\rho_0 a_0^2},$$

where a_R is the radiation constant and a_0 is the equilibrium sound speed. The absorption opacity χ (in units of inverse length) is taken to be a constant, and c is the speed of light.

Choosing an equilibrium temperature defines the speed of sound, which has the same units as the speed of light. The equilibrium density is then determined by choosing the pressure ratio r (the density and temperature must be in a consistent set of units to make r dimensionless). The unit of length or time can be chosen arbitrarily, and the other is then determined through the units of the speed of light. The simplest approach is to set the length scale to be a fixed number of perturbation wavelengths, since otherwise a different mesh (or a rescaling of the mesh) is required for each point in parameter space.

Decomposing the perturbation equations into modes of the form $e^{i(\omega t - kx)}$ yields a dispersion relation that is quadratic in the square of the wave number *k*:

$$c_4 \tau^{-4} + c_2 \tau^{-2} + c_0 = 0,$$

where $\tau^{-1} = k/\chi$ is the wave number in units of the opacity. The coefficients in the dispersion relation are given by

$$c_4 = 1 - i4(\gamma - 1) r \tau_c$$
$$c_2 = 3(1 + i\tau_c^{-1}) + \tau_a^{-2}(-1 + i4\gamma[\gamma - 1] r \tau_c) + 4r(5[\gamma - 1] + 4\gamma[\gamma - 1] r/3 + i\tau_c^{-1}/3)$$
$$c_0 = -3\tau_a^{-2}(1 + 4\gamma[\gamma - 1] r + i\tau_c^{-1})$$

where $\tau_a^{-1} = \omega/(a_0 \chi)$ and $\tau_c^{-1} = \omega/(c\chi)$.

Defining the length unit to be one perturbation wavelength is equivalent to setting $k_r = 2\pi$, where k_r is the real part of *k*. The opacity is then determined by $\chi = k_r / \tau_r^{-1}$, where τ_r^{-1} is the real part of the solution of interest. The time scale is set by $\omega^{-1} = \tau_a \tau_r^{-1} / (a_0 k_r)$, and the simulation is stopped after a fixed multiple of $2\pi\omega^{-1}$ (preferably before the wave propagates to the end of the mesh).

Sample plots of the analytical solution along with numerical results are shown in Figs. 1 and 2. There are two branches to the dispersion relation: a radiatively-modified acoustic wave and a radiative diffusion wave. The former is generally weakly damped, and the latter strongly damped. The fluid is driven at the left boundary, and the snapshots are taken after ten wave periods.

The system response quantities of interest include:

i. Snapshots of perturbation quantities over the entire computational domain.

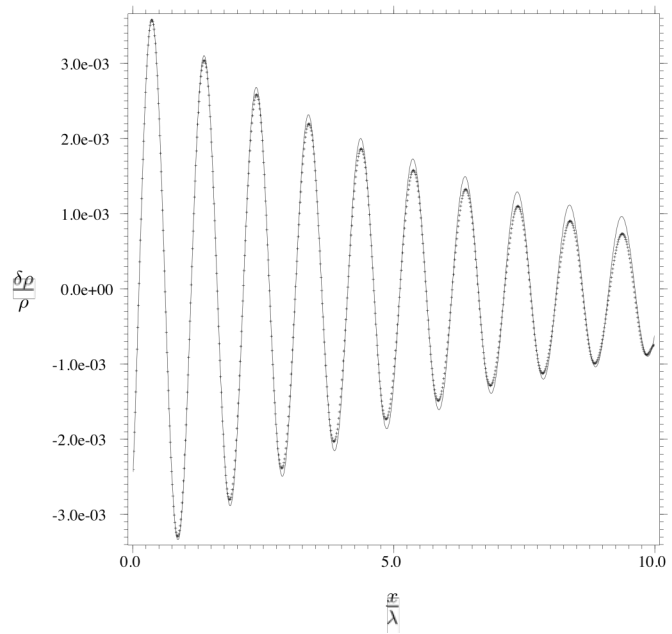

Figure 1. Plot of the density perturbation for a radiative acoustic wave. The solid line is the analytical solution, and the points are computed results. The parameters are: a_0=10^{-4} c, r = 10^{-3}, and τ_a = 10. This corresponds to a mean temperature of 4×10^4 K and mean density of 3×10^{-6} g cm^{-3}.

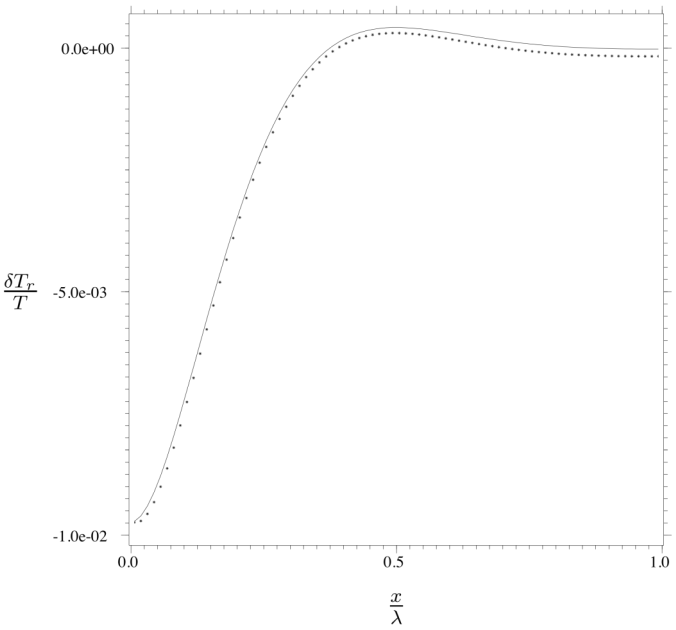

Figure 2. Plot of the radiation temperature perturbation for a radiative diffusion wave. The solid line is the analytical solution, and the points are computed results. The parameters are: a_0=10^{-4} c, r = 10^{-3}, and τ_a = 10, corresponding to a mean temperature of 4×10^4 K and mean density of 3×10^{-6} g cm^{-3}.

IV. **Accuracy Assessment**

i. Calculations will be run on a nominal mesh, which is to include 200 zones in the specified domain (a 10-wavelength mesh for a total of 20 zones per wavelength). Calculations will be run also at mesh resolutions of two, four, and eight times the nominal resolution.
ii. Exact solutions for the density, velocity, material temperature and radiation temperature (perturbed quantities normalized by the equilibrium quantities) will be generated at the positions corresponding to the center of each mesh cell, for each zone in the specified domain.
iii. Values of the L_1, L_2, and L_∞ norm of the difference between the computed and exact density, velocity, material temperature and radiation temperature perturbations at the end of each run are to be evaluated for each mesh resolution at its native resolution. Plots of error versus mesh resolution are to be generated. Inferred convergence properties are to be evaluated both (i) interpolated over all mesh resolutions and (ii) interpolated between each two adjacent mesh resolutions.

V. **Additional User Information**

VI. **References**

[Bog96] Bogdan, T.J, Knoelker, M., MacGregor, K.B., and Kim, E.-J., "Waves in Radiating Fluids," *Astrophys. J.* **456**, pp. 879–901 (1996).

[Mih83] Mihalas, D., and Weibel-Mihalas, B.W., "On the Propagation of Acoustic Waves in a Radiating Fluid," *Astrophys. J.* **273**, pp. 355–362 (1983).

[Mih99] Mihalas, D., and Weibel-Mihalas, B.W., *Foundations of Radiation Hydrodynamics*, Dover, Mineola, NY (1999).

[Obe07] Oberkampf, W.L., and Trucano, T.G., *Verification and Validation Benchmarks*, Sandia National Laboratories report SAND2007-0853 (2007).

[Vin62] Vincenti, W.G., and Baldwin, B.S., "Effect of Thermal Radiation on the Propagation of Plane Acoustic Waves," *J. Fluid Mech.* **12**, pp. 449–477 (1962).

DISTRIBUTION:

1 Rebecca Brannon
Department of Mechanical Engineering
50 S. Central Campus Dr.
Room 2110 - MEB
Salt Lake City, UT 84112

1 Robert Doney
US Army Research Laboratory
AMSRD-ARL-WM-TA
Aberdeen Proving Ground, MD 21005-5066

1 MS 0316
Rob Hoekstra, 1437

1 MS 0316
Eric Keiter, 1437

1 MS 0316
Curt Ober, 1433

1 MS 0316
John Shadid, 1437

1 MS 0321
John Mitchiner, 1430

1 MS 0321
James Peery, 1400

1 MS 0370
Jim Strickland, 1433

1 MS 0370
Timothy G. Trucano, 1411

1 MS 0372
Arne Gullerud, 1524

1 MS 0372
Tim Shelton, 1524

1 MS 0378
Ed Love, 1431

1 MS 0378
John Niederhaus, 1431

1 MS 0378
William J. Rider, 1431

1 MS 0378
Allen C. Robinson, 1431

1 MS 0378
Erik Strack, 1431

1 MS 0378
Randall M. Summers, 1431

1 MS 0378
Tom Voth, 1433

1 MS 0378
V. Gregory Weirs, 1431

1 MS 0380
Martin Heinstein, 1542

1 MS 0380
Joeseph Jung, 1542

1 MS 0380
David Womble, 1540

1 MS 0382
Brian Carnes, 1544

1 MS 0382
Kevin Copps, 1544

1 MS 0382
Steve Bova, 1541

1 MS 0382
Stefan Domino, 1541

1 MS 0382
Basil Hassan, 1541

1 MS 0825
Ryan Bond, 1515

1 MS 0828
Amalia Black, 1544

1 MS 0828
Kevin Dowding, 1544

1 MS 0828
Tony Giunta, 1544

1 MS 0828
Richard Hills, 1544

1 MS 0828
Martin Pilch, 1551

1 MS 0828
Vicente Romero, 1544

1 MS 1146
Kendall Depriest, 1384

1 MS 1152
C. David Turner, 1653

1 MS 1179
Clif Drumm, 1341

1 MS 1179
W. C. Fan, 1341

1 MS 1179
Shawn Pautz, 1341

1 MS 1189
Tom Brunner, 1641

1 MS 1189
Heath Hanshaw, 1641

1 MS 1318
Bruce Hendrickson, 1410

1 MS 1318
Patrick Knupp, 1414

1 MS 1318
Jim Stewart, 1411

1 MS 1318
Laura Swiler, 1411

1 MS 1319
Guglielmo Scovazzi, 1431

1 MS 1322
John Aidun, 1435

1 MS 0899
Technical Library (electronic copy, 9536


Los Alamos
NATIONAL LABORATORY
EST. 1943